Development of Two-Dimensional Photonic Crystal Hydrogel Sensors for Biomolecular Detection

by

Kyeongwoo Jang

Bachelor of Science in Chemistry, Hanyang University, Seoul, South Korea, 2014

Submitted to the Graduate Faculty of the

Dietrich School of Arts and Sciences in partial fulfillment

of the requirements for the degree of

Doctor of Philosophy

University of Pittsburgh

2022

UNIVERSITY OF PITTSBURGH

DIETRICH SCHOOL OF ARTS AND SCIENCES

This dissertation was presented

by

Kyeongwoo Jang

It was defended on

September 28, 2022

and approved by

Dr. Seth Horne, Associate Professor, Department of Chemistry, University of Pittsburgh

Dr. Jennifer Laaser, Assistant Professor, Department of Chemistry, University of Pittsburgh

Dr. Sachin Velankar, Associate Professor, Chemical and Petroleum Engineering, Mechanical Engineering and Materials Science, University of Pittsburgh

Dissertation Director: Dr. Sanford A. Asher, Distinguished Professor of Chemistry, Department of Chemistry, University of Pittsburgh

Development of Two-Dimensional Photonic Crystal Hydrogel Sensors for Biomolecular Detection

Kyeongwoo Jang, PhD

University of Pittsburgh, 2022

The work reported in this dissertation discusses the recent advancements in the development of 2DPC hydrogel sensors for biomolecular detection. The 2DPC hydrogel sensors are fabricated by incorporating 2DPC into responsive hydrogels. Each hydrogel sensor is functionalized with specific recognition groups that interact with the desired target, causing the hydrogel to undergo volume phase transitions (VPTs). We measure the target-induced hydrogel VPTs by monitoring the 2DPC light diffraction and report the analyte concentrations. This sensing platform is simple, does not require sophisticated instrumentation, and could be used in resource-limited environments and point-of-care testing.

We demonstrated the use of oxyamine recognition groups for the detection of phenylpyruvate, an enzymatic reaction product between phenylalanine and phenylalanine dehydrogenase. The chemoselective oxime reaction between the hydrogel oxyamines and phenylpyruvate covalently modifies the hydrogel structure and induces the hydrogel VPTs. This 2DPC hydrogel sensor could be further used to develop a phenylalanine sensor for patients with phenylketonuria and to develop a lactate sensor to evaluate the development of sepsis.

We also developed two other mechanisms for small molecule detection utilizing DNA aptamers as molecular recognition groups. Upon binding targets, the DNA aptamers that are attached to the hydrogel network undergo conformational changes, triggering the hydrogel VPTs. We hypothesize that this sensing motif is generalizable and that other sensors can be easily

fabricated by simply exchanging the aptamer recognition group. We plan to continue to develop this sensing platform for the detection of other small molecules and proteins of interest.

Table of Contents

Preface xx

1.0 Introduction 1

1.1 Two-Dimensional Photonic Crystal Hydrogel Sensors 1

1.1.1 Stimuli-Responsive Hydrogels and Their Volume Phase Transition Mechanisms 1

1.1.1.1 VPTs of non-ionic hydrogels 2

1.1.1.2 VPTs of ionic hydrogels 4

1.1.2 Photonic crystal hydrogel sensing motif 4

1.2 Overview of Research Program 10

1.3 References 11

2.0 Human Serum Phenylpyruvate Quantification Using Responsive 2D Photonic Crystal Hydrogels via Chemoselective Oxime Ligation: Progress toward Developing Phenylalanine-Sensing Elements 16

2.1 Introduction 17

2.2 Experimental 19

2.2.1 Materials 19

2.2.2 Characterization Techniques 20

2.2.2.1 NMR 20

2.2.2.2 Mass Spectrometry 20

2.2.2.3 Scanning Electron Microscopy 21

2.2.3 Preparation of tert-Butyl(2-Acrylamidoethoxy)-Carbamate (TAC) via a Three-Step Sequence of Reactions 21

2.2.3.1 Synthesis of 1[21] 22

2.2.3.2 Synthesis of 2[21,22] 22

2.2.3.3 Synthesis of 3 (TAC)[23] 23

2.2.4 Preparation of 2DPC Hydrogels 23

2.2.5 Hydrogel Boc Deprotection 27

2.2.6 2DPC Particle Spacing Measurements 27

2.2.7 PhPY-Sensing in Buffer Solutions 29

2.2.8 PhPY Sensing in Human Serum 30

2.3 Results and Discussion 30

2.3.1 PhPY-Sensing Motif Using Responsive Hydrogels Containing 2DPC and Oxyamine Recognition Groups 30

2.3.2 Characterizations of PhPY-Sensing Hydrogels 34

2.3.3 PhPY Recognitions in Buffer Solutions 38

2.3.4 PhPY Recognitions in Human Serum 44

2.4 Conclusions 46

2.4.1 Acknowledgements 47

2.5 References 48

3.0 DNA-Crosslinked 2D Photonic Crystal Hydrogels for Detection of Adenosine Actuated by an Adenosine-Binding Aptamer 52

3.1 Introduction 53

3.2 Experimental 55

3.2.1 Materials 55

3.2.2 Annealing DNA Strands 56

3.2.3 PicoGreen Fluorescence Assay.....57

3.2.4 2DPC Hydrogel Fabrication 58

3.2.5 Scanning Electron Microscopy Characterization 60

3.2.6 2DPC Particle Spacing Measurements.....62

3.2.7 Adenosine Sensing in Buffer Solutions.....64

3.2.8 Adenosine Sensing in FBS 64

3.3 Results and Discussion 65

3.3.1 Adenosine Sensing Motif Using DNA-Crosslinked 2DPC Hydrogels That Contain the Adenosine-Binding Aptamer.....65

3.3.2 Optimizing Adenosine-Binding Buffer Conditions via Fluorometric Quantitation of dsDNA Using PicoGreen 67

3.3.3 Adenosine Sensing in Buffer Solutions.....70

3.3.4 Selectivity of Adenosine-Sensing 2DPC Hydrogels.....74

3.3.5 Adenosine Sensing in FBS 75

3.4 Conclusions 78

3.4.1 Acknowledgements.....79

3.5 References 79

4.0 Aptamer-Functionalized 2D Photonic Crystal Hydrogels for Detection of Adenosine..... 85

4.1 Introduction 86

4.2 Experimental..... 89

4.2.1 Materials and Characterization 89

4.2.2 Preparation of AD-Sensing 2DPC Hydrogels 90

4.2.3 2DPC Particle Spacing Measurement 90

4.2.4 AD-Sensing in PBS 92

4.2.5 AD-Sensing in FBS and Human Urine 93

4.3 Results and Discussion 94

4.3.1 Preparation and Characterizations of AD-Sensing 2DPC Hydrogels 94

4.3.2 Reversible AD-Sensing Mechanism Using Aptamer-Functionalized 2DPC Hydrogels 97

4.3.3 AD-sensing in PBS 98

4.3.4 AD-Sensing in FBS and Human Urine 105

4.4 Conclusions 108

4.4.1 Acknowledgements 108

4.5 References 109

5.0 Summary and Future Work 113

5.1 Summary 113

5.2 Future Work 114

5.2.1 Development of L-Phe- and L-Lactate-Sensing Elements Utilizing Enzymes and the Oxyamine-Functionalized 2DPC Hydrogels 114

5.2.2 Future Work in the Aptamer-Functionalized 2DPC Hydrogel Materials 116

5.3 References 121

Appendix A Supporting Information for Chapter 2 122

Appendix A.1 High-Resolution Mass Spectrometry (HRMS) Spectra of Synthesized Compounds 122

Appendix A.2 ^{1}H and ^{13}C NMR Spectra of Synthesized Compounds..... 124

Appendix B Supporting Information for Chapter 3..... 129

Appendix B.1 Calculating Dissociation Constant of the Adenosine-Binding Aptamer 129

Appendix B.2 Optimizing Acrylamide (AAm) Monomer and MBAAm Crosslinker Concentrations in 2DPC Hydrogel Fabrication 131

Appendix C Supporting Information for Chapter 4 133

Appendix C.1 Fabrication of two-dimensional photonic crystal (2DPC) hydrogels .. 133

Appendix C.2 Fourier transform infrared (FTIR) characterization..... 135

Appendix C.3 Optimization of hydrogel sensor composition..... 136

Appendix C.4 An overview on recently reported aptamer-based AD sensors 139

Appendix C.5 Calculating the average % difference in particle spacing changes measured between diluted FBS and pure PBS 140

Appendix C.6 Calculating the % recoveries for the detection of AD in human urine140

Appendix C.7 References..... 141

List of Tables

Table 2-1. Composition of monomer solutions used in the preparation of hydrogel samples 26

Table 3-1. Composition of monomer solutions used in preparation of hydrogel samples ... 59

Table 4-1. Determination of AD in diluted human urine (*n* = 3) 107

Appendix Table B-1. Concentrations of AAm and MBAAm used in preparation of 2DPC hydrogels 132

Appendix Table C-1. Compositions of polymerizable monomer solutions used to prepare various 2DPC hydrogels 134

Appendix Table C-2. Comparison of the performance of our 2DPC hydrogels with other aptasensors for AD detection 139

List of Figures

Figure 1-1. Schematic representation of photonic crystals. The periodicity of photonic crystals ranges from one- to three-dimensional.[31] 5

Figure 1-2. CCA with a body-centered cubic structure. Highly charged colloidal particles are self-assembled into the lattice structure due to the electrostatic repulsion.[34] 6

Figure 1-3. The PCCA sensing motif. The CCA diffraction measurement allows for the sensitive monitoring of the shits in the diffracted wavelength, which is used to report the analyte concentration.[34] 6

Figure 1-4. Preparation of 2DPC on a glass substrate. (a-b) Inject a solution containing polystyrene particles on water surface to fabricate a hexagonally-closed-packed 2DPC array. (c-d) The 2DPC on water is transferred to a glass substrate and air-dried.[2] 8

Figure 1-5. (a) Schematic diagram and (b) the experimental setup showing the 2DPC light diffraction. When irradiated by a monochromatic light along the array normal, 2DPC diffracts light at an angle depending on the particle spacing, producing a Debye ring on the bottom screen.[4] 9

Figure 1-6. Example particle spacing curve reporting the analyte concentration. The 2DPC hydrogel sensor contains biotin recognition groups that form additional crosslinks with avidin via avidin-biotin binding. As the avidin concentration increases, the particle spacing decreases.[4] 9

Figure 2-1. Method for fabricating 2DPC hydrogels. (a−d) First, a hexagonally close-packed PS 2DPC array was prepared on a glass substrate using the steps of our previously

reported needle-tip-flow technique. (e) Polymerizable monomer solution was layered on top of a preformed 2DPC array on a glass slide. A cover slip sealed the solution, (f) after which a free radical polymerization was initiated by UV light. This cross-linked polymer incorporated the ordered 2DPC within the hydrogel network (2DPC hydrogel). 25

Figure 2-2. Debye ring diffraction measurement. A 5 × 5 mm^2 piece of the 2DPC hydrogels was placed parallel to a white screen below. (a) Experimental setup and (b) schematic diagram depicting the diffraction of the 2DPC hydrogel illuminated by 532 nm light from a laser pointer at normal incidence. 28

Figure 2-3. Schematic diagram of the PhPY-sensing hydrogel. The covalent attachment of PhPY changes the hydrogel composition, which causes the hydrogel to swell. The swelling increases the embedded 2DPC particle spacing in proportion to the PhPY concentration. 33

Figure 2-4. (a) SEM image of the hexagonally close-packed 2DPC consisting of PS particles of a diameter of 1.23 μm. (b) SEM image of the non-close-packed 2DPC embedded in the swollen hydrogel. As the hydrogel swelled, the array particle spacing homogeneously increased, maintaining the hexagonal ordering. 35

Figure 2-5. HRMAS 1H NMR spectra of hydrogels (a) before and (b) after sensing PhPY. The new phenyl ring protons at δ = 7.2−7.3 demonstrate the attachment of PhPY to the hydrogel. The residual water signal at δ = 4.7 was suppressed by presaturation. 37

Figure 2-6. (a) Monitoring of the 2DPC particle spacing during PhPY-sensing reactions. p-PDA (100 mM) was employed in each reaction. (b) RPS was calculated and plotted to

normalize the variance in the initial 2DPC particle spacings across the different hydrogel samples. Error bars represent standard deviations (n = 3). 39

Figure 2-7. RPS curves demonstrating chemoselectivity of PhPY sensing. Only when the hydrogels had oxyamine groups and PhPY was present, the RPS increased. Error bars represent standard deviations (n = 3). 41

Figure 2-8. Quantification of PhPY for a detection time of 30 min. To decrease the detection time, the reaction vials were agitated at 500 rpm using a vortex mixer. The RPS at 0.7 mM PhPY had a much larger standard deviation compared to the other data points. The large standard deviation is potentially attributed to the relatively poorly ordered 2DPCs embedded into the corresponding hydrogel samples. The red line shows a linear fit (adjusted R-squared = 0.9968). Error bars represent standard deviations (n = 3). 43

Figure 2-9. Quantification of PhPY in protein-removed human serum (detection time = 30 min). *p*-PDA (500 mM) was employed in each reaction. The red line shows a linear fit (adjusted R-squared = 0.9958). Error bars represent standard deviations (n = 3). . 45

Figure 3-1. Method for fabricating 2DPC hydrogels. (a−e) A polymerizable monomer solution was layered on the top of a preformed 2DPC array on a glass slide. A cover glass sealed the solution, after which polymerization was allowed to proceed for 30 min at room temperature. (f) The resulting crosslinked polymer embedded the ordered 2DPC array monolayer within the hydrogel network (2DPC hydrogel). ... 59

Figure 3-2. SEM images of (a) close-packed 2DPC monolayer and (b) non-close-packed 2DPC monolayer embedded in a hydrogel. 61

Figure 3-3. 2DPC hydrogel particle spacing measurement. A 2DPC hydrogel piece was placed on a stand above a white screen. (a) Experimental setup and (b) schematic diagram showing the Debye ring illuminated by a 532 nm laser. 63

Figure 3-4. (a) Sequences of DNA strands that form adenosineresponsive crosslinks in the hydrogel. (b) Schematic diagram of the adenosine-sensing mechanism using a DNA-crosslinked 2DPC hydrogel. 66

Figure 3-5. Quantification of aptamer−adenosine binding using the PicoGreen assay in different buffer solutions. TNM buffer contains Tris, NaCl, and $MgCl_2$. PicoGreen fluorescence is enhanced more upon binding to dsDNA (hybridized DNA) than to ssDNA. Aptamer−adenosine binding actuates the DNA conformational change from dsDNA to ssDNA. Thus, a decrease in the fluorescence emission upon the addition of adenosine indicates that more aptamer−adenosine binding has occurred. Error bars indicate standard deviations (n = 3). 69

Figure 3-6. Time dependence of 2DPC hydrogel particle spacing on the concentration of adenosine. Error bars indicate standard deviations (n = 3). 71

Figure 3-7. Particle spacing changes' dependence on adenosine concentration in buffer solutions (detection time = 30 min). The X-axis is in a logarithmic scale. The red line shows a linear fit (adjusted R-squared = 0.9874). Error bars indicate standard deviations (n = 3). 73

Figure 3-8. Selectivity of adenosine-sensing 2DPC hydrogels. The 2DPC hydrogel particle spacing was measured in a blank sample containing no nucleosides and in samples containing a 1 mM concentration of adenosine, cytidine, guanosine, or uridine. Each 2DPC hydrogel contained the adenosine-binding aptamer, except for a control

containing no DNA ("hydrogel w/no DNA") and a control containing a mutated aptamer that did not bind adenosine ("hydrogel w/mutated aptamer"). The particle spacing change of each sample was measured after immersion in each solution for 30 min. Error bars indicate standard deviations (n = 3). 74

Figure 3-9. Particle spacing changes' dependence on adenosine concentration in 50% protein-removed FBS (detection time = 30 min). The X-axis is in a logarithmic scale. The red line shows a linear fit (adjusted R-squared = 0.9936). Error bars indicate standard deviations (n = 3). 77

Figure 4-1. (a) Schematic illustration of experimental setup and (b) a photograph of Debye ring. When the 2DPC (hydrogel) is irradiated by a monochromatic light (laser pointer) along the array normal, the diffraction produces a Debye ring on the bottom screen. The 2DPC particle spacing can be calculated by measuring the Debye ring diameter. 91

Figure 4-2. SEM images of (a) the hcp 2DPC on a glass slide, (b) the hcp 2DPC embedded in non-swollen hydrogel, and (c) the non-close-packed 2DPC embedded in swollen hydrogel. Insets: photographs of the corresponding samples showing iridescent colors when they are illuminated by a white flashlight. 96

Figure 4-3. Reversible AD-sensing mechanism using aptamer functionalized 2DPC hydrogels. Upon binding AD, the AD aptamer undergoes a conformational change, which decreases the interparticle spacing of the 2DPC embedded in the hydrogel network. The AD-bound 2DPC hydrogels can be recycled by removing the bound AD with the enzyme ADA. 97

Figure 4-4. Particle spacing changes of different 2DPC hydrogels upon exposure to PBS solutions with and without AD. The mutant DNA does not bind AD. Error bars represent the mean ± standard deviation (*n* = *3*). 99

Figure 4-5. (a) Monitoring of the 2DPC particle spacing change in response to different concentrations of AD. (b) Particle spacing changes' dependence on C_{AD}. The C_{AD} were varied from 0.1 nM to 1 mM. After a fixed AD reaction time of 1 h, each particle spacing change was measured. The inset shows the particle spacing change vs. logC_{AD}. The red line shows a linear fit. Error bars represent the mean ± standard deviation (*n* = 3). 101

Figure 4-6. (a) Selectivity and anti-interference ability of the AD-sensing 2DPC hydrogels. 2DPC hydrogels were reacted with other chemically relevant nucleosides individually (thymidine, guanosine, cytidine, and uridine). The mixture contained AD, thymidine, guanosine, cytidine, and uridine together. After a reaction time of 1 h, each particle spacing change was monitored. (b) Reversible detection of AD. Fresh 2DPC hydrogels were alternately reacted with AD (100 μM) and ADA (1.67 units/mL). After each reaction, the particle spacing was monitored. Error bars represent the mean ± standard deviation (*n* = 3). 104

Figure 4-7. Particle spacing changes' dependence on C_{AD}, measured in tenfold diluted FBS. The *X*-axis has a logarithmic scale. Error bars represent the mean ± standard deviation (*n* = 3)..... 106

Figure 5-1. Proposed mechanisms for (a) L-Phe and (b) L-lactate detection..... 115

Figure 5-2. Proposed thrombin detection mechanism 1..... 117

Figure 5-3. Proposed thrombin detection mechanism 2..... 118

Figure 5-4. Proposed thrombin detection mechanism 3. 119

Figure 5-5. Proposed thrombin detection mechanism 4. 120

Appendix Figure A-1. HRMS spectrum of compound 1. 122

Appendix Figure A-2. HRMS spectrum of compound 3. 123

Appendix Figure A-3. ^{1}H NMR spectrum of compound 1. 124

Appendix Figure A-4. ^{13}C NMR spectrum of compound 1. 125

Appendix Figure A-5. ^{1}H NMR spectrum of compound 2. 126

Appendix Figure A-6. ^{1}H NMR spectrum of compound 3. 127

Appendix Figure A-7. ^{13}C NMR spectrum of compound 3. 128

Appendix Figure B-1. Log ([adenosine]) vs. particle spacing change. A weighted-least square method in OriginLab was used to generate a linear fit of $y = 30.65366x - 8.49099$ (adjusted R-Squared = 0.9746). 130

Appendix Figure C-1. Schematic illustration of 2DPC hydrogel fabrication. 134

Appendix Figure C-2. FTIR spectra of hydrogels before and after the aptamer functionalization reaction. The appearance of a new absorption peak at 1232 cm^{-1}, which derives from the P=O vibration of the DNA phosphate backbone,[2] demonstrates that the aptamer was covalently attached to the hydrogel polymer network. 135

Appendix Figure C-3. Particle spacing changes of various 2DPC hydrogels in response to 10 mM AD in PBS for 1 h. The 2DPC hydrogels were prepared with different (a) C_{AAc}, (b) C_{Bis}, and (c) $C_{Aptamer}$. 137

List of Schemes

Scheme 2-1. Three-Step Sequence for the Preparation of TAC 21

Scheme 2-2. Hydrogel PhPY-Sensing Chemistry..... 31

Scheme 4-1. Reactions used to prepare aptamer functionalized AD-sensing hydrogels..... 94

Preface

I would like to thank my research advisor, Dr. Sanford A. Asher, for the support, encouragement, and patience that he generously provided during my graduate studies at the University of Pittsburgh. I am grateful for his help and for the opportunity to work in the Asher Lab.

I would like to thank all past and present members of the group, David Punihaole, Katie L. Gares, Kyle T. Hufziger, Ryan S. Jakubek, Lily (Tsung-Yu) Wu, Andrew E. Coukouma, Ryan Roppel, Sarah A. Goda, Zhongyu Cai, Sergei V. Bykov, Ivan G. Pallares, Dipak Rout, and Sharon Mansfield, for their help and for their friendship. I am especially grateful for the support of Natasha Smith and James H. Westbay. I also would like to thank all the collaborators, including Dr. W. Seth Horne and Dr. Yuqi Zhang, for many enjoyable hours of work and discussions.

Finally, I would like to express special thanks to my parents, Inok Jang and Jungwhan Lim, and my brother, Wonyoung Jang, for their support. Most of all, I would like to thank my wife Seunghyun Lee and lovely son Green Jang. Thank you for your encouragement and love.

1.0 Introduction

1.1 Two-Dimensional Photonic Crystal Hydrogel Sensors

The Asher group has developed a variety of chemical sensors utilizing two-dimensional photonic crystal (2DPC) hydrogels.[1-12] The 2DPC hydrogel sensors consist of two main components: responsive hydrogels and 2DPC. Hydrogels are crosslinked polymers that can exhibit selective volume phase transitions (VPTs) in response to external stimuli including pH, temperature, light, chemicals, etc.[13-17] The incorporation of 2DPC into the responsive hydrogels enables sensitive monitoring of the hydrogel VPT upon target recognition by measuring the 2DPC light diffraction. Therefore, we measure the target-induced 2DPC light diffraction shifts to report the analyte concentrations. The 2DPC light diffraction measurement only requires a simple laser pointer without the need for sophisticated instruments, ideally positioning the sensing motif for potential use in resource-limited environments. This chapter describes the background theory behind the development of 2DPC hydrogel sensors and provides an overview of the research topics presented in this dissertation.

1.1.1 Stimuli-Responsive Hydrogels and Their Volume Phase Transition Mechanisms

Hydrogels are cross-linked polymers that contain large quantities of water. In response to selective external stimuli, some hydrogels can undergo VPTs, thus acting as smart materials. The external stimuli include pH, temperature, light, small molecules, proteins, etc.[13-17] Depending on the interactions between the hydrogel polymer networks, solvent (water), and stimuli, the

hydrogels may swell or shrink. These stimuli-induced VPTs are very selective and sensitive to the targets. Thus, responsive hydrogels have been of great interest in sensing applications.

Our hypothesis is that we can create chemical sensors by monitoring the hydrogel VPTs. Understanding the mechanisms of the hydrogel VPTs allows the design and fabrication of responsive hydrogels for the selective and sensitive detection of analytes. The VPTs of hydrogels are caused by the changes in the Gibbs free energy within the system, as explained by the Flory-Rehner theory. Flory and Rehner's insights on the thermodynamic properties of polymer network swelling are incorporated into the theory.[18-20]

1.1.1.1 VPTs of non-ionic hydrogels

The VPTs of non-ionic hydrogels were analyzed by the Flory-Rehner swelling equilibrium theory.[19,21] According to the theory, the hydrogel volume change is directly related to the magnitude of the osmotic pressure induced by the Gibbs free energy change. Flory and Rehner discovered that the total Gibbs free energy difference, ΔG_{total} consists of ΔG_{mixing} and $\Delta G_{elastic}$ where ΔG_{mixing} is the change in the free energy of mixing and $\Delta G_{elastic}$ is the change in the elastic free energy.

$$\Delta G_{total} = \Delta G_{mixing} + \Delta G_{elastic} \tag{1-1}$$

The volume derivative of ΔG is equal to the osmotic pressure Π. Thus, the ΔG_{total} generates the osmotic pressures Π_{mixing} and $\Pi_{elastic}$ where Π_{mixing} is the osmotic pressure induced by ΔG_{mixing} and $\Pi_{elastic}$ is the osmotic pressure induced by $\Delta G_{elastic}$. The total osmotic pressure Π_{total} is the sum of the two osmotic pressures Π_{mixing} and $\Pi_{elastic}$.

$$\Pi_{total} = \frac{\partial}{\partial V}(\Delta G_{mixing} + \Delta G_{elastic}) = \Pi_{mixing} + \Pi_{elastic} \tag{1-2}$$

The Flory-Huggins theory explains that ΔG_{mixing} and Π_{mixing} arise from the spontaneous mixing process between the hydrogel polymer chains and the solvent, water.[18,20] When the mixing is spontaneous ($\Delta G_{mixing} < 0$), Π_{mixing} is induced in the hydrogel network, causing the hydrogel to swell. The other components $\Delta G_{elastic}$ and $\Pi_{elastic}$ are derived from the rubber elasticity theory.[22] As the volume of the hydrogel increases due to the spontaneous mixing, the polymer chains lose the conformational entropy, making $\Delta G_{elastic}$ unfavorable ($\Delta G_{elastic} > 0$). This induces the corresponding osmotic pressure $\Pi_{elastic,}$ making the polymer volume resistant to swelling. At equilibrium, these two components are balanced, $\Delta G_{total} = \Pi_{total} = 0$, and the hydrogel maintains its volume. When the hydrogel is not in equilibrium ($\Pi_{total} \neq 0$), the volume of the hydrogel changes until establishing an equilibrium by absorbing or expelling water.[23]

Equations 1-3 and 1-4 further define Π_{mixing} and $\Pi_{elastic}$ by the Flory-Rehner theory, where R is the ideal gas constant, T is the temperature, $\bar{v}_1$ is the molar volume of the solvent, V_0 is the volume of the polymer in the dry state, V is the volume of the polymer in its swollen state, χ is the Flory-Huggins interaction parameter, V_r is the volume of the polymer when initially polymerized, and n_{cr} is the number of crosslinks.[24,25]

$$\Pi_{mixing} = -\frac{RT}{\bar{v}_1}\left[\ln\left(1-\frac{V_0}{V}\right)+\frac{V_0}{V}+\chi\left(\frac{V_0}{V}\right)^2\right] \quad (1\text{-}3)$$

$$\Pi_{elastic} = -\frac{RT}{V_r}n_{cr}\left[\left(\frac{V_r}{V}\right)^{\frac{1}{3}}-\frac{1}{2}\left(\frac{V_r}{V}\right)\right] \quad (1\text{-}4)$$

For the sensor development, we attach specific recognition groups to the hydrogel polymer network.[26] These recognition groups interact with a specific target, resulting in changes in χ or n_{cr}.[4,27] As a result, Π_{total} becomes non-zero and the hydrogel undergoes VPTs. Importantly, the magnitude of the VPTs is proportional to the target concentration. Thus, the target-induced VPTs are monitored and used to report the target concentrations.

1.1.1.2 VPTs of ionic hydrogels

When the hydrogel polymer network contains ionic groups (ionic hydrogels), changes in the ionic free energy ΔG_{ionic} and the corresponding osmotic pressure Π_{ionic} also contribute to ΔG_{total} and Π_{total}, as shown in eqs 1-5 and 1-6.[20]

$$\Delta G_{total} = \Delta G_{mixing} + \Delta G_{elastic} + \Delta G_{ionic} \quad (1\text{-}5)$$

$$\Pi_{total} = \frac{\partial}{\partial V}[\Delta G_{mixing} + \Delta G_{elastic} + \Delta G_{ionic}] = \Pi_{mixing} + \Pi_{elastic} + \Pi_{ionic} \quad (1\text{-}6)$$

Equation 1-7 further describes Π_{ionic} where C_i is the concentration of the mobile ion species i and the superscripts g and s denote the gel (inside of gel) and solution (outside of gel) phases, respectively.

$$\Pi_{ionic} = RT \sum_i \left(c_i^g - c_i^s\right) \quad (1\text{-}7)$$

When the number of mobile ions between the inside and outside of the gel are not in equilibrium, the non-uniform distribution of mobile counterions creates a Donnan potential, leading to the hydrogel VPTs.[28] Thus, hydrogel sensors can be developed by selectively inducing Π_{ionic} in the ionic hydrogels.[1] The ion-induced VPT allows the development of highly sensitive hydrogel sensors in solutions with low ionic strength.[29] However, the VPTs induced by Π_{ionic} are less effective in solutions with high ionic strength because the relative change in the number of ions becomes smaller.

1.1.2 Photonic crystal hydrogel sensing motif

Photonic crystals (PC) are optical nanostructures that are composed of periodic dielectric materials (Figure 1-1).[17,30,31] Due to their ability to control the flow of light, PC have been applied

in many areas, including chemical sensing, light filters, antireflective coatings, waveguiding, etc.[17,32,33]

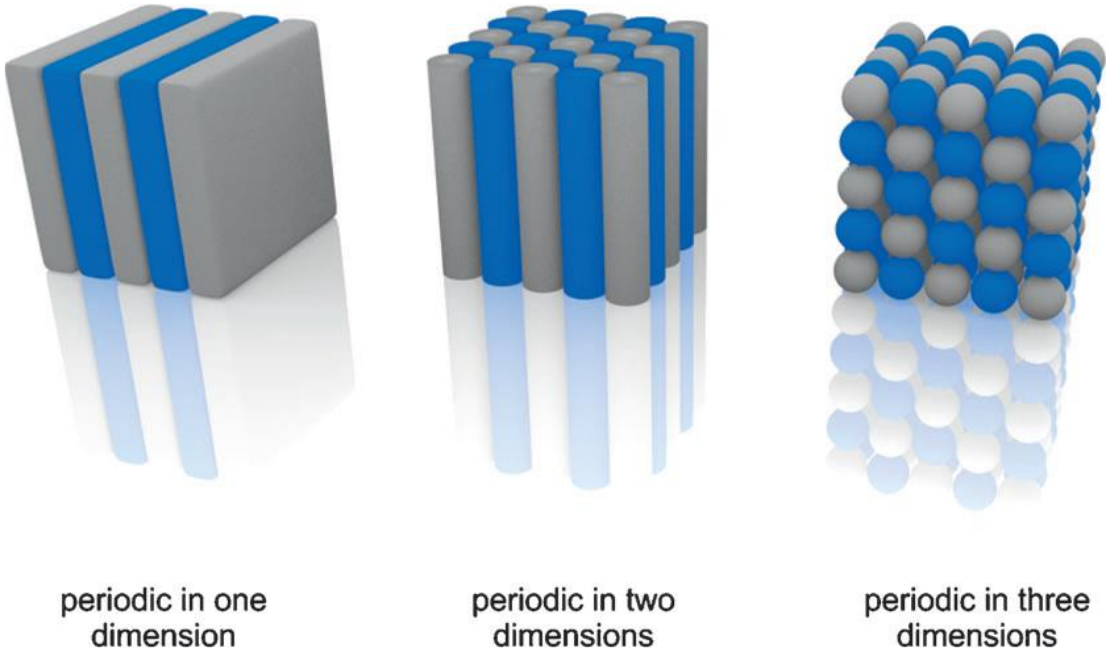

Figure 1-1. Schematic representation of photonic crystals. The periodicity of photonic crystals ranges from one- to three-dimensional.[31]

The Asher group is the first to develop a novel PC hydrogel sensing material called a polymerized crystalline colloidal array (PCCA).[34-36] The PCCA is fabricated by polymerizing a crystalline colloidal array (CCA), a body- or face-centered cubic structure of highly charged colloidal particles (Figure 1-2), into a responsive hydrogel. The responsive hydrogel has molecular recognition groups that interact with the desired target, causing the hydrogel VPTs in proportion to the analyte concentration. The hydrogel VPTs alter the periodicity of the CCA, shifting the diffracted wavelength (Figure 1-3). Thus, the target-induced wavelength shifts are monitored and can be used to report the analyte concentration. Based on this three-dimensional PC hydrogel sensing motif, numerous sensors have been developed to detect stimuli including pH,[24,37]

temperature,[35,38] solvents,[24,37] metal ions,[30,39-42] light,[43,44] gases,[34,45] magnetic field,[46] and small molecules.[29,47-54]

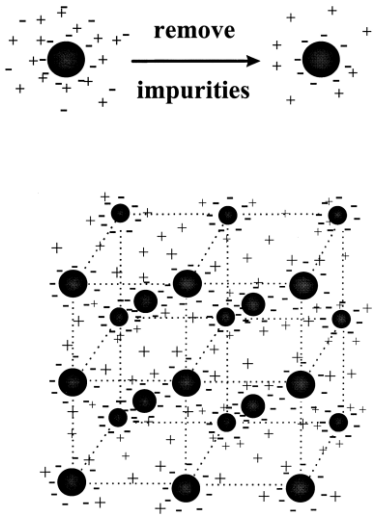

Figure 1-2. CCA with a body-centered cubic structure. Highly charged colloidal particles are self-assembled into the lattice structure due to the electrostatic repulsion.[34]

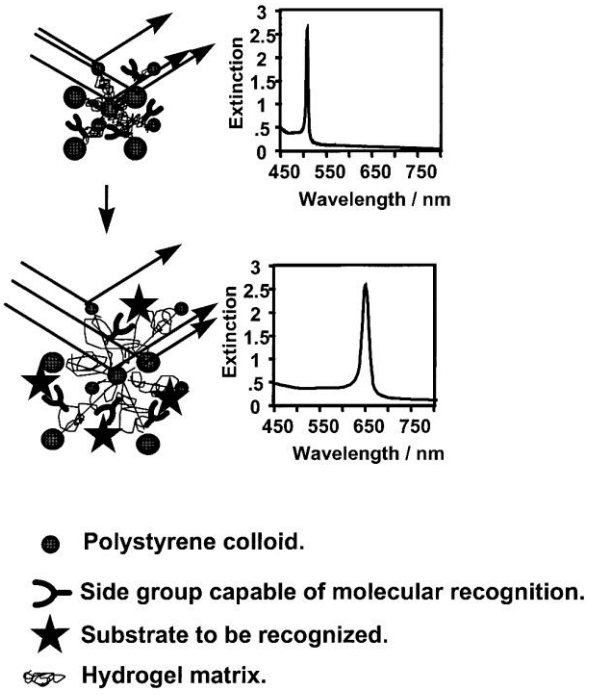

Figure 1-3. The PCCA sensing motif. The CCA diffraction measurement allows for the sensitive monitoring of the shits in the diffracted wavelength, which is used to report the analyte concentration.[34]

The PCCA sensing motif has a limitation in that the CCA is sensitive to the ionic impurities.[34] As the polystyrene particles self-assemble into an ordered lattice due to the electrostatic repulsion, the presence of ionic impurities can disturb the CCA ordering and greatly degrade the CCA diffraction quality. Therefore, any polymerizable monomers with ionic groups cannot be used during the PCCA fabrication. If such groups are required as molecular recognition groups, they need to be attached to the PCCA hydrogel network via post-polymerization modifications that require additional steps. Also, for highly sensitive monitoring, the PCCA sensors need a spectrometer for the diffraction measurement, limiting their potential applications in resource-limited environments.

The Asher group recently reported a new 2DPC hydrogel sensing motif that eliminates the shortcomings of the PCCA sensors.[1,2,55] As an initial fabrication step, a hexagonally-closed-packed 2DPC array is prepared on water, transferred to a glass substrate, and dried (Figure 1-4).[2] The dry 2DPC array is now highly stable on the glass substrate, and the hexagonal ordering is not disturbed by the addition of polymerizable monomer solutions containing ionic groups. This allows the preparation of 2DPC hydrogels even using monomer solutions containing charged species.

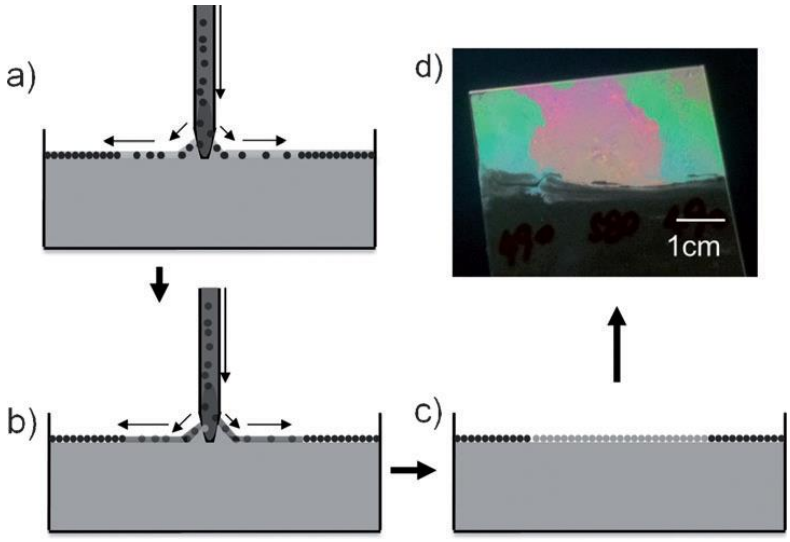

Figure 1-4. Preparation of 2DPC on a glass substrate. (a-b) Inject a solution containing polystyrene particles on water surface to fabricate a hexagonally-closed-packed 2DPC array. (c-d) The 2DPC on water is transferred to a glass substrate and air-dried.[2]

In addition, the 2DPC diffraction measurement requires only a laser pointer without any sophisticated spectrometer. When irradiated by a monochromatic light along the array normal, the 2DPC array forward diffracts light at an angle, producing a Debye ring on the bottom screen (Figure 1-5).[4] By measuring the Debye ring diameter, the 2DPC particle spacing can be calculated and used to determine the analyte concentration (Figure 1-6).[4] Due to its ease of fabrication, low cost, and the potential application in resource-limited setting, the 2DPC hydrogel sensing motif has been widely used to detect pH,[1,2] gases,[7] metal ions,[1] small molecules,[3,11,12,56-59] proteins,[4-6,9,10] microorganisms,[8,60] etc.

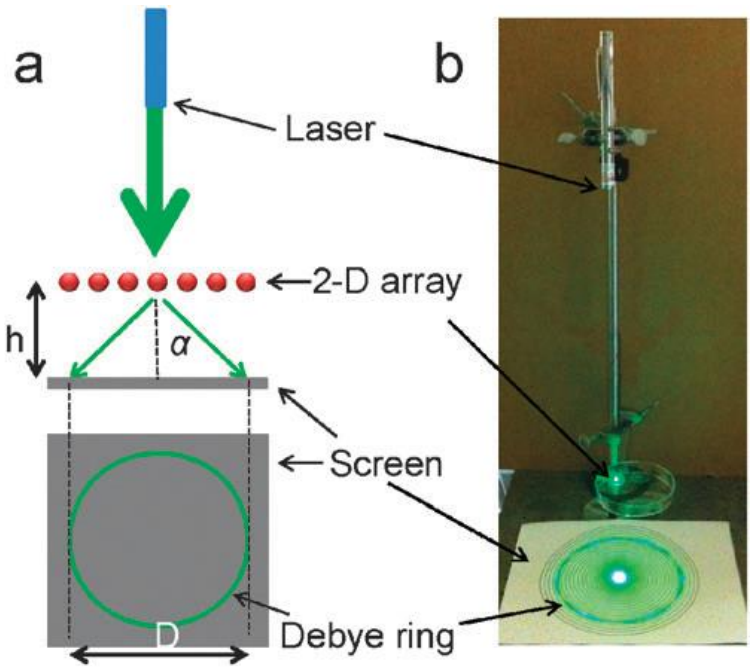

Figure 1-5. (a) Schematic diagram and (b) the experimental setup showing the 2DPC light diffraction. When irradiated by a monochromatic light along the array normal, 2DPC diffracts light at an angle depending on the particle spacing, producing a Debye ring on the bottom screen.[4]

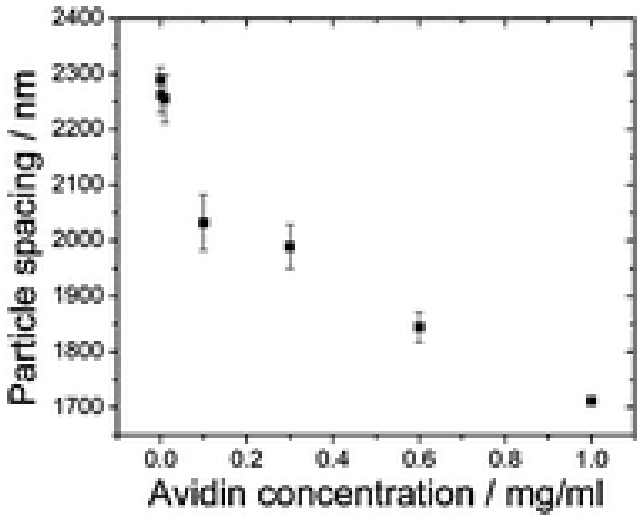

Figure 1-6. Example particle spacing curve reporting the analyte concentration. The 2DPC hydrogel sensor contains biotin recognition groups that form additional crosslinks with avidin via avidin-biotin binding. As the avidin concentration increases, the particle spacing decreases.[4]

1.2 Overview of Research Program

The work reported in this dissertation discusses the advancements in the development of 2DPC hydrogel sensors for biomolecular detection. This 2DPC hydrogel sensing motif requires only a laser pointer and does not require any sophisticated instrumentation or complicated sample preparation. Thus, the hydrogel sensors could potentially be used for resource-limited settings and point-of-care testing.

Chapter 2 describes the development of phenylpyruvate (PhPY)-sensing 2DPC hydrogels. PhPY is the reaction product between phenylalanine and the enzyme phenylalanine dehydrogenase. With the goal of developing phenylalanine sensor for phenylketonuria patients, we first developed the PhPY sensor. The 2DPC hydrogel sensor for PhPY used an oxyamine recognition group to form a chemoselective oxime bond with the carbonyl group of PhPY. The PhPY-induced covalent modification attached additional charged groups to the hydrogel network, resulting in the hydrogel swelling. This in turn increased the 2DPC particle spacing in proportion to the PhPY concentration.

Chapter 3 demonstrates the development of new 2DPC hydrogel sensing motif utilizing the DNA aptamers as molecular recognition groups. Aptamers are short, single-stranded oligonucleotides that bind specific targets with high binding affinities. For this proof-of-concept study, we polymerized the adenosine-binding aptamer into the hydrogel network. The long aptamer strand was partially duplexed with another short DNA strand that was also polymerized in the hydrogel network. In the absence of adenosine, the hybridized DNA strands acted as crosslinks in the hydrogels; however, when adenosine was added, the DNA crosslinks broke as the adenosine-binding aptamer now competitively bound adenosine. This reduced the elastic restoring

force of the hydrogel network, causing the hydrogel to swell. The adenosine-induced particle spacing increases were monitored to report the adenosine concentrations.

Chapter 4 shows another 2DPC hydrogel sensor for the detection of adenosine using a different sensing mechanism. In the hydrogels, the adenosine-binding aptamers were again used as recognition groups. The difference is that now both ends of the DNA strand were covalently attached to the hydrogel network. Upon binding adenosine, the aptamer changed its conformation from an elongated structure to a short hair-pin loop structure. These adenosine-induced aptamer conformational changes induced the hydrogel shrinkage and decreased the 2DPC particle spacing.

Chapter 5 summarizes the research program and describes its future directions.

1.3 References

(1) Zhang, J. T.; Wang, L.; Luo, J.; Tikhonov, A.; Kornienko, N.; Asher, S. A., 2-D Array Photonic Crystal Sensing Motif. *J. Am. Chem. Soc.* **2011,** 133, 9152-9155.

(2) Zhang, J.-T.; Wang, L.; Lamont, D. N.; Velankar, S. S.; Asher, S. A., Fabrication of Large-Area Two-Dimensional Colloidal Crystals. *Angew. Chem. Int. Ed.* **2012,** 51, 6117-6120.

(3) Zhang, J. T.; Smith, N.; Asher, S. A., Two-Dimensional Photonic Crystal Surfactant Detection. *Anal. Chem.* **2012,** 84, 6416-6420.

(4) Zhang, J.-T.; Chao, X.; Liu, X.; Asher, S. A., Two-Dimensional Array Debye Ring Diffraction Protein Recognition Sensing. *Chem. Commun.* **2013,** 49, 6337-6339.

(5) Zhang, J.-T.; Cai, Z.; Kwak, D. H.; Liu, X.; Asher, S. A., Two-Dimensional Photonic Crystal Sensors for Visual Detection of Lectin Concanavalin A. *Anal. Chem.* **2014,** 86, 9036-9041.

(6) Cai, Z.; Zhang, J.-T.; Xue, F.; Hong, Z.; Punihaole, D.; Asher, S. A., 2D Photonic Crystal Protein Hydrogel Coulometer for Sensing Serum Albumin Ligand Binding. *Anal. Chem.* **2014,** 86, 4840-4847.

(7) Smith, N. L.; Hong, Z.; Asher, S. A., Responsive Ionic Liquid-Polymer 2D Photonic Crystal Gas Sensors. *Analyst* **2014,** 139, 6379-6386.

(8) Cai, Z.; Kwak, D. H.; Punihaole, D.; Hong, Z.; Velankar, S. S.; Liu, X.; Asher, S. A., A Photonic Crystal Protein Hydrogel Sensor for *Candida Albicans*. *Angew. Chem. Int. Ed.* **2015,** 54, 13036-13040.

(9) Cai, Z.; Luck, L. A.; Punihaole, D.; Madura, J. D.; Asher, S. A., Photonic Crystal Protein Hydrogel Sensor Materials Enabled by Conformationally Induced Volume Phase Transition. *Chem. Sci.* **2016,** 7, 4557-4562.

(10) Cai, Z.; Sasmal, A.; Liu, X.; Asher, S. A., Responsive Photonic Crystal Carbohydrate Hydrogel Sensor Materials for Selective and Sensitive Lectin Protein Detection. *ACS Sens.* **2017,** 2, 1474-1481.

(11) Jang, K.; Horne, W. S.; Asher, S. A., Human Serum Phenylpyruvate Quantification Using Responsive 2D Photonic Crystal Hydrogels via Chemoselective Oxime Ligation: Progress toward Developing Phenylalanine-Sensing Elements. *ACS Appl. Mater. Interfaces* **2020,** 12, 39612-39619.

(12) Jang, K.; Westbay, J. H.; Asher, S. A., DNA-Crosslinked 2D Photonic Crystal Hydrogels for Detection of Adenosine Actuated by an Adenosine-Binding Aptamer. *ACS Sensors* **2022,** 7, 1648-1656.

(13) Roy, D.; Cambre, J. N.; Sumerlin, B. S., Future Perspectives and Recent Advances in Stimuli-Responsive Materials. *Prog. Polym. Sci.* **2010,** 35, 278-301.

(14) Yetisen, A. K.; Butt, H.; Volpatti, L. R.; Pavlichenko, I.; Humar, M.; Kwok, S. J. J.; Koo, H.; Kim, K. S.; Naydenova, I.; Khademhosseini, A.; Hahn, S. K.; Yun, S. H., Photonic Hydrogel Sensors. *Biotechnol. Adv.* **2016,** 34, 250-271.

(15) Tavakoli, J.; Tang, Y., Hydrogel Based Sensors for Biomedical Applications: An Updated Review. *Polymers* **2017,** 9, 364.

(16) Sun, X.; Agate, S.; Salem, K. S.; Lucia, L.; Pal, L., Hydrogel-Based Sensor Networks: Compositions, Properties, and Applications—A Review. *ACS Appl. Bio Mater.* **2021,** 4, 140-162.

(17) Cai, Z.; Li, Z.; Ravaine, S.; He, M.; Song, Y.; Yin, Y.; Zheng, H.; Teng, J.; Zhang, A., From Colloidal Particles to Photonic Crystals: Advances in Self-Assembly and Their Emerging Applications. *Chem. Soc. Rev.* **2021,** 50, 5898-5951.

(18) Huggins, M. L., Thermodynamic Properties of Solutions of Long-chain Compounds. *Ann. N.Y. Acad. Sci.* **1942,** 43, 1-32.

(19) Flory, P. J.; Rehner Jr, J., Statistical Mechanics of Cross-Linked Polymer Networks I. Rubberlike Elasticity. *J. Chem. Phys.* **1943,** 11, 512-520.

(20) Flory, P. J., *Principles of Polymer Chemistry*. Cornell University Press: **1953**.

(21) Hiemenz, P. C.; Lodge, T. P., *Polymer Chemistry*. CRC press: **2007**.

(22) Flory, P. J.; Rehner Jr, J., Statistical Mechanics of Cross-Linked Polymer Networks I. Rubberlike Elasticity. *J. Chem. Phys.* **1943,** 11, 512-520.

(23) Arndt, K.-F.; Krahl, F.; Richter, S.; Steiner, G., Swelling-Related Processes in Hydrogels. In *Hydrogel Sensors and Actuators: Engineering and Technology*. Springer: **2009,** 69-136.

(24) Xu, X.; Goponenko, A. V.; Asher, S. A., Polymerized PolyHEMA Photonic Crystals: pH and Ethanol Sensor Materials. *J. Am. Chem. Soc.* **2008,** 130, 3113-3119.

(25) Goponenko, A. V.; Asher, S. A., Modeling of Stimulated Hydrogel Volume Changes in Photonic Crystal PB^{2+} Sensing Materials. *J. Am. Chem. Soc.* **2005,** 127, 10753-10759.

(26) Shibayama, M.; Tanaka, T., Volume Phase Transition and Related Phenomena of Polymer Gels. *Adv. Polym. Sci.* **1993,** 109, 1-62.

(27) Zhang, J. T.; Wang, L.; Chao, X.; Asher, S. A., Periodicity-Controlled Two-Dimensional Crystalline Colloidal Arrays. *Langmuir* **2011,** 27, 15230-15235.

(28) Durmaz, S.; Okay, O., Acrylamide/2-Acrylamido-2-Methylpropane Sulfonic Acid Sodium Salt-Based Hydrogels: Synthesis and Characterization. *Polymer* **2000,** 41, 3693-3704.

(29) Walker, J. P.; Asher, S. A., Acetylcholinesterase-Based Organophosphate Nerve Agent Sensing Photonic Crystal. *Anal. Chem.* **2005,** 77, 1596-1600.

(30) Holtz, J. H.; Asher, S. A., Polymerized Colloidal Crystal Hydrogel Films as Intelligent Chemical Sensing Materials. *Nature* **1997,** 389, 829-832.

(31) Fenzl, C.; Hirsch, T.; Wolfbeis, O. S., Photonic Crystals for Chemical Sensing and Biosensing. *Angew. Chem. Int. Ed.* **2014,** 53, 3318-3335.

(32) Tikhonov, A.; Kornienko, N.; Zhang, J.-T.; Wang, L.; Asher, S. A., Reflectivity Enhanced Two-Dimensional Dielectric Particle Array Monolayer Diffraction. *J. Nanophotonics* **2012,** 6, 063509.

(33) Prevo, B. G.; Velev, O. D., Controlled, Rapid Deposition of Structured Coatings from Micro- and Nanoparticle Suspensions. *Langmuir* **2004,** 20, 2099-2107.

(34) Holtz, J. H.; Holtz, J. S. W.; Munro, C. H.; Asher, S. A., Intelligent Polymerized Crystalline Colloidal Arrays: Novel Chemical Sensor Materials. *Anal. Chem.* **1998,** 70, 780-791.

(35) Asher, S. A.; Weissman, J.; Sunkara, H. B.; Pan, G.; Holtz, J.; Liu, L.; Kesavamoorthy, R., Novel Optically Responsive and Diffracting Materials Derived from Crystalline Colloidal Array Self-Assembly. In *Photonic and Optoelectronic Polymers*. American Chemical Society: **1997**, 495-506.

(36) Asher, S.; Sunkara, H.; Weissman, J.; Penn, B.; Frazier, D., Design of Intelligent Mesoscale Periodic Array Structures Utilizing Smart Hydrogel. *Polymer Preprints-America* **1996,** 37, 453-454.

(37) Lee, K.; Asher, S. A., Photonic Crystal Chemical Sensors: pH and Ionic Strength. *J. Am. Chem. Soc.* **2000,** 122, 9534-9537.

(38) Weissman, J. M.; Sunkara, H. B.; Tse, A. S.; Asher, S. A., *Thermally Switchable Periodicities and Diffraction from Novel Mesoscopically Ordered Materials*. DTIC Document: **1996**.

(39) Asher, S. A.; Peteu, S. F.; Reese, C. E.; Lin, M.; Finegold, D., Polymerized Crystalline Colloidal Array Chemical-Sensing Materials for Detection of Lead in Body Fluids. *Anal. Bioanal. Chem.* **2002,** 373, 632-638.

(40) Asher, S. A.; Sharma, A. C.; Goponenko, A. V.; Ward, M. M., Photonic Crystal Aqueous Metal Cation Sensing Materials. *Anal. Chem.* **2003,** 75, 1676-1683.

(41) Reese, C. E.; Asher, S. A., Photonic Crystal Optrode Sensor for Detection of Pb^{2+} in High Ionic Strength Environments. *Anal. Chem.* **2003,** 75, 3915-3918.

(42) Yan, F.; Asher, S., Cation Identity Dependence of Crown Ether Photonic Crystal Pb^{2+} Sensing. *Anal. Bioanal. Chem.* **2007,** 387, 2121-2130.

(43) Kamenjicki, M.; Lednev, I. K.; Mikhonin, A.; Kesavamoorthy, R.; Asher, S. A., Photochemically Controlled Photonic Crystals. *Adv. Funct. Mater.* **2003,** 13, 774-780.

(44) Kamenjicki, M.; Lednev, I. K.; Asher, S. A., Photoresponsive Azobenzene Photonic Crystals. *J. Phys. Chem. B* **2004,** 108, 12637-12639.

(45) Hong, W.; Chen, Y.; Feng, X.; Yan, Y.; Hu, X.; Zhao, B.; Zhang, F.; Zhang, D.; Xu, Z.; Lai, Y., Full-Color CO_2 Gas Sensing by an Inverse Opal Photonic Hydrogel. *Chem. Commun.* **2013,** 49, 8229-8231.

(46) Xu, X.; Friedman, G.; Humfeld, K. D.; Majetich, S. A.; Asher, S. A., Superparamagnetic Photonic Crystals. *Adv. Mater.* **2001,** 13, 1681-1684.

(47) Asher, S. A.; Holtz, J. H., Glucose Sensing Intelligent Polymerized Crystalline Colloidal Arrays. *Polymer* **1993,** 34, 4531.

(48) Alexeev, V. L.; Sharma, A. C.; Goponenko, A. V.; Das, S.; Lednev, I. K.; Wilcox, C. S.; Finegold, D. N.; Asher, S. A., High Ionic Strength Glucose-Sensing Photonic Crystal. *Anal. Chem.* **2003,** 75, 2316-2323.

(49) Asher, S. A.; Alexeev, V. L.; Goponenko, A. V.; Sharma, A. C.; Lednev, I. K.; Wilcox, C. S.; Finegold, D. N., Photonic Crystal Carbohydrate Sensors: Low Ionic Strength Sugar Sensing. *J. Am. Chem. Soc.* **2003,** 125, 3322-3329.

(50) Alexeev, V. L.; Das, S.; Finegold, D. N.; Asher, S. A., Photonic Crystal Glucose-Sensing Material for Noninvasive Monitoring of Glucose in Tear Fluid. *Clin. Chem.* **2004,** 50, 2353-2360.

(51) Sharma, A. C.; Jana, T.; Kesavamoorthy, R.; Shi, L.; Virji, M. A.; Finegold, D. N.; Asher, S. A., A General Photonic Crystal Sensing Motif: Creatinine in Bodily Fluids. *J. Am. Chem. Soc.* **2004,** 126, 2971-2977.

(52) Walker, J. P.; Kimble, K. W.; Asher, S. A., Photonic Crystal Sensor for Organophosphate Nerve Agents Utilizing the Organophosphorus Hydrolase Enzyme. *Anal. Bioanal. Chem.* **2007,** 389, 2115-2124.

(53) Cui, Q.; Ward Muscatello, M. M.; Asher, S. A., Photonic Crystal Borax Competitive Binding Carbohydrate Sensing Motif. *Analyst* **2009,** 134, 875-880.

(54) Ward Muscatello, M. M.; Stunja, L. E.; Asher, S. A., Polymerized Crystalline Colloidal Array Sensing of High Glucose Concentrations. *Anal. Chem.* **2009,** 81, 4978-4986.

(55) Cai, Z.; Smith, N. L.; Zhang, J.-T.; Asher, S. A., Two-Dimensional Photonic Crystal Chemical and Biomolecular Sensors. *Anal. Chem.* **2015,** 87, 5013-5025.

(56) Rizvi, A. S.; Murtaza, G.; Yan, D.; Irfan, M.; Xue, M.; Meng, Z. H.; Qu, F., Development of Molecularly Imprinted 2D Photonic Crystal Hydrogel Sensor for Detection of L-Kynurenine in Human Serum. *Talanta* **2020,** 208, 120403.

(57) Wang, Y.; Xie, T.; Yang, J.; Lei, M.; Fan, J.; Meng, Z.; Xue, M.; Qiu, L.; Qi, F.; Wang, Z., Fast Screening of Antibiotics in Milk Using a Molecularly Imprinted Two-Dimensional Photonic Crystal Hydrogel Sensor. *Anal. Chim. Acta* **2019,** 1070, 97-103.

(58) Qi, F.; Lan, Y.; Meng, Z.; Yan, C.; Li, S.; Xue, M.; Wang, Y.; Qiu, L.; He, X.; Liu, X., Acetylcholinesterase-Functionalized Two-Dimensional Photonic Crystals for the Detection of Organophosphates. *RSC Advances* **2018,** 8, 29385-29391.

(59) Chen, C.; Dong, Z.-Q.; Shen, J.-H.; Chen, H.-W.; Zhu, Y.-H.; Zhu, Z.-G., 2D Photonic Crystal Hydrogel Sensor for Tear Glucose Monitoring. *ACS Omega* **2018,** 3, 3211-3217.

(60) Murtaza, G.; Rizvi, A. S.; Irfan, M.; Yan, D.; Khan, R. U.; Rafique, B.; Xue, M.; Meng, Z. H.; Qu, F., Glycated Albumin Based Photonic Crystal Sensors for Detection of Lipopolysaccharides and Discrimination of Gram-Negative Bacteria. *Anal. Chim. Acta* **2020,** 1117, 1-8.

2.0 Human Serum Phenylpyruvate Quantification Using Responsive 2D Photonic Crystal Hydrogels via Chemoselective Oxime Ligation: Progress toward Developing Phenylalanine-Sensing Elements

This chapter was previously published in the journal *ACS Applied Materials & Interfaces* as Jang, K.; Horne, W. S.; Asher, S. A., Human Serum Phenylpyruvate Quantification Using Responsive 2D Photonic Crystal Hydrogels via Chemoselective Oxime Ligation: Progress toward Developing Phenylalanine-Sensing Elements. *ACS Appl. Mater. Interfaces* **2020**, 12, 39612-39619, and is reprinted with permission. K.J. collected and analyzed the data. This manuscript was prepared by K.J. with the assistance of W.S.H. and S.A.A.

There is a need to develop at-home phenylalanine (Phe) test kits, analogous to home glucose meters, for phenylketonuria patients who must measure their blood Phe levels frequently to adjust their diet. Unfortunately, such test kits are not available yet because of the lack of simple and inexpensive Phe-sensing elements. With the goal of developing a Phe-sensing element, we fabricated two-dimensional photonic crystal (2DPC) hydrogels that quantify human serum phenylpyruvate (PhPY), which is the product of the reaction between Phe and the enzyme phenylalanine dehydrogenase. The PhPY-sensing hydrogels have oxyamine recognition groups that link PhPY to the hydrogel polymer network via chemoselective oxime ligation. This structural modification induces the hydrogel to swell, which then increases interparticle spacings within the embedded 2DPC. The PhPY-induced particle spacing changes are measured from light diffraction and used to quantify the PhPY concentrations. The estimated limit of detection of PhPY in human serum for a detection time of 30 min is 19 μM, which is comparable to the minimum blood Phe concentrations of healthy people. Besides the potential application for developing Phe-sensing

elements, this new hydrogel sensing approach via chemoselective oxime ligation is generalizable to the development of other chemical sensors working in complex biological environments.

2.1 Introduction

Phenylketonuria (PKU) is a rare inborn error of metabolism that is caused by the deficiency of phenylalanine hydroxylase, which metabolizes phenylalanine (Phe) to tyrosine.[1] Untreated PKU patients have abnormally high blood Phe levels that can result in severe neurological disorders as well as symptoms including eczema, microcephaly, and seizures. Few medications, including sapropterin, have been developed to decrease Phe levels, and these are only effective for less than half of those with PKU.[2] The most common treatment for PKU is dietary, which involves the consumption of Phe-free medical formulas and reduced intake of natural protein. The treatment should be continued for life to maintain the blood Phe levels within 120−360 μM.[1] This requires PKU patients to frequently monitor their blood Phe levels and adjust their diet because excessively low Phe levels can also impede normal growth and development.[2]

To measure Phe levels, patients must take blood samples at home and mail these samples to clinics or laboratories or alternatively visit clinics to have blood samples taken. The typical turnaround time is 5−10 days, precluding real-time diet adjustment based on current conditions. Thus, there is a need to develop at-home Phe test kits analogous to home glucose meters because PKU patients would highly benefit from frequent feedback on their blood Phe levels as such data enable real-time diet adjustment.[2,3] Unfortunately, such test kits are not available yet.

Currently, three main clinical methods are used to measure blood Phe levels:[2] the Guthrie bacterial inhibition assay,[4] fluorometric analysis,[5,6] and tandem mass spectrometry.[7,8] Various

laboratory techniques have also been developed to detect blood Phe utilizing high-performance liquid chromatography,[9,10] colorimetric assays,[11−13] electrochemistry,[14,15] chemiluminescence,[16,17] etc. None of these techniques has yet been successfully applied to develop at-home Phe test kits, largely because of the lack of simple and inexpensive Phe-sensing elements that can function in blood without the need for sophisticated instruments or trained personnel.

With the goal of developing a Phe-sensing element, we fabricated two-dimensional photonic crystal (2DPC) hydrogels capable of chemoselectively detecting phenylpyruvate (PhPY), which is the product of the reaction between Phe and the enzyme phenylalanine dehydrogenase (PheDH). The responsive 2DPC hydrogels, made of inexpensive materials, contain oxyamine functional groups that serve as molecular recognition agents. These hydrogel oxyamines chemoselectively react with the ketone in PhPY and covalently link PhPY to the hydrogel. This hydrogel structural modification gives rise to osmotic pressures, which cause hydrogel volume increases in response to increased concentrations of PhPY. The PhPY-induced volume changes are measured by light diffraction from the embedded 2DPCs, providing simple visible readouts that are used to quantify PhPY concentrations. The estimated limit of detection (LoD) of PhPY in human serum for a detection time of 30 min is 19 μM, which is comparable to the minimum blood Phe concentrations of healthy people. This proof-of-concept study demonstrates the capability of PhPY quantification in human serum via oxime formation which is widely used for bioconjugation applications.[18]

Although requiring further studies, our hypothesis is that the PhPY-sensing materials developed here could be applied to develop Phe-sensing elements by coupling with the enzyme PheDH. Prior studies have shown that the enzyme converts Phe to PhPY in whole blood and the concentrations of enzymatically produced PhPY are proportional to the Phe concentrations.[19,20]

Thus, our PhPY-sensing hydrogels will be tested to quantify enzymatically produced PhPY to determine the concentration of Phe. These enzyme-coupled Phe-sensing elements could be utilized to develop at-home Phe test kits more inexpensively and efficiently than with existing Phe-sensing elements. The new hydrogel sensing approach via chemoselective oxime ligation appears generalizable and can be used to develop other chemical sensors, including those for a wide range of biomedically relevant targets.

2.2 Experimental

2.2.1 Materials

Acrylamide (AAm), acrylic acid (AAc), 2-hydroxy-4′-(2-hydroxyethoxy)-2-methylpropiophenone (Irgacure 2959), *N,N′*-methylenebisacrylamide (MBAAm), 1-propanol, anhydrous dimethylformamide (DMF), *p*-phenylenediamine (p-PDA), sodium phenylpyruvate (NaPhPY), L-phenylalanine (Phe), L-(−)-3-phenyllactic acid (PLA), phenylpropanoic acid (PPA), human serum (from human male AB plasma, U.S. origin, sterile-filtered), and an Amicon Ultra-15 Centrifugal Filter Unit (UFC 900308) were purchased from Sigma-Aldrich. *N*-(2-bromoethyl)phthalimide, 1,8-diazabicyclo[5.4.0]undec-7-ene (DBU), anhydrous acetonitrile (MeCN), hydrazine hydrate, and *N*,*N*-diisopropylethylamine (DIPEA) were purchased from Acros Organics. Hydroxybenzotriazole hydrate (HOBT), 1-ethyl-3-(3-dimethylaminopropyl) carbodiimide hydrochloride (EDC), and N-Boc-hydroxylamine were purchased from Oakwood Products. Ethanol (200 proof) and hydrochloric acid were purchased from Decon Labs, Inc. and Thermo Fisher Scientific, respectively. All chemicals were used as received unless otherwise

specified. AAc was purified by passing it through a glass pipette filled with alumina to remove the inhibitor. Human serum was centrifuged for 60 min at 5000 g in Amicon Ultra-15 Centrifugal Filter Units to filter out serum proteins above 3 kDa. Ultrapure water (18.2 mΩ·cm) obtained from a Milli-Q Reference A+ was used for all experiments.

2.2.2 Characterization Techniques

2.2.2.1 NMR

^{1}H and ^{13}C NMR spectra of the synthesized compounds (**1**−**3**) were recorded on Bruker AVANCE III 400 or 500 MHz spectrometers. Chemical shifts (δ) were reported relative to the residual $CHCl_3$ signal. High-resolution magic-angle spinning (HRMAS) ^{1}H NMR spectra of the hydrogels were recorded on a Bruker AVANCE 600 MHz wide-bore NMR spectrometer, equipped with a HRMAS accessory at a rotation rate of 4200 Hz at 300 K. For NMR spectroscopic studies, the hydrogels were prepared without 2DPCs. These hydrogels were thoroughly washed with Milli-Q water, freeze-dried, and placed in a 4 mm rotor. Approximately 40 μL of D_2O was added to 10 mg of each dry hydrogel. Chemical shifts (δ) were reported relative to the residual H_2O signal.

2.2.2.2 Mass Spectrometry

The high-resolution molecular masses of the synthesized compounds (**1**, **3**) were determined with a Thermo QExactive Instrument utilizing the positive electrospray ionization (ESI) technique at 70 K resolution.

2.2.2.3 Scanning Electron Microscopy

Periodic ordering of the 2DPC was monitored using a field emission scanning electron microscope (Zeiss Sigma 500) with an SE2 detector at an accelerating voltage of 3 kV after sputter-coating (PELCO SC-7, auto sputter coater) the samples with gold for 75 s at 30 mA.

2.2.3 Preparation of tert-Butyl(2-Acrylamidoethoxy)-Carbamate (TAC) via a Three-Step Sequence of Reactions

Synthesis of the TAC monomer (Scheme 2-1) proceeded as follows.

Scheme 2-1. Three-Step Sequence for the Preparation of TAC

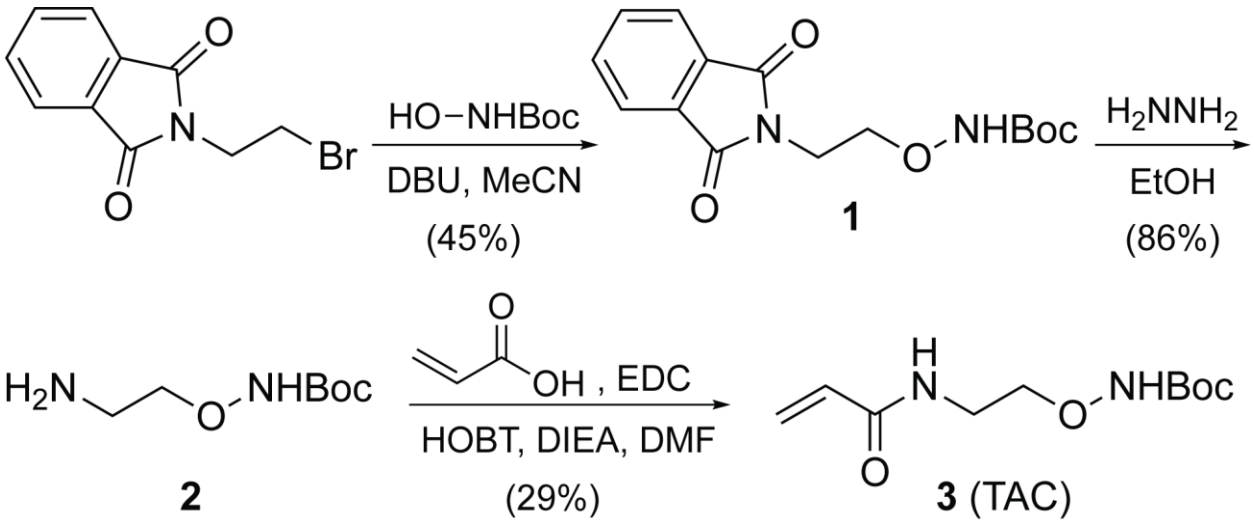

2.2.3.1 Synthesis of 1[21]

N-Boc-hydroxylamine (10.10 g, 75.83 mmol, 1.0 equiv) and DBU (33.98 mL, 227.5 mmol, 3.0 equiv) were dissolved in dry MeCN (50 mL) and stirred for 10 min under N_2. The solution was cooled to 0 °C, and *N*-(2-bromoethyl)phthalimide (38.53 g, 151.7 mmol, 2 equiv) was added. The mixture was stirred for 2 h at 0 °C and 70 h at room temperature. The reaction mixture was diluted with 5% $NaHSO_4$ (30 mL), and the organic phase was extracted with ethyl acetate (EtOAc, 3 × 100 mL). The combined organic phases were brine washed, dried over $MgSO_4$, and concentrated by rotary evaporation. The crude material was purified by column chromatography (silica, hexane/EtOAc = 7:3) to yield product **1** (10.5 g, 34.2 mmol, 45%). R_f = 0.32 (hexane/EtOAc = 7:3). ^{1}H NMR ($CDCl_3$, 500 MHz): δ 1.47 (s, 9H), 4.00 (m, 4H), 7.73 (m, 2H), 7.76 (br, 1H), 7.86 (m, 2H). ^{13}C NMR ($CDCl_3$, 125 MHz): δ 28.4, 36.1, 73.2, 81.8, 123.6, 132.2, 134.3, 156.7, 168.8. HR-ESI-MS m/z: 307.13108 ($[M + H]^+$, calcd for $C_{15}H_{19}O_5N_2$, 307.12885).

2.2.3.2 Synthesis of 2[21,22]

Hydrazine hydrate (4.53 mL, 93.3 mmol, 3 equiv) was added to a solution of **1** (9.54 g, 31.1 mmol, 1 equiv) and 100 mL of ethanol under N_2. The reaction mixture was stirred at 80 °C for 24 h. The solvent was removed by rotary evaporation, and 50 mL of cold dichloromethane was added to the residue. The amine product was extracted from the solid byproduct, phthalhydrazide, by stirring the mixture. The precipitated phthalhydrazide was filtered off, and the residue was washed with 50 mL of cold dichloromethane. Then, the combined filtrate and washings were mixed with 20 mL of saturated K_2CO_3 solution. The product was extracted with dichloromethane, and the organic layer was brine washed, dried over $MgSO_4$, and concentrated. The resulting crude product **2** (4.73 g, 26.8 mmol, 86%) was used without further purification. ^{1}H NMR ($CDCl_3$, 500 MHz): δ 1.48 (s, 9H), 2.99 (t, 2H, J = 9.8 Hz), 3.93 (t, 2H, J = 9.9 Hz).

2.2.3.3 Synthesis of 3 (TAC)[23]

HOBT (0.7758 g, 5.067 mmol, 1.3 equiv) and **2** (4.73 g, 26.8 mmol, 1 equiv) were dissolved in dry DMF (50 mL) at 0 °C under Ar. After 10 min stirring, acrylic acid (2.39 mL, 34.9 mmol, 1.3 equiv) was added and the mixture was stirred for another 10 min. DIPEA (14.0 mL, 80.6 mmol, 3 equiv) was added, and the mixture was stirred for 15 min. EDC (7.72 g, 40.3 mmol, 1.5 equiv) was added, and the reaction mixture was stirred at room temperature for 20 h. The solution was diluted with 100 mL of water and extracted using EtOAc. The organic layer was washed with 5% $NaHSO_4$(aq), 5% $NaHCO_3$(aq), water, and brine in sequence. The solution was dried over $MgSO_4$ and concentrated under reduced pressure. The crude product was purified using column chromatography (silica, hexane/EtOAc = 2:8) to yield product **3** (1.70 g, 7.77 mmol, 29%). ^{1}H NMR ($CDCl_3$, 400 MHz): δ 1.49 (s, 9H), 3.58 (q, 2H, J = 5.2 Hz), 3.91 (t, 2H, J = 4.8 Hz), 5.65 (dd, 1H, J = 10.1, 1.6 Hz), 6.18 (dd, 1H, J = 17.1, 10.2 Hz), 6.31 (dd, 1H, J = 17.0, 1.6 Hz), 7.09 (br, 1H), 7.34 (s, 1H). ^{13}C NMR (CDCl3, 125 MHz): δ 28.3, 37.6, 76.0, 82.5, 126.3, 131.3, 158.0, 165.9. HR-ESI-MS m/z: 231.13476 ($[M + H]^+$, calcd for $C_{10}H_{19}O_4N_2$, 231.13393).

2.2.4 Preparation of 2DPC Hydrogels

First, negatively charged polystyrene (PS) spheres of a diameter of 1.23 μm were synthesized by dispersion polymerization. The detailed procedures were reported by Zhang et al.[24] These PS spheres (3 mL, 16% w/w in water) and 1 mL of 1-propanol were mixed. Then, using our previously reported needle-tip-flow technique (Figure 2-1a,b), a hexagonally close-packed PS 2DPC array was self-assembled on a water surface.[25] The self-assembled 2DPC array was transferred to a glass substrate (24 × 40 mm^2) and air dried (Figure 2-1c,d). Polymerizable monomer solutions were prepared following the composition listed in Table 2-1. The solutions

were deoxygenated by injecting N_2 gas with a needle for 15 min (1 or 2 bubbles per second). After the initiator (8 μL of 33% w/v Irgacure 2959 in dimethyl sulfoxide) was added, the solutions were mildly vortexed for 15 s at 100 rpm. A 96 μL aliquot of the polymerizable solutions was layered on top of the preformed 2DPC array on a glass slide (Figure 2-1e). A cover slip was placed onto the 2DPC array to uniformly spread the polymerization solution. The free radical polymerization was then initiated by irradiating 365 nm UV light from a UVP Compact and Handheld UV Lamp (UVGL-55) for 15 min at room temperature (Figure 2-1f). The resulting cross-linked polymer chains incorporated the hexagonally ordered 2DPC array within the hydrogel network. Finally, the polymerized 2DPC hydrogel was peeled from the glass substrates and thoroughly washed with a phosphate-buffered saline solution (pH 7.2).

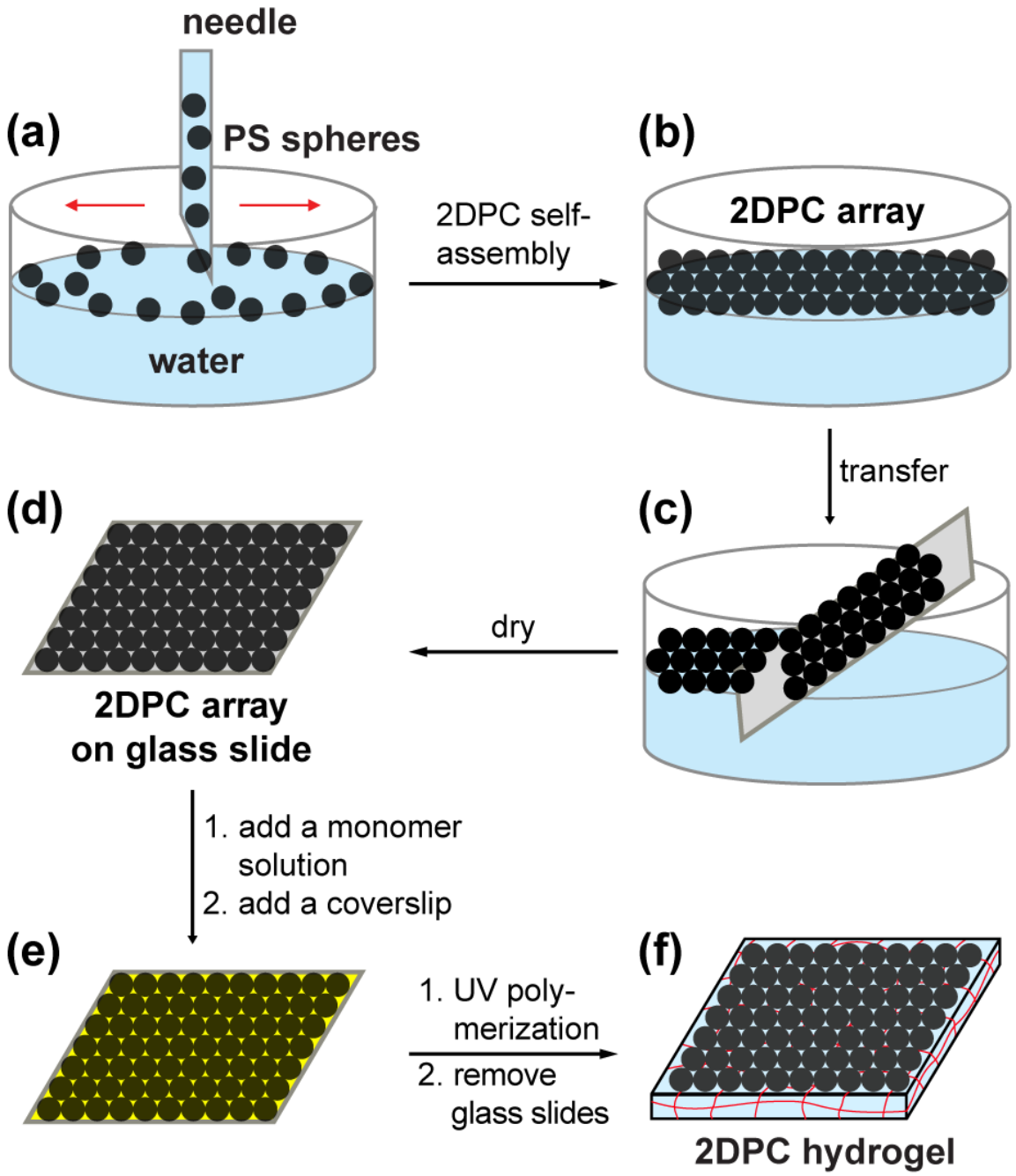

Figure 2-1. Method for fabricating 2DPC hydrogels. (a−d) First, a hexagonally close-packed PS 2DPC array was prepared on a glass substrate using the steps of our previously reported needle-tip-flow technique. (e) Polymerizable monomer solution was layered on top of a preformed 2DPC array on a glass slide. A cover slip sealed the solution, (f) after which a free radical polymerization was initiated by UV light. This cross-linked polymer incorporated the ordered 2DPC within the hydrogel network (2DPC hydrogel).

Table 2-1. Composition of monomer solutions used in the preparation of hydrogel samples

component	% (w/w)	mass (mg)
AAm	8	32
TAC	10	40
AAc	2	8
MBAAm	0.5	2
PG	45	180
H_2O	34.5	138
total	100	400

2.2.5 Hydrogel Boc Deprotection

After preparation of 2DPC hydrogels as described above, the Boc protecting groups in the polymer networks were removed by treatment with HCl. The as-prepared hydrogel was immersed in 12 mL of 1 M HCl and allowed to stand for 10 min. The HCl concentration was increased and decreased in increments to minimize osmotic shock to the hydrogel samples. The sequence of reagents added to the reaction were as follows: (1) 3 mL of 12 M HCl (final concentration 3 M HCl), (2) 5 mL of 12 M HCl (final concentration 5 M HCl), (3) 16 mL of water (final concentration 3 M HCl), and (4) 72 mL of water (final concentration 1 M HCl). The reaction was allowed to stand for 10 min after each addition. After the above sequence of steps, Boc-deprotected hydrogels were soaked in 100 mM acetate buffer (pH 5.5) overnight, cut into 5 × 5 mm^2 pieces with a razor blade, and stored in 100 mM acetate buffer (pH 5.5). The thickness of PhPY sense-ready hydrogels was estimated to be 145 μm.

2.2.6 2DPC Particle Spacing Measurements

PhPY-induced hydrogel volume changes were monitored by measuring the 2DPC particle spacing, d, from the Debye diffraction ring diameters (Figure 2-2).[26] Hexagonally ordered 2DPCs diffract light according to the Bragg diffraction condition of eq 2-1, where m is the diffraction order, λ is the wavelength of the incident light, d is the spacing between each particle of the 2DPC, α is the incident angle of the light, and β is the diffracted angle of the light.

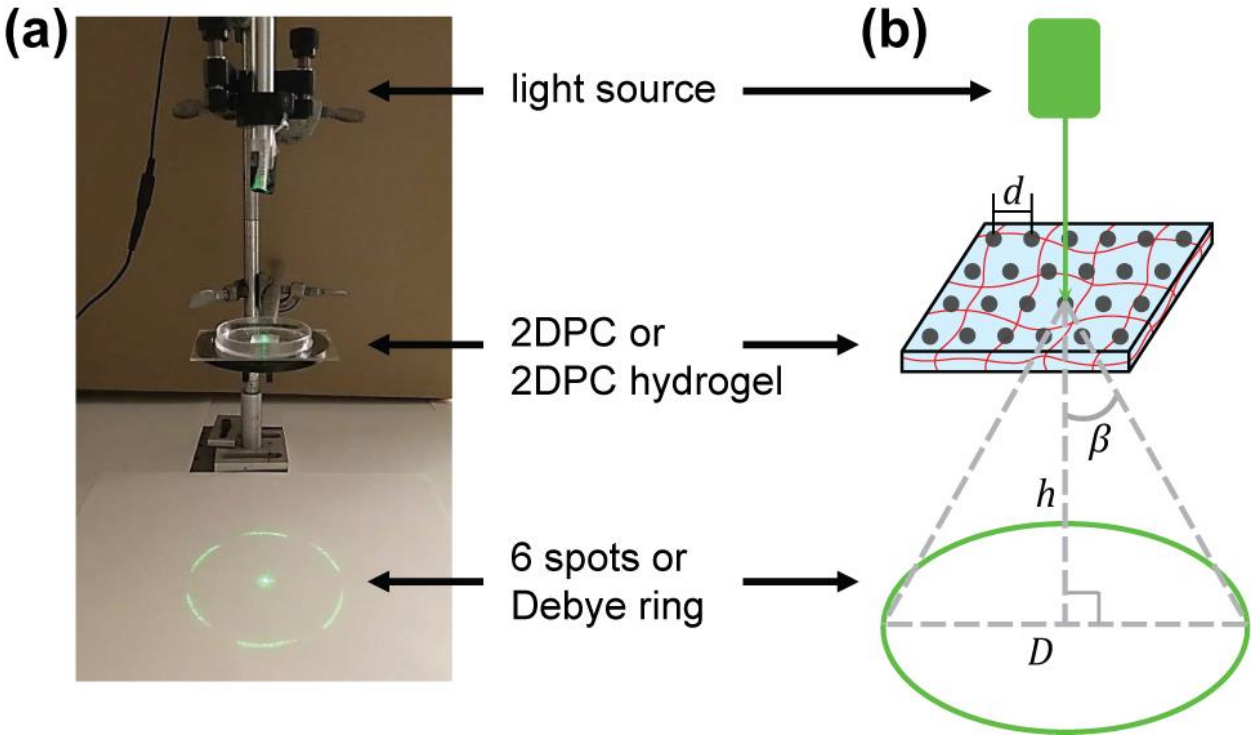

Figure 2-2. Debye ring diffraction measurement. A 5 × 5 mm^2 piece of the 2DPC hydrogels was placed parallel to a white screen below. (a) Experimental setup and (b) schematic diagram depicting the diffraction of the 2DPC hydrogel illuminated by 532 nm light from a laser pointer at normal incidence.

$$m\lambda = \frac{\sqrt{3}}{2} d(\sin\alpha + \sin\beta) \quad (2\text{-}1)$$

When 2DPCs or 2DPC hydrogels are irradiated using a 532 nm green laser pointer along the array normal (α = 0°), eq 2-1 reduces to

$$d = \frac{2(532\ \text{nm})}{\sqrt{3}\sin\beta} \quad (2\text{-}2)$$

For a perfectly ordered 2DPC, the light is strongly forward-diffracted at an angle β, producing six bright diffraction spots.[27] In our case where the sample is microcrystalline, consisting of numerous small rotationally disordered crystals, the diffraction formed a Debye ring on the screen below (Figure 2-2a). Equation 2-3 relates D, h, and β, where D is the diameter of the Debye ring and h is the distance between the 2DPC plane and the bottom white paper (Figure 2-2b).

$$\beta = \tan^{-1}\frac{D}{2h} \quad (2\text{-}3)$$

Combining eqs 2-2 and 2-3 gives eq 2-4.

$$d = \frac{2(532\ \text{nm})}{\sqrt{3}\sin(\tan^{-1}\frac{D}{2h})} \quad (2\text{-}4)$$

h is typically fixed at 15 cm. Thus, the particle spacing d was calculated by measuring only D. To determine d of each sample, we measured nine different D's from three different positions within the same hydrogel sample and averaged them.

2.2.7 PhPY-Sensing in Buffer Solutions

For each reaction, a 5 × 5 mm^2 hydrogel was placed in a 10 mL solution of 100 mM acetate buffer (pH 5.5) containing 100 mM *p*-PDA. The hydrogel was equilibrated in the solution for 10 min, and the initial particle spacing was measured. A small aliquot of 100 mM of NaPhPY solution was added to initiate the PhPY-sensing reaction. For the first set of samples, the 2DPC particle

spacings were measured every 5 min for 1 h. For the second set of samples, the reaction vials were mounted in a vortex mixer and agitated at 500 rpm. After the PhPY reaction proceeded for 30 min, the 2DPC particle spacings were measured again.

2.2.8 PhPY Sensing in Human Serum

The hydrogels (5 × 5 mm^2 pieces) were washed with 10 mM of acetate buffer solutions (pH 5.7) overnight. After the particle spacings were measured, each hydrogel was transferred to 10 mL of protein-removed human serum containing 500 mM *p*-PDA (pH 5.2, HCl was added to adjust the pH). A small aliquot of 100 mM of NaPhPY solution was added to each serum solution. The reaction vials were mounted in a vortex mixer and agitated at 500 rpm. After the PhPY reaction proceeded for 30 min, the hydrogels were thoroughly washed with 10 mM acetate buffer (pH 5.7) for 30 min, replacing the washing buffer every 10 min. Then, the 2DPC particle spacings were measured again.

2.3 Results and Discussion

2.3.1 PhPY-Sensing Motif Using Responsive Hydrogels Containing 2DPC and Oxyamine Recognition Groups

Scheme 2-2 shows the hydrogel network and its PhPY-sensing chemistry. The copolymer structures shown are simplified representations of cross-linked networks. During polymerization, the newly synthesized monomer TAC was Boc-protected to mask the oxyamine nucleophilicity

that could cause unwanted side reactions. Post-polymerization deprotection removed the Boc groups and released the free oxyamine groups, serving as PhPY recognition agents. Additionally, AAc and AAm monomers were copolymerized with TAC to increase the hydrophilicity of the resulting hydrogels.

Scheme 2-2. Hydrogel PhPY-Sensing Chemistry

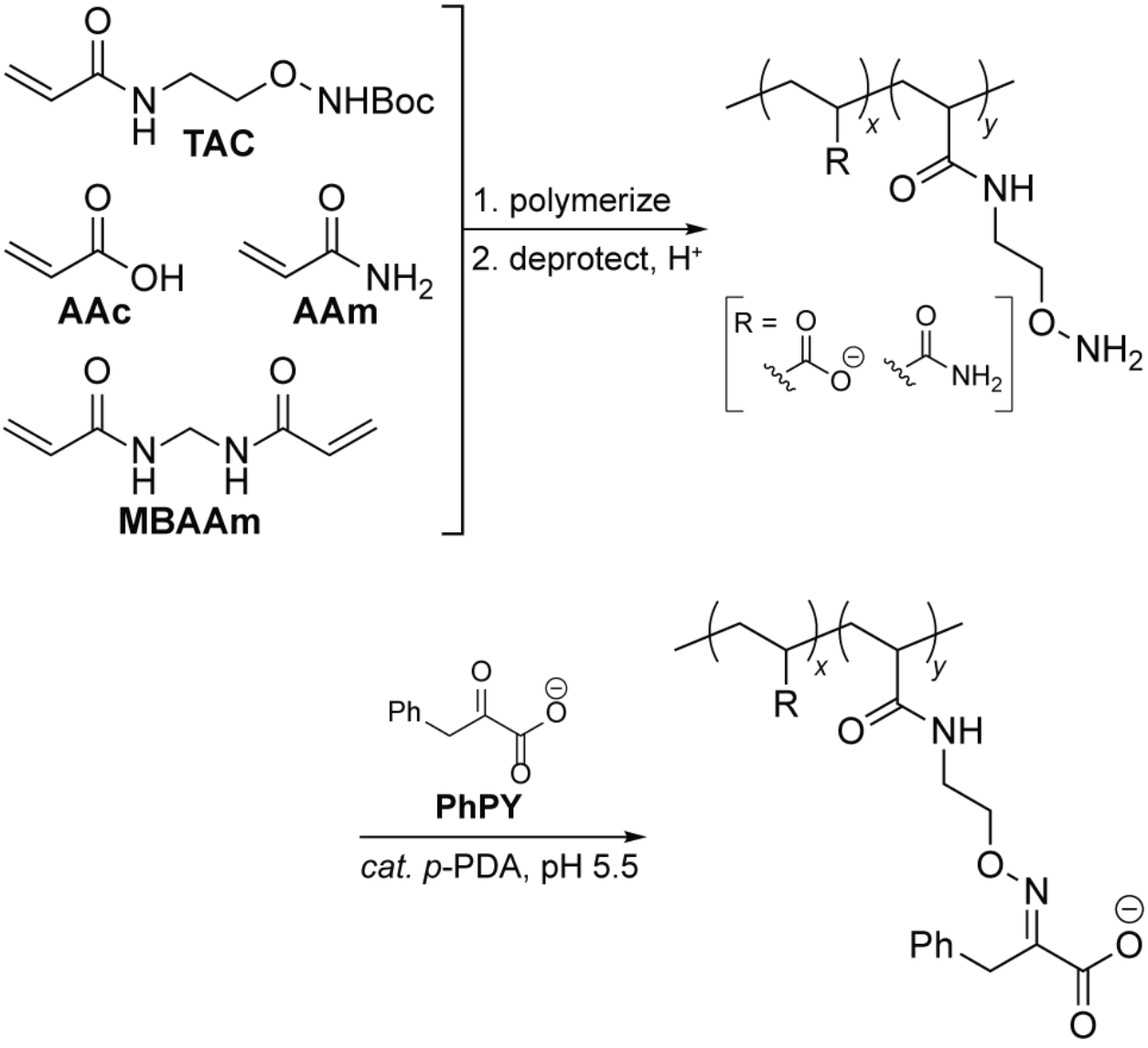

Our design of the sensor was based on the hypothesis that the formation of oxime bonds between the PhPY carbonyl groups and the hydrogel oxyamine groups would serve as the basis for PhPY sensing. We employed the catalyst *p*-PDA to increase the oxime reaction rate in order to reduce the PhPY detection time. While oxime ligation is slow between pH 5 and 7 without a catalyst,[28,29] *p*-PDA increases the reaction rates 50- to 120-fold.[30–32]

The covalent attachment of PhPY changes the hydrogel composition, which causes the hydrogel volume to swell (Figure 2-3). The addition of PhPY carboxylates makes the hydrogel more hydrophilic and also localizes counterions. These characteristics generate a reaction-induced osmotic pressure, Π, in the hydrogel. The resulting change in Π causes the hydrogel volume to increase until the system reaches an equilibrium, where the osmotic pressure is uniform in both the hydrogel and the surrounding solution reservoir.[33,34] Furthermore, the hydrogel swelling increases the embedded 2DPC particle spacing, which is directly proportional to the PhPY concentration.

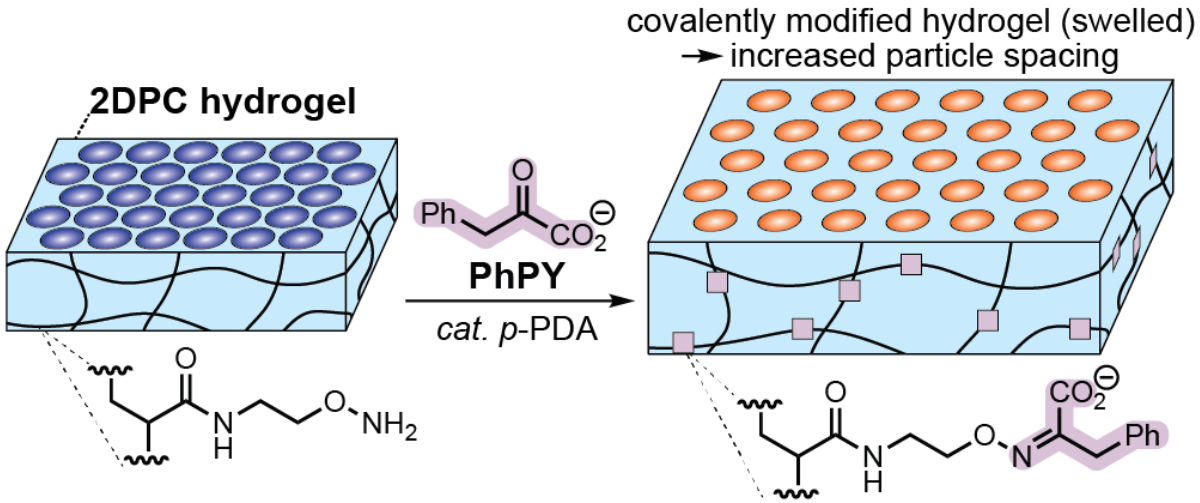

Figure 2-3. Schematic diagram of the PhPY-sensing hydrogel. The covalent attachment of PhPY changes the hydrogel composition, which causes the hydrogel to swell. The swelling increases the embedded 2DPC particle spacing in proportion to the PhPY concentration.

2.3.2 Characterizations of PhPY-Sensing Hydrogels

Figure 2-4a shows a scanning electron microscopy (SEM) image of the hexagonally close-packed PS 2DPC, which diffracts light according to the Bragg diffraction condition. The subsequent polymerization incorporated the 2DPC into the newly formed cross-linked polymer network. As the hydrogel swelled, the spacing of the embedded particles increased homogeneously, and the PS particles formed a non-close-packed 2DPC (Figure 2-4b). The hexagonal ordering of the embedded array was retained, which enabled the sensitive monitoring of the hydrogel volume change by measuring the 2DPC light diffraction. To prevent the non-close-packed particles from collapsing during the drying process, swollen 2DPC hydrogels were sandwiched between two glass substrates and dried in a desiccator before being sputter-coated.

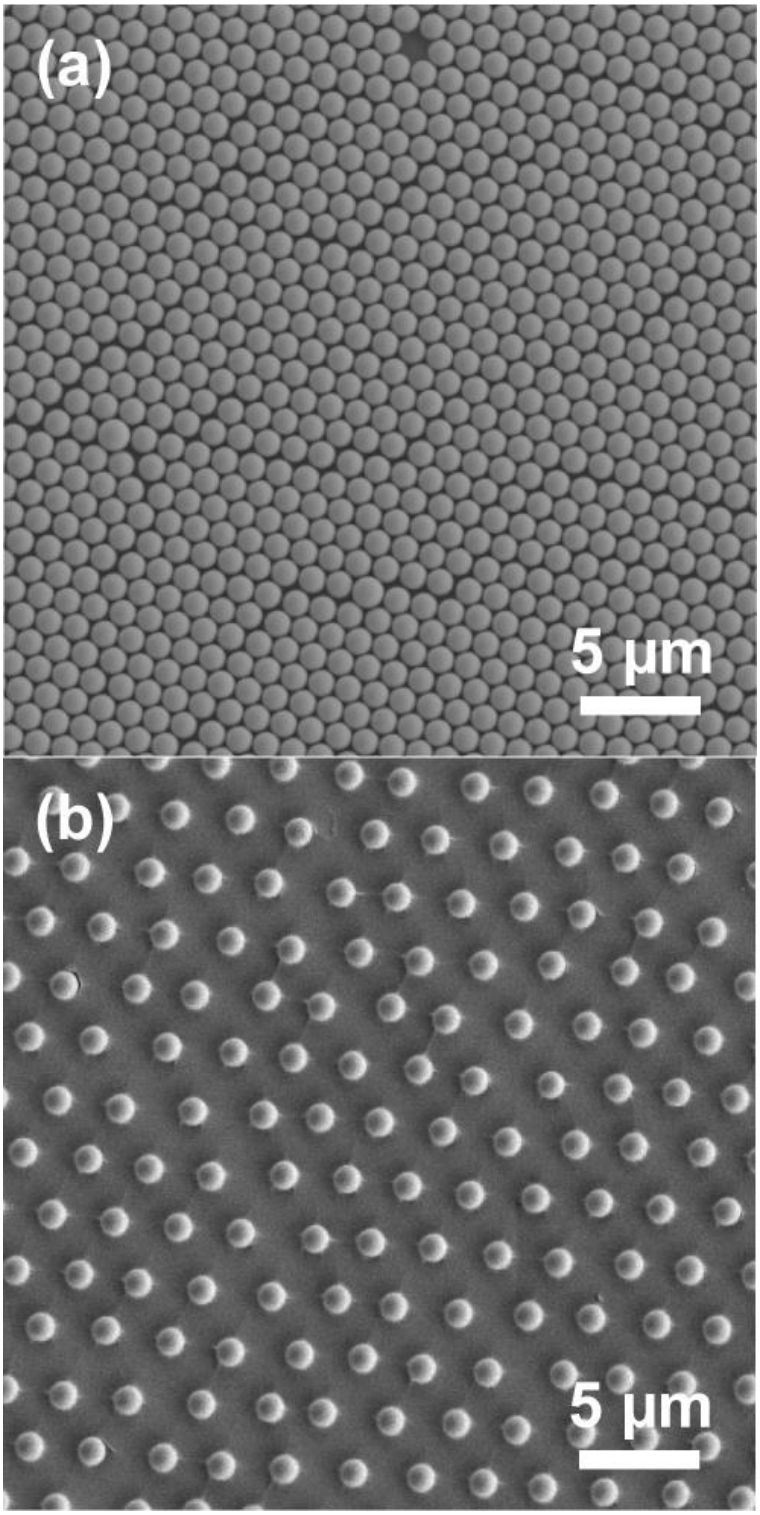

Figure 2-4. (a) SEM image of the hexagonally close-packed 2DPC consisting of PS particles of a diameter of 1.23 μm. (b) SEM image of the non-close-packed 2DPC embedded in the swollen hydrogel. As the hydrogel swelled, the array particle spacing homogeneously increased, maintaining the hexagonal ordering.

NMR spectroscopy was used to characterize the PhPY-sensing hydrogels. Because of the reduced mobility of the individual backbone chains in the cross-linked polymer network, solution NMR spectra of most hydrogels show significant line broadening.[35,36] To improve the spectral resolution, a smaller amount (0.1% w/w) of the cross-linker (MBAAm) was used to prepare the hydrogels, and the magic-angle spinning (MAS) technique was employed.[37,38]

Figure 2-5a shows the water-suppressed ^{1}H NMR spectrum of the hydrogel before treatment with PhPY. The two sets of signals around $\delta = 1.56$ and 2.11 ppm correspond to the polymer backbone CH_2 and CH groups, respectively. The other two sets of signals around $\delta = 3.34$ and 3.73 ppm correspond to the side-chain CH_2 groups of TAC monomers. Before sensing PhPY, no proton peaks were observed at $\delta > 4$ ppm (except the residual water signal). However, after sensing PhPY, new peaks were observed at $\delta = 7.2-7.3$ ppm (Figure 2-5b), which correspond to the phenyl ring groups of the attached PhPY. The integrated areas of the phenyl protons at $\delta = 7.2$ ppm and the polymer backbone protons at $\delta = 1.54$ and 2.12 ppm roughly correspond to the hydrogel monomer composition. The NMR data obtained clearly demonstrate the covalent attachment of PhPY to the hydrogels.

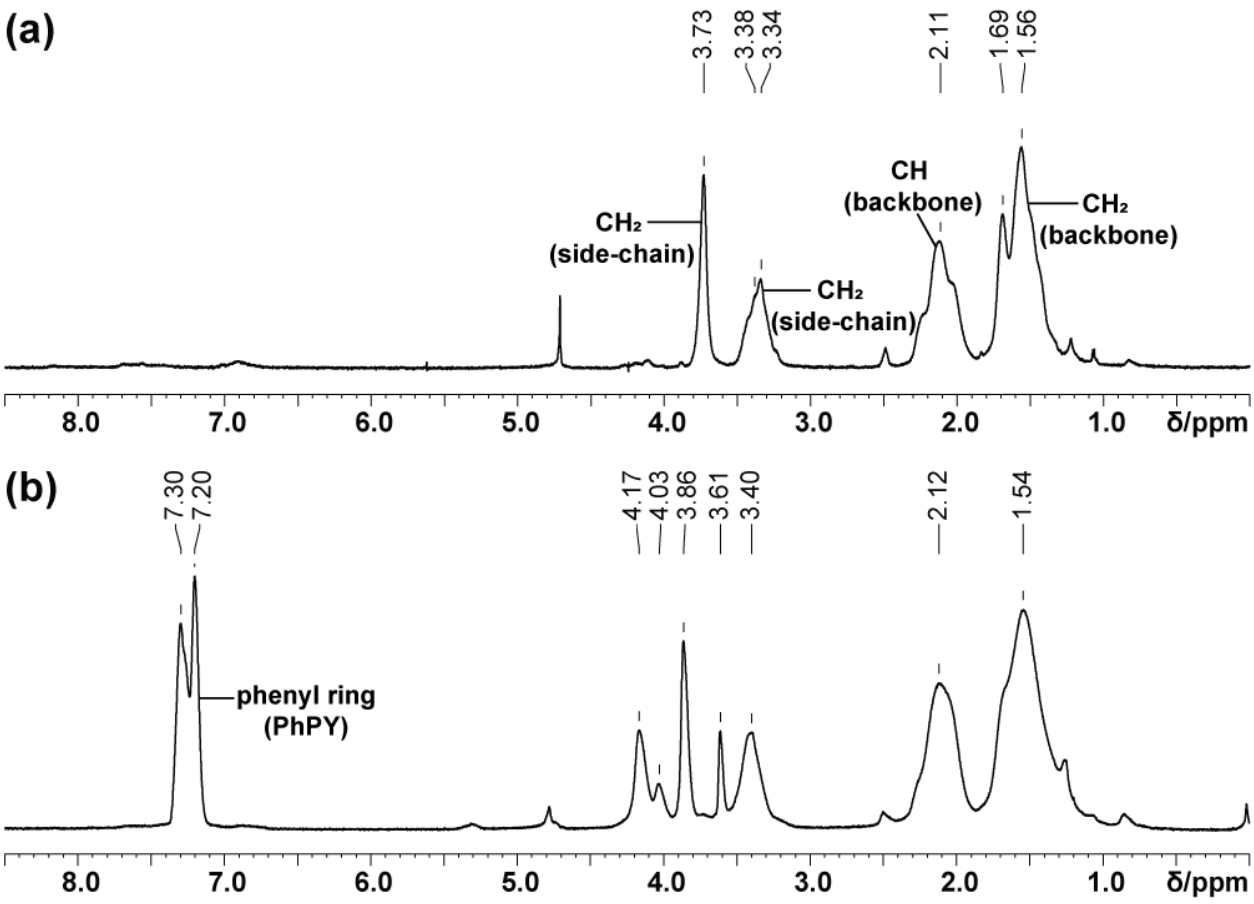

Figure 2-5. HRMAS 1H NMR spectra of hydrogels (a) before and (b) after sensing PhPY. The new phenyl ring protons at δ = 7.2−7.3 demonstrate the attachment of PhPY to the hydrogel. The residual water signal at δ = 4.7 was suppressed by presaturation.

2.3.3 PhPY Recognitions in Buffer Solutions

The PhPY-induced hydrogel swelling was monitored by measuring the embedded 2DPC particle spacings. First, each 5 × 5 mm^2 piece of the hydrogel was placed in a solution of acetate buffer (pH 5.5) containing 100 mM of *p*-PDA, and the initial particle spacing was measured. The average was 1740 nm (Figure 2-6a where time = 0 min), which is a 45% increase over the individual PS sphere diameter of 1.23 μm. This means that the hydrogel volumes were already swollen even before detecting PhPY, which is attributed to the presence of hydrophilic monomers. These PhPY-sensing hydrogels were mechanically robust and easy to handle.

Next, a different aliquot of 100 mM of NaPhPY solution was added to each hydrogel sample to initiate the PhPY-sensing reaction, and the particle spacing was measured every 5 min (Figure 2-6a). The hydrogels underwent larger particle spacing increases (or volume swellings) with faster reaction rates at higher PhPY concentrations. For example, 5 mM PhPY increased the particle spacing by 260 nm in 30 min, while 1 mM PhPY increased the particle spacing by only 110 nm in 1 h. The reason for this difference is that the magnitude of the swelling is proportional to the analyte concentration because the higher the PhPY concentration, the more PhPY molecules are attached to the hydrogels, generating a higher Π. In addition, the PhPY molecules are more likely to diffuse into the hydrogel network at higher PhPY concentrations, resulting in faster reaction rates. If no PhPY was present (0 mM), the particle spacings remained constant, showing that the hydrogel volume swellings were induced by the PhPY reactions.

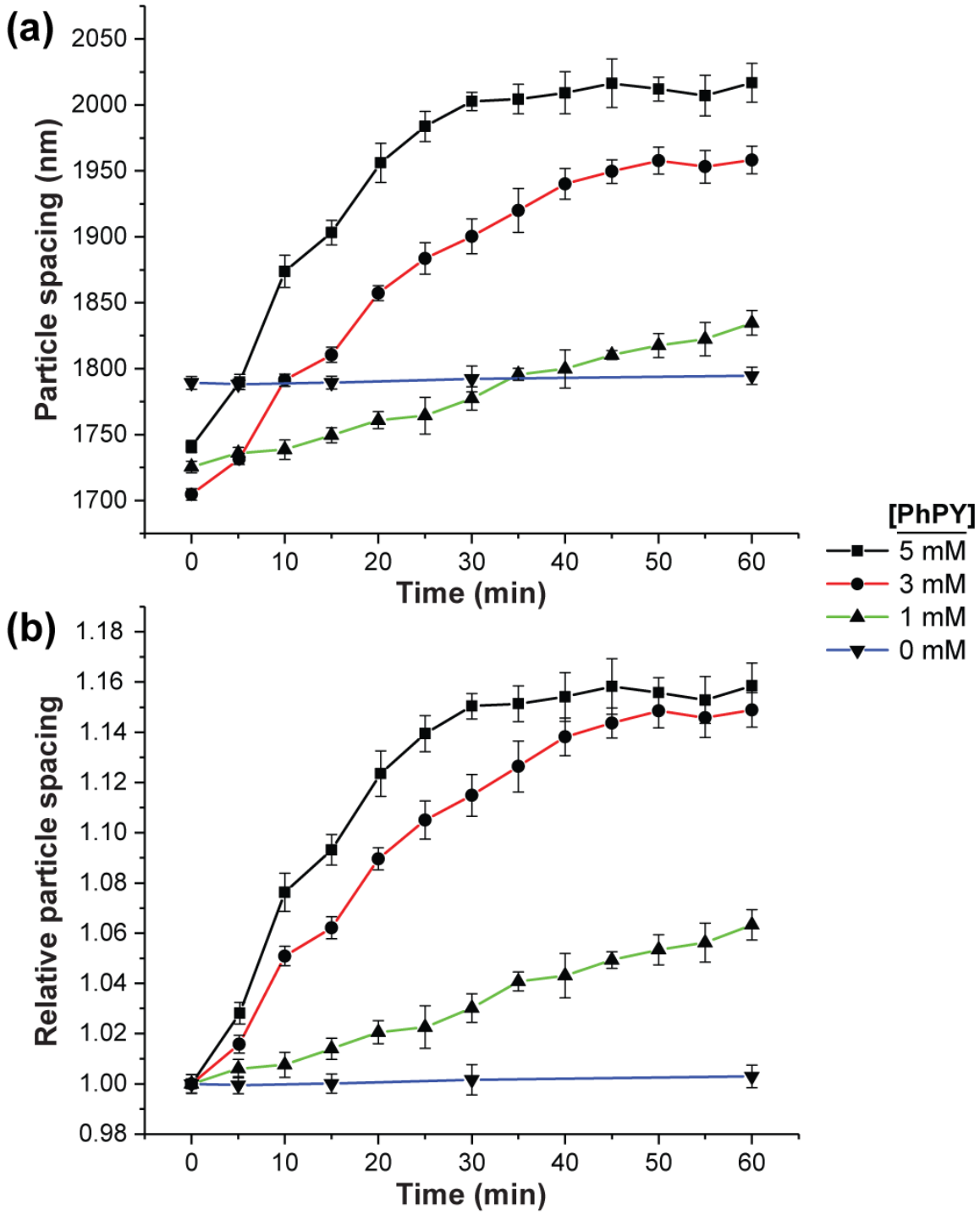

Figure 2-6. (a) Monitoring of the 2DPC particle spacing during PhPY-sensing reactions. p-PDA (100 mM) was employed in each reaction. (b) RPS was calculated and plotted to normalize the variance in the initial 2DPC particle spacings across the different hydrogel samples. Error bars represent standard deviations (n = 3).

Although the relative standard deviation is only 2%, the initial particle spacings varied across the different hydrogel samples, which makes it more difficult to analyze the data. To circumvent this issue, the individual particle spacing curve was scaled, and the relative particle spacing (RPS) curves were plotted instead (Figure 2-6b). For instance, all of the particle spacing data points in the 5 mM PhPY curve of Figure 2-6a were divided by the curve initial particle spacing, 1741 nm. The relative standard deviation of each data point was also calculated following the propagation of uncertainty. Then, the initial RPS value, where time = 0 min, always becomes 1, and the remaining data points show their relative changes compared with the initial point. The other particle spacing curves were calculated in the same way. As a result, all of the RPS curves have the same initial value, which enables the different curves from various samples to be compared without bias. Thus, only RPS curves, calculated from the raw particle spacing curves, are discussed in the following results.

Figure 2-7 shows data supporting the chemoselectivity of the PhPY-sensing reaction. While PhPY induced a significant RPS increase, changes were negligible when testing close structural analogues: Phe, PLA, and PPA. This shows that the ketone group is vital and supports the hypothesis that the formation of an oxime with the hydrogel gives rise to the observed swelling. As an additional control, hydrogels lacking oxyamine groups were prepared by replacing TAC monomers with AAm. The RPS of these nonfunctional hydrogels did not increase after the incubation in PhPY. Thus, only when the hydrogels had oxyamine groups and PhPY was present, the RPS increased.

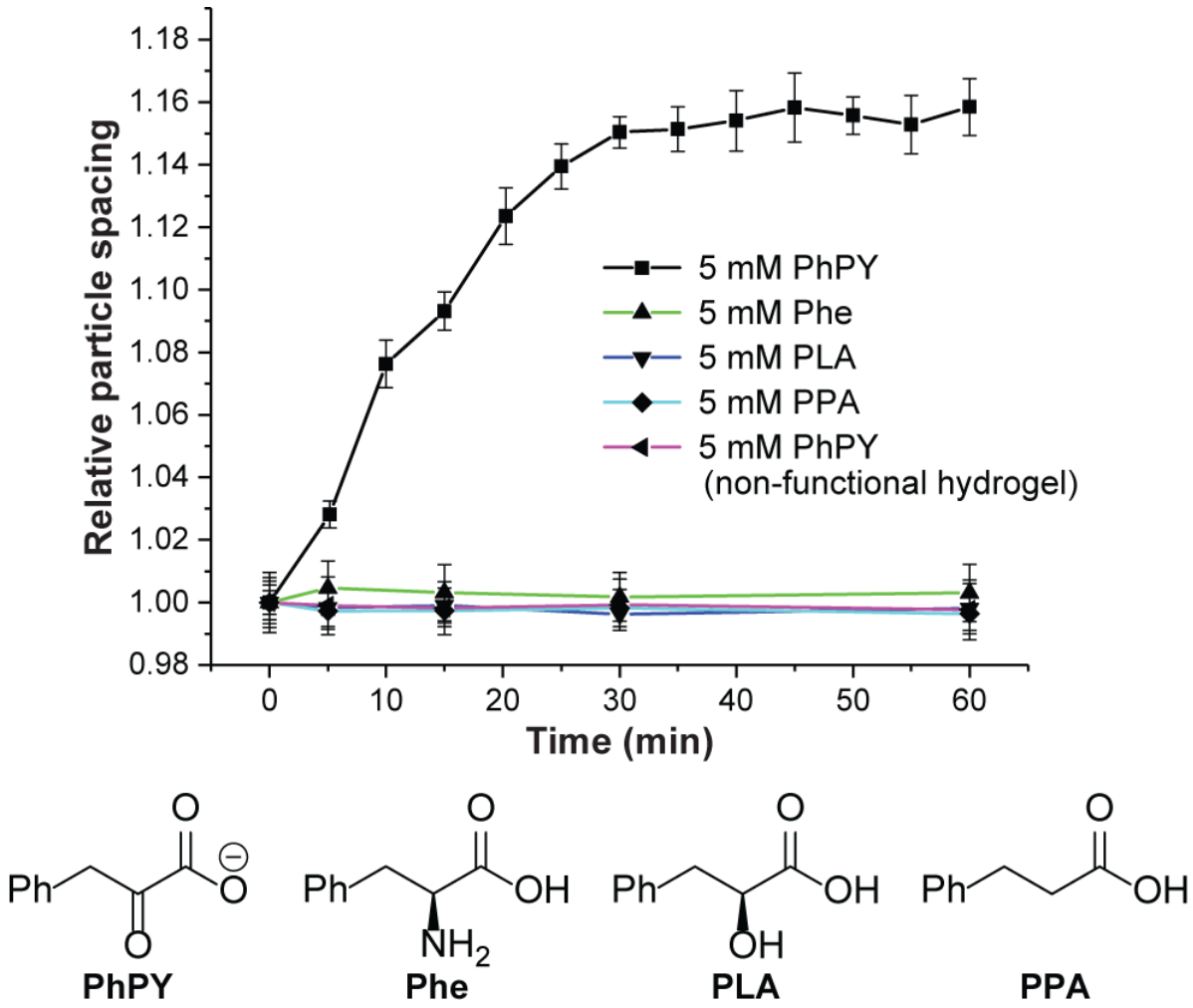

Figure 2-7. RPS curves demonstrating chemoselectivity of PhPY sensing. Only when the hydrogels had oxyamine groups and PhPY was present, the RPS increased. Error bars represent standard deviations (n = 3).

Figure 2-8 shows the concentration-dependent response of the sensor to PhPY at a fixed detection time of 30 min. To decrease the PhPY detection time, the reaction vials were agitated at 500 rpm using a vortex mixer. This agitation accelerated the diffusion rate of PhPY so that more PhPY molecules reached the oxyamines located inside the hydrogels, leading to larger and faster RPS increases in a shorter time. The effect of agitation can be clearly seen by comparing Figure 2-6b with Figure 2-8 at T = 30 min and [PhPY] = 1 mM. The RPS was only 1.030 when no agitation was employed (Figure 2-6b), but the RPS increased significantly to 1.125 when accompanied by agitation (Figure 2-8). Under these detection conditions, the LoD, estimated from the linear fit, was 93 μM (3*SD of y-intercept/slope).

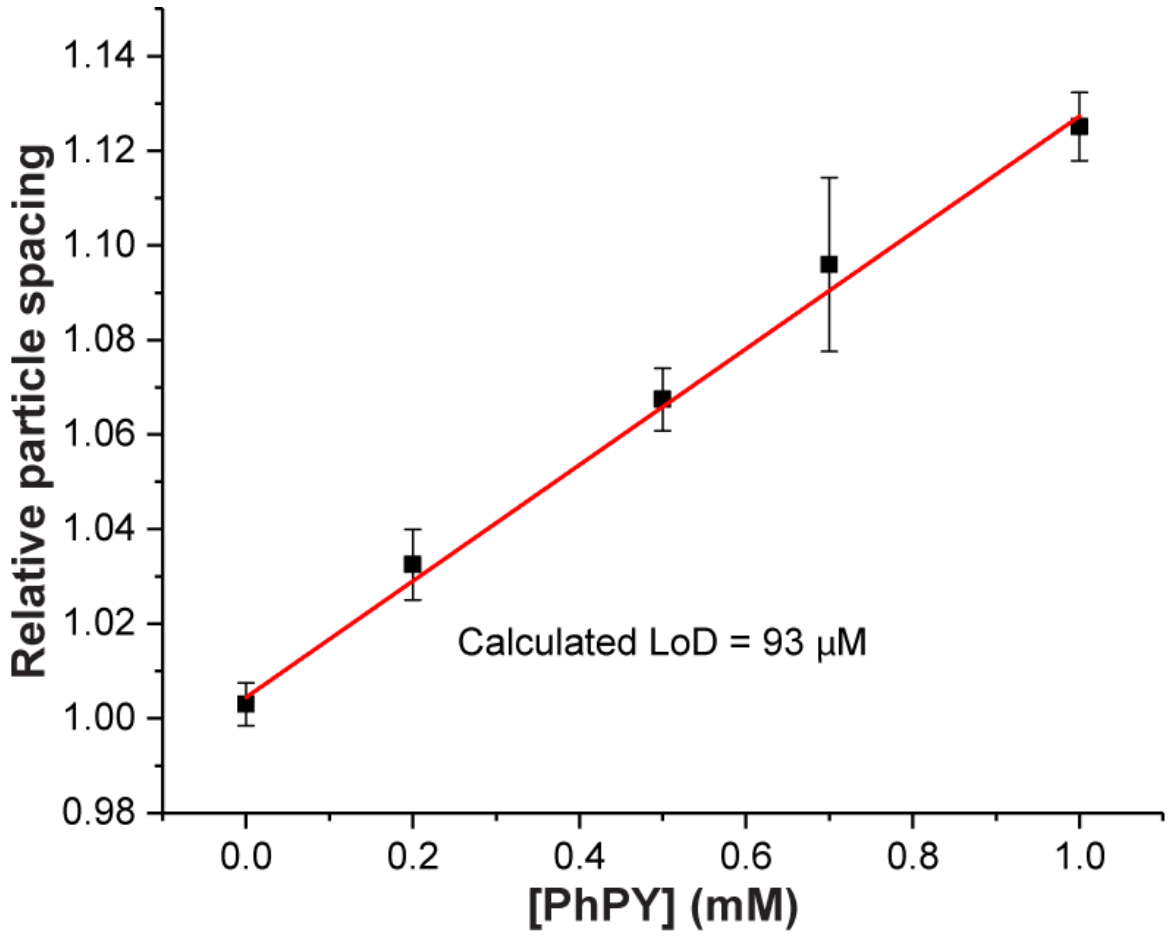

Figure 2-8. Quantification of PhPY for a detection time of 30 min. To decrease the detection time, the reaction vials were agitated at 500 rpm using a vortex mixer. The RPS at 0.7 mM PhPY had a much larger standard deviation compared to the other data points. The large standard deviation is potentially attributed to the relatively poorly ordered 2DPCs embedded into the corresponding hydrogel samples. The red line shows a linear fit (adjusted R-squared = 0.9968). Error bars represent standard deviations (n = 3).

2.3.4 PhPY Recognitions in Human Serum

The PhPY-sensing hydrogels were also tested in more complex biological milieu, human serum. Based on the preliminary results, we removed serum proteins to minimize interference. As in the previous experiments, we initially used a 100 mM concentration of *p*-PDA. However, because *p*-PDA showed a substantially lower solubility at physiological pH, it was necessary to add a relatively large amount of HCl to lower the pH and completely dissolve *p*-PDA. As a result, serum solutions containing 100 mM of *p*-PDA had much higher ionic strength than acetate buffer solutions containing the same concentration of *p*-PDA. This increased ionic strength of the serum solution screened the negative charges, which were attached to the hydrogels after detecting PhPY, thus minimizing Π and the hydrogel volume increase.

To avoid the ionic strength issue and increase the sensor responsivity, the hydrogels were washed with acetate buffer solutions with a low ionic strength of 10 mM before and after detecting PhPY. In this case, the ionic strength of the serum solution did not affect the particle spacing measurements, and the hydrogels showed larger volume changes after detecting PhPY. Further, 500 mM of *p*-PDA, much higher than 100 mM, was employed for PhPY sensing to maximize the oxime reaction rate.

Figure 2-9 shows the RPS data as a result of detecting various PhPY concentrations in protein-removed human serum (detection time = 30 min). The degree of increase in RPS was greater in the serum solutions than in the buffer solutions. This is because, as aforementioned, the *p*-PDA concentration was increased during the PhPY detection, and the hydrogels were washed with low-ionic-strength solutions after the reaction. For instance, where [PhPY] = 0.5 mM, the RPS in the buffer solutions was 1.067 (Figure 2-8); however, the RPS in the serum solutions was noticeably higher at 1.158 (Figure 2-9).

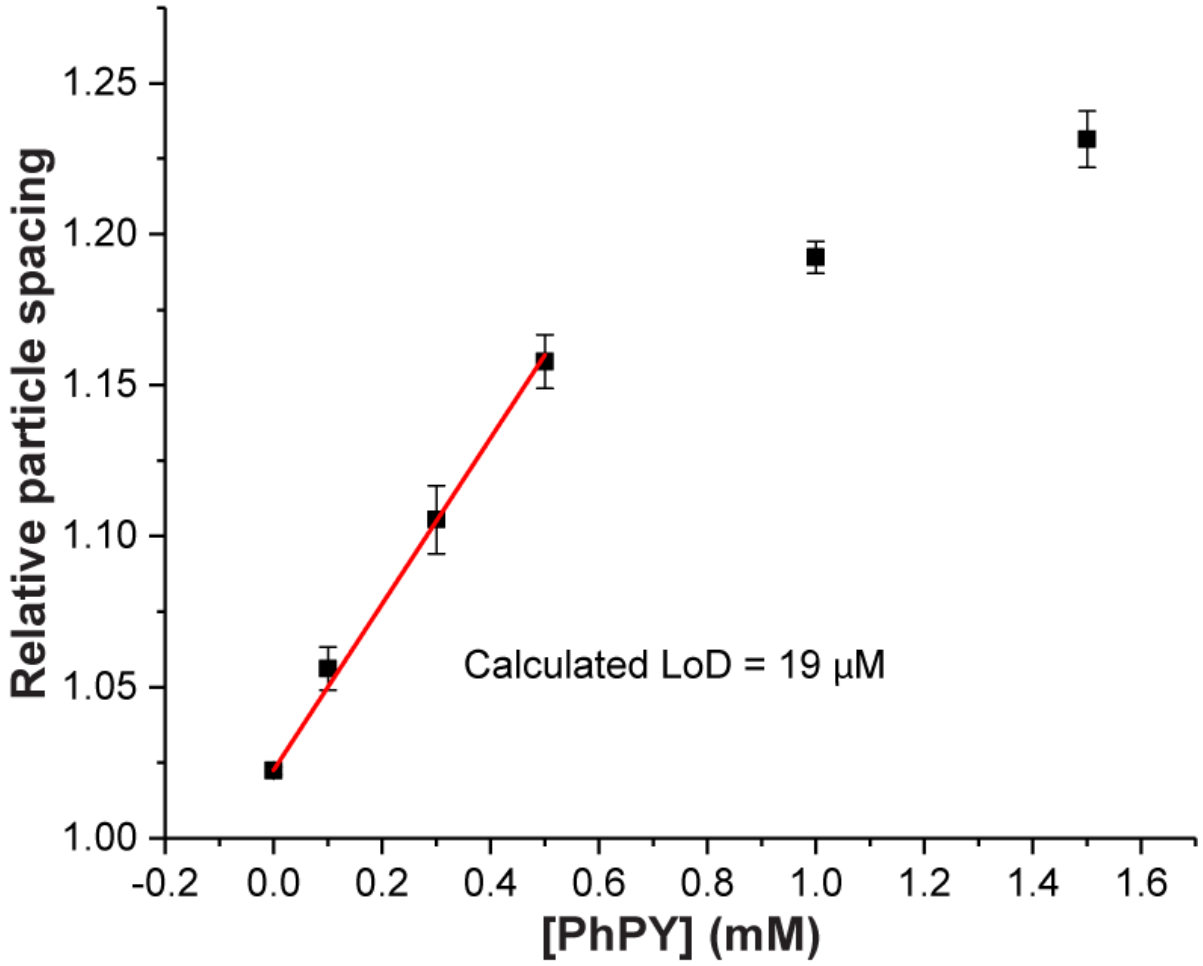

Figure 2-9. Quantification of PhPY in protein-removed human serum (detection time = 30 min). *p*-PDA (500 mM) was employed in each reaction. The red line shows a linear fit (adjusted R-squared = 0.9958). Error bars represent standard deviations (n = 3).

The red line shows a linear fit where [PhPY] ≤ 0.5 mM, and the LoD was estimated to be 19 μM (3*SD of y-intercept/slope). The change in the RPS began to level off when [PhPY] > 0.5 mM because the PhPY reaction gradually reached equilibrium. The results demonstrate that the 2DPC hydrogel sensor could be used to precisely determine the analyte concentrations in biological samples.

When [PhPY] = 0 mM in protein-removed human serum, the RPS was not 1 but slightly increased to 1.022. We hypothesize that this is due to the presence of other ketones or aldehydes that are normally present in blood at low levels. We do not anticipate that this would pose a problem in the potential future application of the reported material in the development of a blood Phe sensor by coupling the enzymatic conversion of Phe to PhPY with the PhPY-sensing hydrogels. The background RPS of untreated blood will be measured first without the enzymatic conversion and subtracted from the RPS determined after the enzymatic conversion.

The long-term stability of PhPY-sensing hydrogels was tested. After being stored in 100 mM acetate buffer solutions (pH 5.5) for 4 months at 4 °C, the hydrogel samples reacted with 0.5 mM of PhPY in protein-removed human serum as described above (n = 3). The aged samples showed a negligible difference in the RPS values compared with the data shown in Figure 2-9. This demonstrates that the hydrogels can be stored for a long time without losing their responsivity.

2.4 Conclusions

We have described here responsive 2DPC hydrogels for the chemoselective detection of PhPY, the reaction product of Phe with the enzyme PheDH. The PhPY-sensing hydrogels chemoselectively react with PhPY, leading to a change in hydrogel volume that is quantified by

light diffraction from the embedded 2DPC. This covalent structural modification enables the hydrogels to be vigorously washed with a buffer solution of low ionic strength after PhPY reactions, resulting in greatly improved sensor responsivity. The estimated LoD of PhPY in protein-removed human serum for a detection time of 30 min is 19 μM, which is comparable to the minimum blood Phe concentrations of healthy people.

In future work, we plan to test our hypothesis that it is possible to couple the enzymatic conversion of Phe to PhPY with the newly reported PhPY-sensing hydrogels to develop a blood Phe sensor. The recognition of enzymatically produced PhPY would be able to quantify the Phe concentration because Phe produces a stoichiometric amount of PhPY from the reaction. Our ultimate goal is to incorporate this Phe sensor into an at-home test kit for PKU patients. Although these plans present technical challenges that must be addressed, with sufficient optimization, we propose that the sensor material presented here can be applied more inexpensively and efficiently than with existing Phe-sensing elements. This new hydrogel sensing approach via covalent oxime ligation, widely used in bioconjugation applications, can be generalized to develop other chemical sensors.

2.4.1 Acknowledgements

The authors acknowledge Krishnan Damodaran and Mike Delk for assistance in obtaining NMR spectra. The authors acknowledge the University of Pittsburgh and the Defense Threat Reduction Agency (grant no. HDTRA1-15-1-0038) for providing instrumentation and financial support.

2.5 References

(1) Mitchell, J. J.; Trakadis, Y. J.; Scriver, C. R., Phenylalanine Hydroxylase Deficiency. *Genet. Med.* **2011**, 13, 697-707.

(2) Camp, K. M.; Parisi, M. A.; Acosta, P. B.; Berry, G. T.; Bilder, D. A.; Blau, N.; Bodamer, O. A.; Brosco, J. P.; Brown, C. S.; Burlina, A. B.; Burton, B. K.; Chang, C. S.; Coates, P. M.; Cunningham, A. C.; Dobrowolski, S. F.; Ferguson, J. H.; Franklin, T. D.; Frazier, D. M.; Grange, D. K.; Greene, C. L.; Groft, S. C.; Harding, C. O.; Howell, R. R.; Huntington, K. L.; Hyatt-Knorr, H. D.; Jevaji, I. P.; Levy, H. L.; Lichter-Konecki, U.; Lindegren, M. L.; Lloyd-Puryear, M. A.; Matalon, K.; MacDonald, A.; McPheeters, M. L.; Mitchell, J. J.; Mofidi, S.; Moseley, K. D.; Mueller, C. M.; Mulberg, A. E.; Nerurkar, L. S.; Ogata, B. N.; Pariser, A. R.; Prasad, S.; Pridjian, G.; Rasmussen, S. A.; Reddy, U. M.; Rohr, F. J.; Singh, R. H.; Sirrs, S. M.; Stremer, S. E.; Tagle, D. A.; Thompson, S. M.; Urv, T. K.; Utz, J. R.; van Spronsen, F.; Vockley, J.; Waisbren, S. E.; Weglicki, L. S.; White, D. A.; Whitley, C. B.; Wilfond, B. S.; Yannicelli, S.; Young, J. M., Phenylketonuria Scientific Review Conference: State of the Science and Future Research Needs. *Mol. Genet. Metab.* **2014**, 112, 87-122.

(3) American Academy of Pediatrics. National Institutes of Health Consensus Development Conference Statement: phenylketonuria: screening and management, October 16-18, 2000. *Pediatrics* **2001**, 108, 972-982.

(4) Guthrie, R.; Susi, A., A Simple Phenylalanine Method for Detecting Phenylketonuria in Large Populations of Newborn Infants. *Pediatrics* **1963**, 32, 338-343.

(5) Gerasimova, N. S.; Steklova, I. V.; Tuuminen, T., Fluorometric Method for Phenylalanine Microplate Assay Adapted for Phenylketonuria Screening. *Clin. Chem.* **1989**, 35, 2112-2115.

(6) Mishra, D. R.; Darjee, S. M.; Bhatt, K. D.; Modi, K. M.; Jain, V. K., Calix Protected Gold Nanobeacon as Turn-Off Fluorescent Sensor for Phenylalanine. *J. Inclusion Phenom. Macrocyclic Chem.* **2015**, 82, 425-436.

(7) Chace, D. H.; Sherwin, J. E.; Hillman, S. L.; Lorey, F.; Cunningham, G. C., Use of Phenylalanine-to-Tyrosine Ratio Determined by Tandem Mass Spectrometry to Improve Newborn Screening for Phenylketonuria of Early Discharge Specimens Collected in the First 24 Hours. *Clin. Chem.* **1998**, 44, 2405-2409.

(8) Corso, G.; Paglia, G.; Garofalo, D.; D'Apolito, O., Neutral Loss Analysis of Amino Acids by Desorption Electrospray Ionization Using an Unmodified Tandem Quadrupole Mass Spectrometer. *Rapid Commun. Mass Spectrom.* **2007**, 21, 3777-3784.

(9) Roesel, R. A.; Blankenship, P. R.; Hommes, F. A., HPLC Assay of Phenylalanine and Tyrosine in Blood Spots on Filter Paper. *Clin. Chim. Acta* **1986**, 156, 91-96.

(10) Neurauter, G.; Scholl-Bürgi, S.; Haara, A.; Geisler, S.; Mayersbach, P.; Schennach, H.; Fuchs, D., Simultaneous Measurement of Phenylalanine and Tyrosine by High Performance Liquid Chromatography (HPLC) with Fluorescence Detection. *Clin. Biochem.* **2013**, 46, 1848-1851.

(11) De Silva, V.; Oldham, C. D.; May, S. W., L-Phenylalanine Concentration in Blood of Phenylketonuria Patients: A Modified Enzyme Colorimetric Assay Compared with Amino Acid Analysis, Tandem Mass Spectrometry, and HPLC Methods. *Clin. Chem. Lab. Med.* **2010**, 48, 1271-1279.

(12) Thiessen, G.; Robinson, R.; De Los Reyes, K.; Monnat, R. J.; Fu, E., Conversion of a Laboratory-Based Test for Phenylalanine Detection to a Simple Paper-Based Format and Implications For PKU Screening in Low-Resource Settings. *Analyst* **2015**, 140, 609-615.

(13) Robinson, R.; Wong, L.; Monnat, R.; Fu, E., Development of a Whole Blood Paper-Based Device for Phenylalanine Detection in the Context of PKU Therapy Monitoring. *Micromachines* **2016**, 7, 28-37.

(14) Omidinia, E.; Shadjou, N.; Hasanzadeh, M., Immobilization of Phenylalanine-Dehydrogenase on Nano-Sized Polytaurine: A New Platform for Application of Nano-Polymeric Materials on Enzymatic Biosensing Technology. *Mater. Sci. Eng., C* **2014**, 42, 368-373.

(15) Idili, A.; Parolo, C.; Ortega, G.; Plaxco, K. W., Calibration-Free Measurement of Phenylalanine Levels in the Blood Using an Electrochemical Aptamer-Based Sensor Suitable for Point-of-Care Applications. *ACS Sens.* **2019**, 4, 3227-3233.

(16) Qiu, H.; Xi, Y.; Lu, F.; Fan, L.; Luo, C., Determination of L-Phenylalanine On-Line Based on Molecularly Imprinted Polymeric Microspheres and Flow Injection Chemiluminescence. *Spectrochim. Acta, Part A* **2012**, 86, 456-460.

(17) Borghei, Y.-S.; Hosseini, M.; Khoobi, M.; Ganjali, M. R., Copper Nanocluster-Enhanced Luminol Chemiluminescence for High- Selectivity Sensing of Tryptophan and Phenylalanine. *Luminescence* **2017**, 32, 1045-1050.

(18) Kölmel, D. K.; Kool, E. T., Oximes and Hydrazones in Bioconjugation: Mechanism and Catalysis. *Chem. Rev.* **2017**, 117, 10358-10376.

(19) Hummel, W.; Schütte, H.; Kula, M.-R., Enzymatic Determination of L-Phenylalanine and Phenylpyruvate with L-Phenylalanine Dehydrogenase. *Anal. Biochem.* **1988**, 170, 397-401.

(20) Wendel, U.; Hummel, W.; Langenbeck, U., Monitoring of Phenylketonuria: a Colorimetric Method for the Determination of Plasma Phenylalanine Using L-Phenylalanine Dehydrogenase. *Anal. Biochem.* **1989**, 180, 91-94.

(21) Peschke, B.; Zundel, M.; Bak, S.; Clausen, T. R.; Blume, N.; Pedersen, A.; Zaragoza, F.; Madsen, K., C-Terminally PEGylated hGH-derivatives. *Bioorg. Med. Chem.* **2007**, 15, 4382-4395.

(22) Harjani, J. R.; Liang, C.; Jessop, P. G., A Synthesis of Acetamidines. *J. Org. Chem.* **2011**, 76, 1683-1691.

(23) Hermanson, G. T., *Bioconjugate Techniques*; Academic Press, 2013.

(24) Zhang, F.; Cao, L.; Yang, W., Preparation of Monodisperse and Anion-Charged Polystyrene Microspheres Stabilized with Polymerizable Sodium Styrene Sulfonate by Dispersion Polymerization. *Macromol. Chem. Phys.* **2010**, 211, 744-751.

(25) Zhang, J.-T.; Wang, L.; Lamont, D. N.; Velankar, S. S.; Asher, S. A., Fabrication of Large-Area Two-Dimensional Colloidal Crystals. *Angew. Chem., Int. Ed.* **2012**, 51, 6117-6120.

(26) Zhang, J.-T.; Chao, X.; Liu, X.; Asher, S. A., Two-Dimensional Array Debye Ring Diffraction Protein Recognition Sensing. *Chem. Commun.* **2013**, 49, 6337-6339.

(27) Prevo, B. G.; Velev, O. D., Controlled, Rapid Deposition of Structured Coatings from Micro- and Nanoparticle Suspensions. *Langmuir* **2004**, 20, 2099-2107.

(28) Dirksen, A.; Dirksen, S.; Hackeng, T. M.; Dawson, P. E., Nucleophilic Catalysis of Hydrazone Formation and Transimination: Implications for Dynamic Covalent Chemistry. *J. Am. Chem. Soc.* **2006**, 128, 15602-15603.

(29) Dirksen, A.; Hackeng, T. M.; Dawson, P. E., Nucleophilic Catalysis of Oxime Ligation. *Angew. Chem., Int. Ed.* **2006**, 45, 7581-7584.

(30) Crisalli, P.; Kool, E. T., Water-Soluble Organocatalysts for Hydrazone and Oxime Formation. *J. Org. Chem.* **2013**, 78, 1184-1189.

(31) Wendeler, M.; Grinberg, L.; Wang, X.; Dawson, P. E.; Baca, M., Enhanced Catalysis of Oxime-Based Bioconjugations by Substituted Anilines. *Bioconjugate Chem.* **2013**, 25, 93-101.

(32) Rashidian, M.; Mahmoodi, M. M.; Shah, R.; Dozier, J. K.; Wagner, C. R.; Distefano, M. D., A Highly Efficient Catalyst for Oxime Ligation and Hydrazone−Oxime Exchange Suitable for Bioconjugation. *Bioconjugate Chem.* **2013**, 24, 333-342.

(33) Flory, P. J.; Rehner, J., Jr., Statistical Mechanics of Cross-Linked Polymer Networks I. Rubberlike Elasticity. *J. Chem. Phys.* **1943**, 11, 512-520.

(34) Hiemenz, P. C.; Lodge, T. P., *Polymer Chemistry*; CRC Press, 2007.

(35) Bain, A. D.; Eaton, D. R.; Hamielec, A. E.; Mlekuz, M.; Sayer, B. G., Line Broadening in the Carbon-13 NMR Spectra of Cross-Linked Polymers. *Macromolecules* **1989**, 22, 3561-3564.

(36) Shapiro, Y. E., Structure and Dynamics of Hydrogels and Organogels: An NMR Spectroscopy Approach. *Prog. Polym. Sci.* **2011**, 36, 1184-1253.

(37) Mathur, A. M.; Scranton, A. B., Characterization of Hydrogels Using Nuclear Magnetic Resonance Spectroscopy. *Biomaterials* **1996**, 17, 547-557.

(38) Shestakova, P.; Willem, R.; Vassileva, E., Elucidation of the Chemical and Morphological Structure of Double-Network (DN) Hydrogels by High-Resolution Magic Angle Spinning (HRMAS) NMR Spectroscopy. *Chem. Eur. J.* **2011**, 17, 14867-14877.

3.0 DNA-Crosslinked 2D Photonic Crystal Hydrogels for Detection of Adenosine Actuated by an Adenosine-Binding Aptamer

This chapter was previously published in the journal *ACS Sensors* as Jang, K.; Westbay, J. H.; Asher, S. A., DNA-Crosslinked 2D Photonic Crystal Hydrogels for Detection of Adenosine Actuated by an Adenosine-Binding Aptamer. *ACS Sens.* **2022**, 7, 1648-1656, and is reprinted with permission. K.J. and J.H.W. contributed equally. This manuscript was prepared by K.J. and J.H.W. with the assistance of S.A.A.

There is a need to develop versatile sensing motifs that can be used to detect a variety of chemical targets in resource-limited settings, for example, at the point of care. While numerous sensing technologies have been developed toward this effort, these technologies can be overly complex and require a skilled technician, extensive sample preparation, or sophisticated instrumentation to use, limiting their generalizability and application in resource-limited settings. Here, we report a novel sensing motif that utilizes DNA-crosslinked two-dimensional photonic crystal (2DPC) hydrogels. These hydrogel sensors contain a DNA aptamer recognition group that binds a target analyte. As proof of concept, we fabricated 2DPC hydrogels using a well-studied adenosine-binding aptamer. This adenosine aptamer is duplexed with a partially complementary strand and forms responsive crosslinks in the hydrogel polymer network. When adenosine is introduced, aptamer−adenosine binding occurs, breaking the DNA crosslinks and causing the hydrogel to swell. This in turn increases the particle spacing of an embedded 2DPC array, shifting the 2DPC Bragg diffraction. Thus, adenosine concentration can be monitored through 2DPC Bragg diffraction measurements. A linear range of 20 μM to 2 mM was observed. The detection limits were calculated to be 13.9 μM in adenosine-binding buffer and 26.7 μM in fetal bovine serum.

This reported sensing motif has a readout that is simple and rapid and requires minimal equipment. We hypothesize that this sensing motif is generalizable and that other sensors can be easily fabricated by simply exchanging the aptamer that serves as a molecular recognition group.

3.1 Introduction

There is a need to develop sensing motifs that are generalizable and can be used in resource-limited settings, especially at the point of care.[1] Developing accessible point-of-care sensors that operate outside of a laboratory without the need for skilled technicians would save time, improve patient compliance, and reduce health care costs.[2,3] For example, easy-to-use glucose monitoring devices have significantly improved outcomes for patients with insulin-dependent diabetes mellitus.[4]

Recently, various sensing methods have been reported utilizing aptamers. Aptamers are short, single-stranded RNA or DNA that are selected using the systemic evolution of ligands via the exponential enrichment (SELEX) process to specifically bind chemical targets.[5,6] Aptamers have specificities and binding affinities analogous to antibodies but are generally more stable, easier to engineer, and less expensive to produce; thus, they have been widely used in recent sensor development.[7,8] For example, aptasensors have been developed utilizing technologies such as fluorescence resonance energy transfer,[9,10] fluorescence,[11,12] surface plasmon resonance spectroscopy,[13,14] and electrochemistry.[15,16] While these sensing methods offer high specificity and sensitivity, they can require a skilled technician, extensive sample preparation, and/or sophisticated instrumentation, limiting their application in resource-limited environments.

Low-cost photonic crystal (PC) hydrogel sensors are a simple sensing platform that have been fabricated for a variety of chemical targets including pH,[17,18] ions,[19,20] small molecules,[17,21–26] and proteins.[27,28] PC hydrogels consist of a periodic PC array embedded in a stimuli-responsive hydrogel. The stimuli-responsive hydrogel contains molecular recognition groups that actuate specific volume phase transitions (VPT) in the presence of target analytes. The target-induced VPT are monitored by shifts in the PC Bragg diffraction and used to quantify analyte concentrations.[29,30] These PC sensors require minimal or no sample preparation and have simple, colorimetric readouts, ideally positioning the PC hydrogels for use in resource-limited settings.

Recently, the Gu group utilized PC hydrogels with aptamers to develop sensors for metal ions.[19,31] They covalently attached Pb^{2+}-, Hg^{2+}-, and Ag^{+}-binding aptamers to PC hydrogels. Upon binding the target metal ion, each aptamer underwent a specific hairpin-like conformational change that shrank the hydrogel, blue-shifting the PC array diffraction. This specific sensing motif is limited in versatility because not all aptamers undergo these hairpin-like conformational changes that trigger hydrogel VPT and PC diffraction shifts on binding target molecules.

Here, we report the development of novel DNA-crosslinked two-dimensional PC (2DPC) hydrogels. This sensing motif utilizes duplexed DNA crosslinks that do not rely on a specific conformational change and thus are generalizable to any aptamer-target interaction.[32,33] As proof of concept, we fabricated hydrogel sensors using a well-studied adenosine-binding aptamer.[34,35] Adenosine is an endogenous, regulatory molecule that frequently serves as a model small molecule in aptamer studies.[32,36–39] We fabricated an adenosine-binding PC hydrogel by attaching a 2DPC array to a DNA-crosslinked hydrogel containing the adenosine-binding aptamer. In the presence of adenosine, competitive aptamer−adenosine binding occurs and breaks the DNA crosslinks. This generates an osmotic pressure in the system that actuates hydrogel swelling. The hydrogel swelling

in turn increases the particle spacing of the embedded 2DPC array and shifts the 2DPC Bragg diffraction. These adenosine-induced particle spacing changes were monitored through 2DPC diffraction measurements and used to quantify the concentration of adenosine. The limits of detection (LoDs) are calculated to be 13.9 μM in adenosine-binding buffer and 26.7 μM in 50% protein-removed fetal bovine serum (FBS) (detection time = 30 min).

The reported DNA-crosslinked 2DPC hydrogels require minimal equipment and sample preparation to use, ideally positioning them for application in resource-limited settings. We hypothesize that this sensing motif is generalizable, and sensors for other targets can be fabricated by simply exchanging the aptamer molecular recognition group. Aptamers for a wide variety of targets including ions,[19,31] small molecules,[40−42] proteins,[43−46] and whole cells[47,48] with sub-micromolar dissociation constants have been reported, enabling the development of versatile sensors with ultralow LoDs.

3.2 Experimental

3.2.1 Materials

Acrydite-modified DNA strands (DNA 1: 5′-acrydite-AGA GAA CCT GGG GGA GTA TTG CGG AGG AAG GT-3′, DNA 2: 5′-acrydite-CCC AGG TTC TCT-3′, and DNA 3: 5′-acrydite-AGA GAA CCT GGG GGA GTA ATG CGG AGC AAG GT-3′, purified using high-performance liquid chromatography) were purchased from Integrated DNA Technologies. Stock solutions of DNA 1, 2, and 3 were prepared separately at a 2 mM concentration in TE buffer [10 mM Tris, pH 8.0, and 0.1 mM ethylenediaminetetraacetic acid (EDTA)] and stored at −20 °C. Tris

base (≥99.9%), magnesium chloride, 4-(2-hydroxyethyl)-1-piperazineethanesulfonic acid (HEPES) (99%), sodium hydroxide pellets (≥97%), sodium styrene sulfonate (NaSS) (≥90%), 2,2'-azobisisobutyronitrile (98%), styrene (99%), acrylamide (≥99%), N,N'-methylenebisacrylamide (MBAAm) (99%), ammonium persulfate (98%), tetramethylethylenediamine (TEMED) (99%), adenosine (≥99%), cytidine (99%), uridine (≥99%), and guanosine (98%) were purchased from Sigma-Aldrich. EDTA (99.5%) was purchased from J.T. Baker. Sodium chloride was purchased from EMD Millipore. Hydrochloric acid (36.5−38% w/w), potassium acetate (99%), methanol (99.8%), and 2-propanol (≥99.5%) were purchased from Thermo Fisher Scientific. Ethanol (200 proof) was purchased from Decon Labs, Inc. A QuantiT PicoGreen double-stranded DNA (dsDNA) assay kit was purchased from Invitrogen. The cover glass (thickness 1, 24 × 60 mm^2) and FBS were purchased from Corning. To remove serum proteins, FBS was filtered using 10 kDa centrifugal filters. Microscope premium frosted glass slides (25 × 75 × 1 mm^3) were purchased from Fisher Scientific. All chemicals were used as received unless otherwise specified. Ultrapure water (18.2 mΩ·cm) obtained from a Milli-Q Reference A+ was used for all experiments.

3.2.2 Annealing DNA Strands

A DNA annealing solution was prepared by adding 20 μL each of stock DNA 1 and DNA 2 solutions (a 2 mM concentration prepared in TE buffer) to a 160 μL solution of 1.25× duplex buffer. The DNA annealing solution contained the following components: 200 μM of DNA 1 and DNA 2; 1× duplex buffer (30 mM HEPES, pH 7.5, and 100 mM potassium acetate); and 0.2× TE buffer. To ensure thorough mixing, the solution was pipetted up and down 20 times and then centrifuged at 1000 RCF for 30 s. The solution was then heated to 95 °C on a Corning LSE Digital

dry bath heater for 5 min and cooled at room temperature for 30 min. For the fluorescence assay, the annealed DNA solution was used as is. For 2DPC hydrogel fabrication, the annealed DNA solution was dried on a Labconco CentriVap Concentrator (78100-00 A) for 6 h.

3.2.3 PicoGreen Fluorescence Assay

A PicoGreen fluorescence assay was used for the optimization of aptamer-adenosine binding buffer. The assay procedure was modified from that of Lv et al.[49] A solution of annealed DNA was diluted using the following three different buffer solutions to a final concentration of 2 μM DNA: (i) duplex buffer (30 mM HEPES, pH 7.5; 100 mM potassium acetate), (ii) TNM (5 mM $MgCl_2$) (20 mM Tris, pH 7.5; 300 mM NaCl; and 5 mM $MgCl_2$), and (iii) TNM (10 mM $MgCl_2$) (20 mM Tris, pH 7.5; 300 mM NaCl; and 10 mM $MgCl_2$). For samples containing only DNA, a 300 μL solution of 40 nM DNA was prepared in each of the three buffers by diluting an aliquot of the 2 μM DNA solution. For samples containing DNA and adenosine, a 300 μL solution of 40 nM DNA and 400 μM adenosine was prepared in each of the three buffers. After mixing the DNA and adenosine solutions, the mixture was stored on a laboratory bench at room temperature under aluminum foil for 30 min to allow time for aptamer−adenosine binding. A 300 μL solution of 200× diluted PicoGreen, prepared in the same buffer as that of each DNA sample, was added to 300 μL of each DNA sample. This final solution was pipetted up and down 15 times and then transferred to a quartz cuvette after 3 min. Fluorescence spectra were measured in triplicate for each sample using a HORIBA Jobin Yvon Fluoromax-3 spectrofluorometer with 480 nm excitation, 525 nm emission, and slit widths of 2 nm for excitation and emission. Blank PicoGreen fluorescence in the three different buffers was measured separately. The background signal in the corresponding buffer was subtracted from each DNA measurement.

3.2.4 2DPC Hydrogel Fabrication

Negatively charged polystyrene (PS) particles with a diameter of 1.21 μm were synthesized via dispersion polymerization using methods described by Zhang et al.[50] These PS particles (12% (w/w) in water) were mixed in a 3:1 ratio with 2-propanol. Using our previously reported needle tip flow method,[51,52] this dispersion was injected at the air−water interface of a crystallization dish (Figure 3-1a). Then, the PS particles were self-assembled into a hexagonally close-packed 2DPC array monolayer (Figure 3-1b). A glass substrate (24 × 60 mm^2, cover glass, Corning) was used to pick up the 2DPC array (Figure 3-1c), and the 2DPC array was dried at room temperature for 24 h (Figure 3-1d). Tape was applied in two layers onto the 2DPC array glass substrate to section off a 2.4 × 1 cm^2 strip of the 2DPC array (Figure 3-1e). Polymerizable monomer solutions were prepared using the compositions described in Table 3-1. The monomer solutions were degassed in a vacuum desiccator for 15 min. After adding initiators [0.7 μL of 5% (v/v) TEMED in water and 0.7 μL of 10% (w/v) ammonium persulfate in water], the mixtures were stirred for 5 s using a micropipette tip and then were deposited onto the preformed 2DPC array glass substrate (2.4 × 1 cm^2) (Figure 3-1e). A glass slide cover (25 × 75 × 1 mm^3, microscope premium frosted glass slides, Fisher Scientific) was placed over the solution. Then, polymerization was allowed to occur under vacuum in a desiccator for 30 min. The resulting crosslinked polymer embedded the 2DPC array into the hydrogel network (Figure 3-1f). After polymerization, the sandwiched glass substrates containing the 2DPC hydrogel were placed in buffer (20 mM Tris, pH 7.5; 10 mM $MgCl_2$; and 300 mM NaCl) for 10 min. The glass substrates were separated using a razor blade, and the 2DPC hydrogel was peeled off of the substrate. The 2DPC hydrogel was washed in buffer for 3 min and cut into 0.4 × 0.5 cm^2 pieces. Each piece was stored in a refrigerated, sealed Petri dish without buffer.

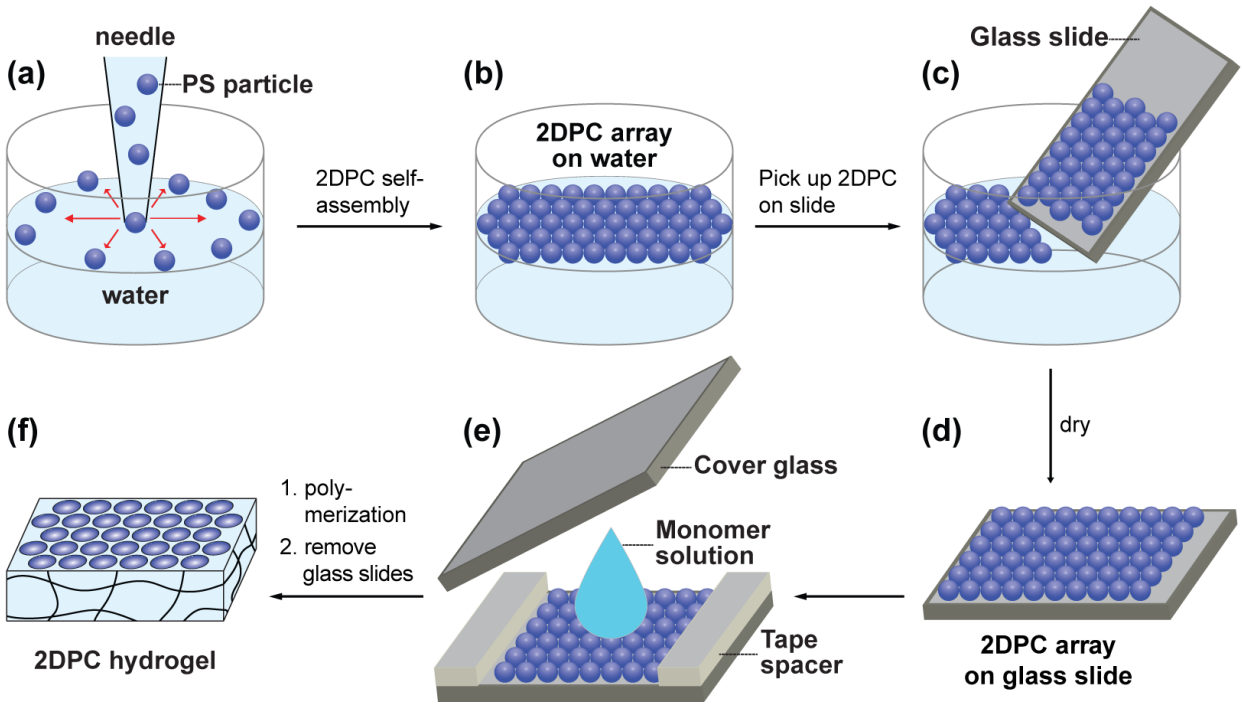

Figure 3-1. Method for fabricating 2DPC hydrogels. (a–e) A polymerizable monomer solution was layered on the top of a preformed 2DPC array on a glass slide. A cover glass sealed the solution, after which polymerization was allowed to proceed for 30 min at room temperature. (f) The resulting crosslinked polymer embedded the ordered 2DPC array monolayer within the hydrogel network (2DPC hydrogel).

Table 3-1. Composition of monomer solutions used in preparation of hydrogel samples

component	concentration
acrylamide	25% (w/v)
MBAAm	0.02% (w/v)
hybridized (annealed) DNA strands	0.8 mM
total volume	50 μL

3.2.5 Scanning Electron Microscopy Characterization

Periodic orderings of the close-packed 2DPC monolayer (Figure 3-2a) and the non-close-packed 2DPC monolayer embedded in swollen hydrogels (Figure 3-2b) were monitored using a field emission scanning electron microscope (Zeiss Sigma 500 VP) with an SE2 detector at an accelerating voltage of 3 kV (2DPC) or 5 kV (2DPC hydrogel). For scanning electron microscopy (SEM) characterization, swollen 2DPC hydrogels were sandwiched between glass slides and dried. Before taking SEM images, the samples were sputter-coated with gold for 75 s at 30 mA using an auto sputter coater (PELCO SC-7).

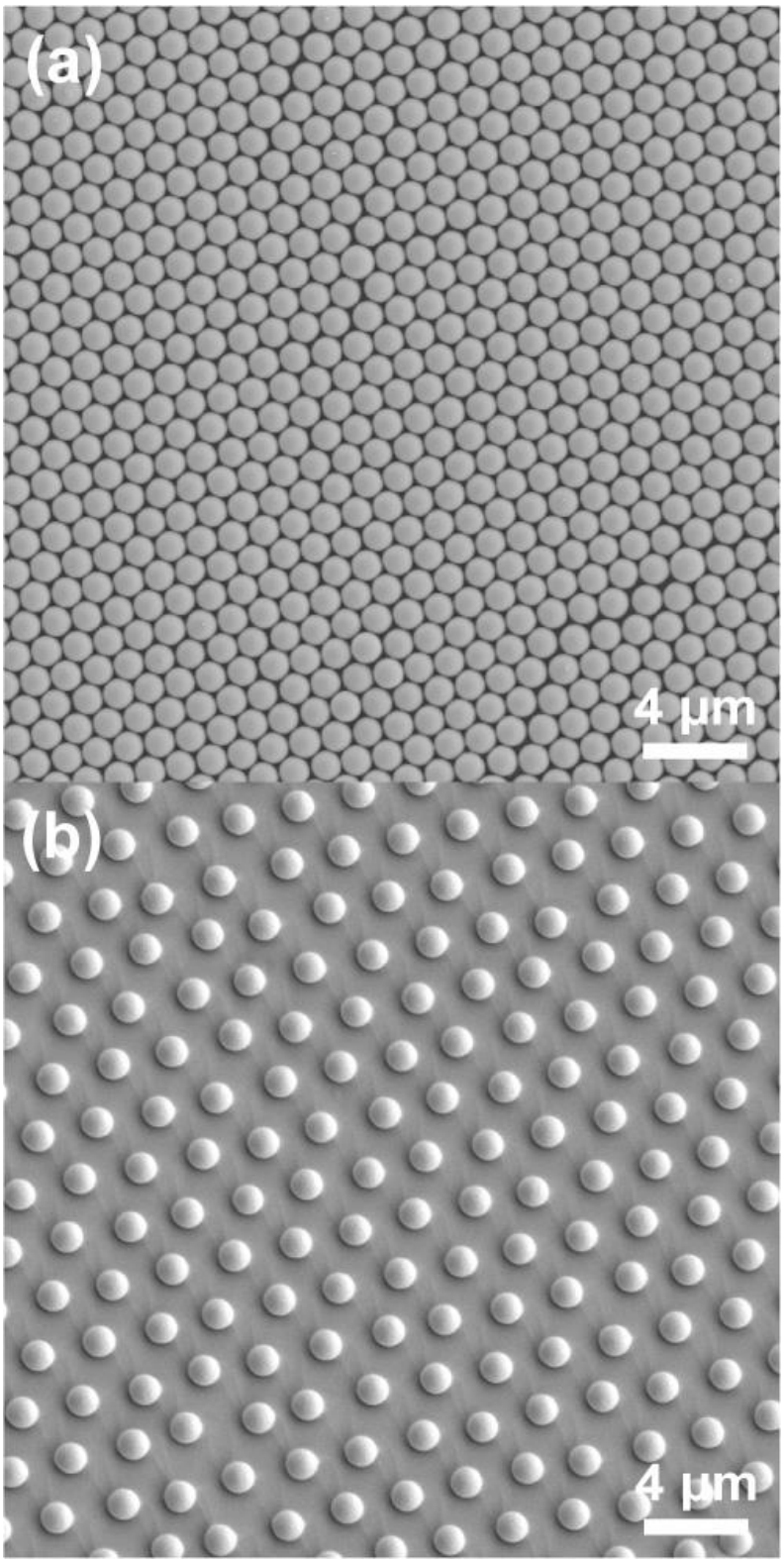

Figure 3-2. SEM images of (a) close-packed 2DPC monolayer and (b) non-close-packed 2DPC monolayer embedded in a hydrogel.

3.2.6 2DPC Particle Spacing Measurements

Adenosine-induced hydrogel swelling was monitored through 2DPC particle spacing measurements using described methods.[53] Briefly, eq 3-1 gives the condition for Bragg diffraction of a hexagonally close-packed 2DPC array where m is the order of diffraction, λ is the wavelength of light, d is the 2DPC array nearest neighbor particle spacing, and α and β are the angles of incidence and diffraction, respectively.

$$m\lambda = \frac{\sqrt{3}}{2} d(\sin\alpha + \sin\beta) \tag{3-1}$$

As shown in Figure 3-3, 2DPC hydrogels were excited along their normal using a 532 nm laser pointer, eliminating dependence on the angle of incidence (α = 0). A perfectly ordered 2DPC array shows six spots diffracted at angle β.[54] 2DPC arrays with a small rotational disorder diffract a Debye ring pattern.[24,53] Equation 3-2 relates the Debye ring diameter to β, where D is the Debye ring diameter and h is the distance between the 2DPC array and the Debye ring plane.

$$\beta = \tan^{-1}\left(\frac{D}{2h}\right) \tag{3-2}$$

Equations 3-1 and 3-2 combine to give eq 3-3.

$$d = \frac{2\lambda}{\sqrt{3}\sin\left(\tan^{-1}\left(\frac{D}{2h}\right)\right)} \tag{3-3}$$

h was fixed at 15 cm, and λ of the light source was known (532 nm). Thus, particle spacing was monitored by measuring D. To calculate d, we measured and averaged different D values from five different positions within each 2DPC hydrogel sample.

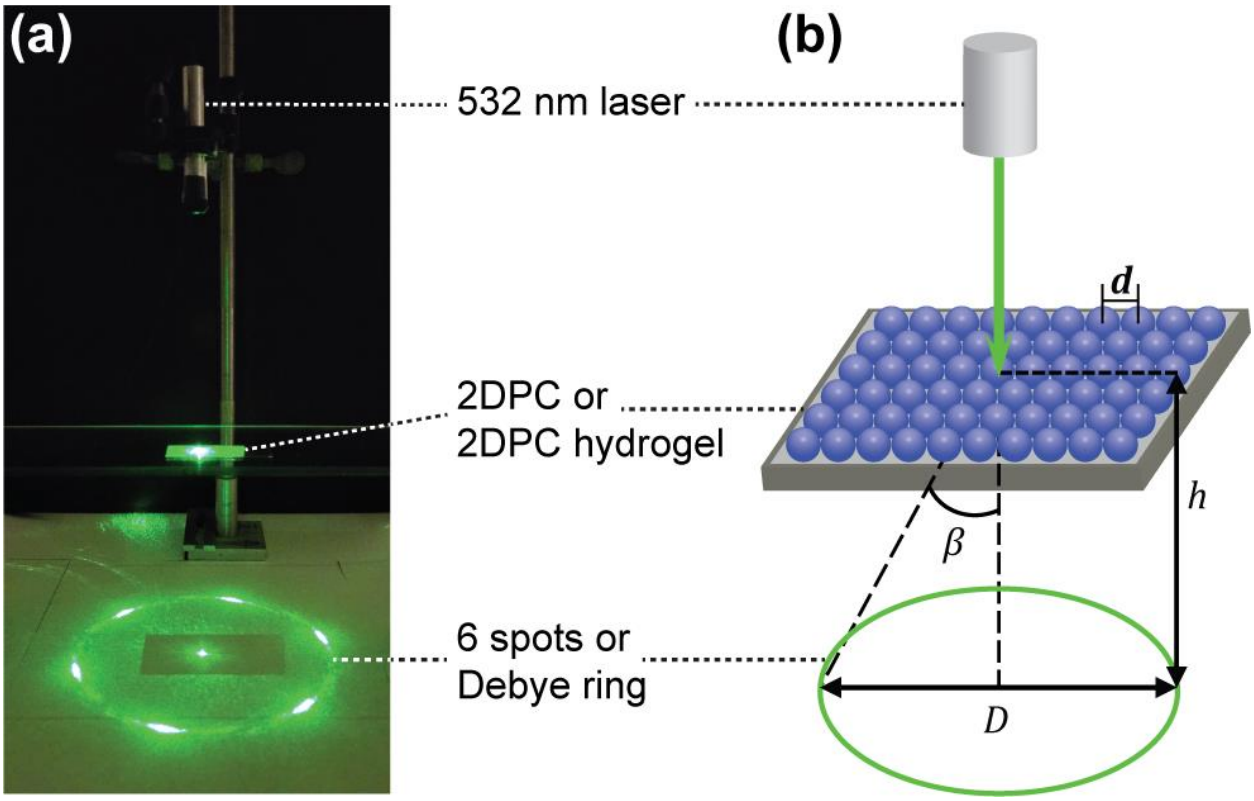

Figure 3-3. 2DPC hydrogel particle spacing measurement. A 2DPC hydrogel piece was placed on a stand above a white screen. (a) Experimental setup and (b) schematic diagram showing the Debye ring illuminated by a 532 nm laser.

3.2.7 Adenosine Sensing in Buffer Solutions

2DPC hydrogel pieces were brought to room temperature on a lab bench, and each was incubated in 10 mL of adenosine-binding buffer solution (20 mM Tris, pH 7.5; 10 mM $MgCl_2$; and 300 mM NaCl). After 10 min, the initial particle spacing of the 2DPC hydrogels was measured. The hydrogel pieces were then each submerged in 20 mL of adenosine-binding buffer solution containing 0 (blank) to 2 mM adenosine. Particle spacing measurements were obtained at time intervals of 5, 15, 30, and 60 min. For control measurements, 2DPC hydrogel pieces were each submerged in 20 mL of adenosine-binding buffer solution containing a 1 mM concentration of either adenosine, cytidine, guanosine, or uridine. The particle spacing was measured after 30 min of incubation. Each measurement was repeated three times using a different gel piece.

3.2.8 Adenosine Sensing in FBS

Protein-removed FBS was diluted to 50% with a serum diluting buffer (40 mM Tris, pH 7.5; 19 mM $MgCl_2$; and 450 mM NaCl). The final salt concentration of the 50% protein-removed FBS was the same as that of the pure adenosine-binding buffer (20 mM Tris, pH 7.5; 10 mM $MgCl_2$; and 300 mM NaCl).

2DPC hydrogel pieces were brought to room temperature on a lab bench, and each was incubated in 10 mL of adenosine-binding buffer solution (20 mM Tris, pH 7.5; 10 mM $MgCl_2$; and 300 mM NaCl). After 10 min, the initial particle spacing of the 2DPC hydrogels was measured. The 2DPC hydrogel pieces were then each submerged in 10 mL of 50% protein-removed FBS containing 0 (blank) to 2 mM adenosine. The particle spacing was measured after 30 min of incubation. Each measurement was repeated three times using a different gel piece.

3.3 Results and Discussion

3.3.1 Adenosine Sensing Motif Using DNA-Crosslinked 2DPC Hydrogels That Contain the Adenosine-Binding Aptamer

Figure 3-4 shows a simplified representation of our DNA-crosslinked 2DPC hydrogel and its adenosine sensing mechanism. As described in Section 2.4, the hydrogels were copolymerized with acrylamide, MBAAm, and the DNA strands onto pre-formed 2DPCs. The polyacrylamide backbone chains and the additional covalent MBAAm crosslinks ensured that the hydrogels were mechanically robust enough to embed the 2DPC array. To find the optimal 2DPC hydrogel fabrication conditions, we systematically varied the concentrations of acrylamide and MBAAm (see the Supporting Information). The DNA strands were modified with acrydite, an acrylic phosphoramidite group with a similar activity to that of the acrylamide monomer.[55] This modification enabled covalent incorporation of the DNA into the hydrogel polymer network.

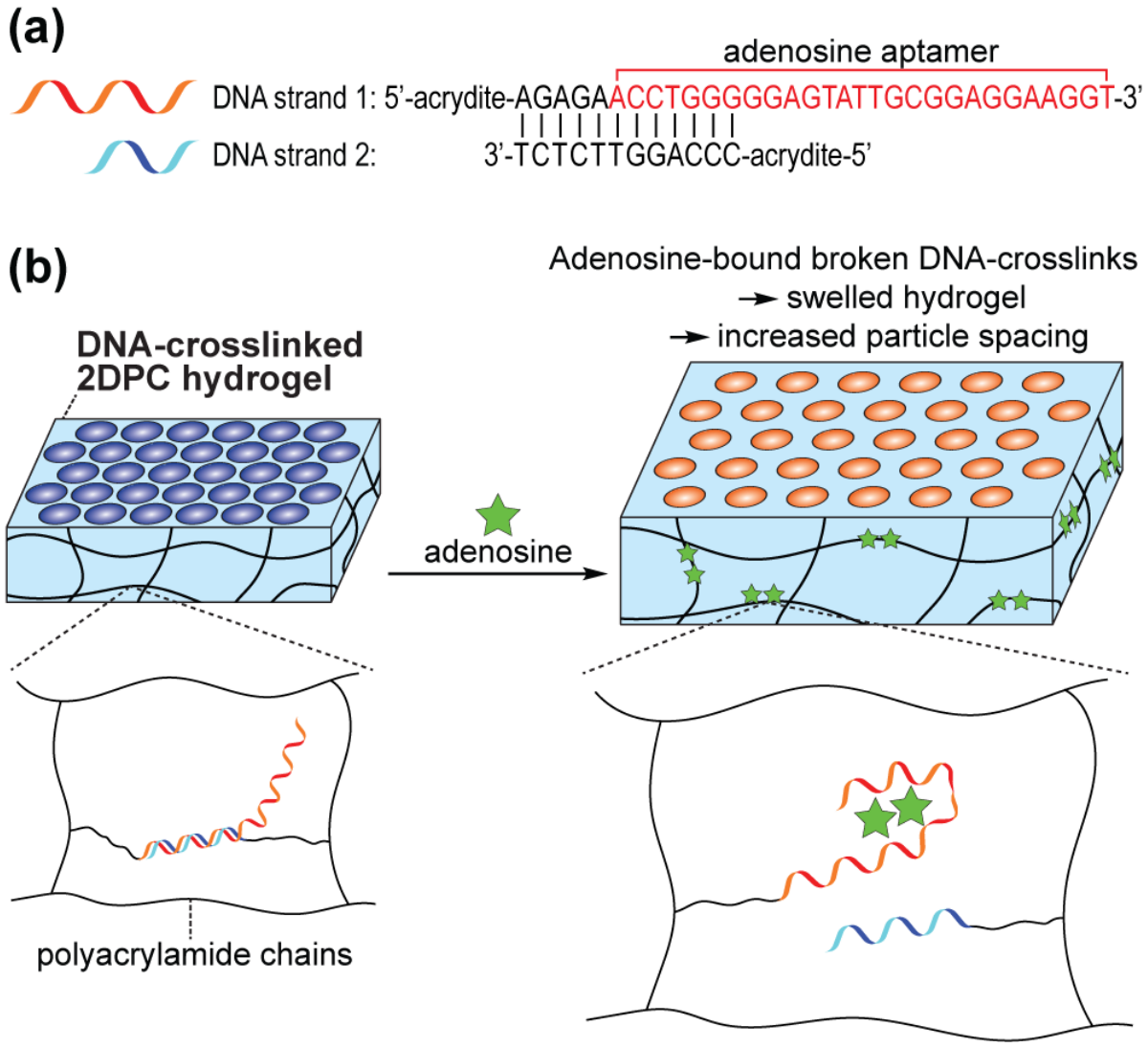

Figure 3-4. (a) Sequences of DNA strands that form adenosineresponsive crosslinks in the hydrogel. (b) Schematic diagram of the adenosine-sensing mechanism using a DNA-crosslinked 2DPC hydrogel.

For this proof-of-concept study, we utilized a 32-mer DNA strand 1 and a 12-mer DNA strand 2 (Figure 3-4a) based on Yang et al.'s work that demonstrated the fabrication of DNA-crosslinked hydrogels.[32] DNA strand 1 contains an adenosine-binding aptamer segment in its sequence. Without adenosine, DNA strand 1 hybridizes with DNA strand 2 and forms 12 base pairs that are stable enough to serve as DNA crosslinks in the hydrogels. Upon the addition of adenosine, the adenosine aptamer segment in DNA strand 1 competitively binds adenosine with high affinity, resulting in an aptamer conformational change (Figure 3-4b). This conformational change breaks the preformed DNA base pairs (or DNA crosslinks), which in turn decreases the elasticity of the hydrogel network and generates an osmotic pressure.[56,57] As a result, the hydrogel swells by absorbing water to relieve this pressure as the system reaches a new equilibrium where the net osmotic pressure evolves to zero.[56,57] This adenosine-induced hydrogel swelling homogeneously increases the particle spacing of the embedded 2DPC array, maintaining the hexagonal ordering. This shifts the Bragg diffraction angle in proportion to the amount of adenosine present. Based on preliminary data, the 2DPC hydrogels were fabricated with the chosen DNA concentration that showed large enough particle spacing changes in response to adenosine.

3.3.2 Optimizing Adenosine-Binding Buffer Conditions via Fluorometric Quantitation of dsDNA Using PicoGreen

Buffer conditions can affect the binding affinity and stability of DNA aptamers.[58,59] For the adenosine-binding aptamer used as a recognition agent, several different salt concentrations were previously examined.[32,34,39,49] In particular, it has been reported that Mg^{2+} may play an important role in assisting the adenosine-binding aptamer because the salt stabilizes the structure

of the aptamer−adenosine complex.[60,61] However, different sources suggest different amounts of Mg^{2+} for optimal aptamer−adenosine binding.

Thus, to optimize buffer conditions in our 2DPC hydrogel system, we utilized a PicoGreen assay. PicoGreen is an intercalating dye that becomes more fluorescent upon binding to dsDNA, compared to single-stranded DNA (ssDNA) or RNA.[62,63] Since our adenosine sensing motif involves a DNA conformational change from dsDNA to ssDNA upon adenosine binding, PicoGreen can be used to monitor the extent of adenosine binding by measuring fluorescence signal changes.

Figure 3-5 shows the PicoGreen assay data for optimization of aptamer−adenosine binding buffer. We compared the PicoGreen fluorescence in samples of hybridized DNA before and after incubation with adenosine under different buffer conditions. When the hybridized DNA aptamer binds adenosine, its competitive binding breaks DNA hybridization and converts dsDNA to ssDNA. As a result, the fluorescence emission decreases because PicoGreen fluorescence is more enhanced in the presence of dsDNA than in ssDNA. Thus, the largest decrease in relative fluorescence indicates maximal aptamer−adenosine binding.[49]

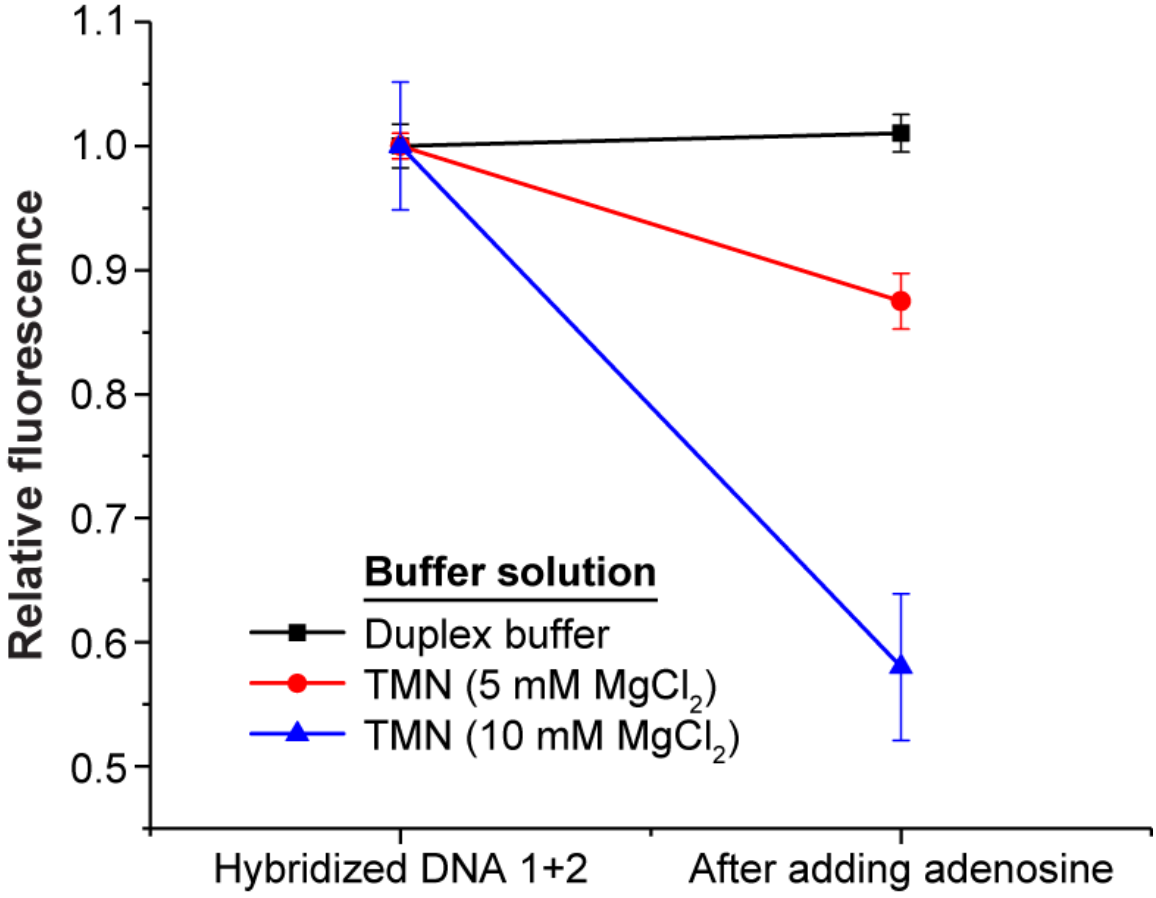

Figure 3-5. Quantification of aptamer−adenosine binding using the PicoGreen assay in different buffer solutions. TNM buffer contains Tris, NaCl, and $MgCl_2$. PicoGreen fluorescence is enhanced more upon binding to dsDNA (hybridized DNA) than to ssDNA. Aptamer−adenosine binding actuates the DNA conformational change from dsDNA to ssDNA. Thus, a decrease in the fluorescence emission upon the addition of adenosine indicates that more aptamer−adenosine binding has occurred. Error bars indicate standard deviations (n = 3).

We first examined PicoGreen fluorescence in duplex buffer (30 mM HEPES, pH 7.5, and 100 mM potassium acetate) that was used to anneal the DNA strands and notably did not contain Mg^{2+}. We observed a negligible change in fluorescence when adenosine was added (Figure 3-5), indicating that the aptamer did not bind adenosine in this buffer. We then tested TNM (5 mM $MgCl_2$) and TNM (10 mM $MgCl_2$) buffers, containing 20 mM Tris (pH 7.5) and 300 mM NaCl with different concentrations of Mg^{2+}. In both TNM buffers, the fluorescence decreased after the addition of adenosine (Figure 3-5). This signal decrease indicates that the aptamer bound adenosine and the structure of DNA strands changed from dsDNA to ssDNA. These results from various buffers support that Mg^{2+} must be present for the aptamer to bind adenosine. We observed that further increases in Mg^{2+} concentration did not induce larger fluorescence quenching (data not shown). Therefore, the TNM (10 mM $MgCl_2$) buffer, which showed the largest decrease in fluorescence, was adopted as the adenosine-binding buffer for future 2DPC hydrogel measurements.

3.3.3 Adenosine Sensing in Buffer Solutions

The adenosine sensing response of our DNA-crosslinked 2DPC hydrogels was monitored by measuring the 2DPC particle spacing. Each 0.4×0.5 cm^2 piece of the 2DPC hydrogel was first immersed in a blank adenosine-binding buffer, TNM (10 mM $MgCl_2$), that did not contain adenosine for 10 min. After measuring the particle spacing, each hydrogel sample was then immersed in a buffer solution additionally containing adenosine ranging in concentration from 0 to 2 mM.

Figure 3-6 shows the changes in the particle spacing of 2DPC hydrogels over time at different concentrations of adenosine. The particle spacing change was calculated by subtracting

the initial particle spacing (at time = 0) from each sample. At larger concentrations of adenosine, the 2DPC hydrogel particle spacing increased more rapidly and to a greater extent than at smaller concentrations of adenosine. For example, at 2 mM adenosine, the particle spacing increased by more than 90 nm in 5 min, while at 20 μM adenosine, the particle spacing increased by only 30 nm after 60 min. Regardless of adenosine concentration, the adenosine-induced particle spacing changes began to level off as the aptamer−adenosine binding reaction gradually reached equilibrium over time.

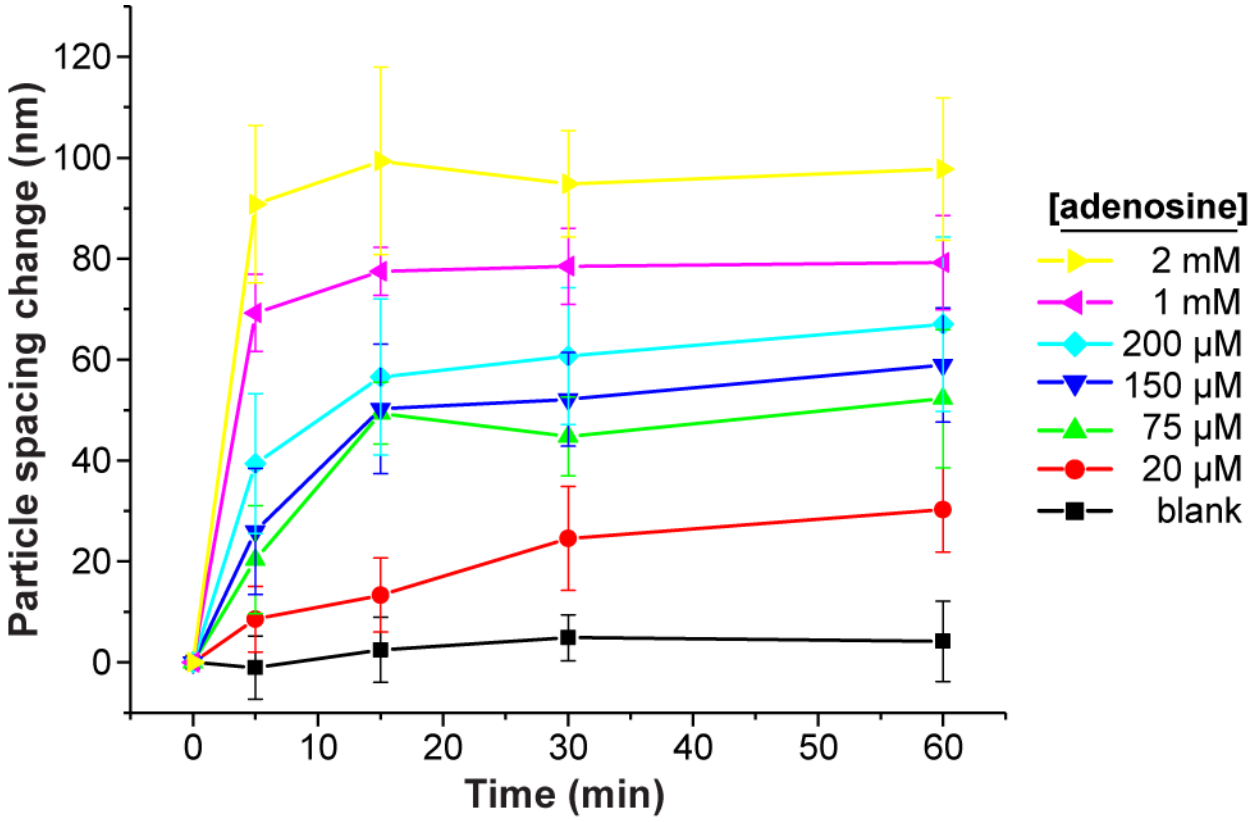

Figure 3-6. Time dependence of 2DPC hydrogel particle spacing on the concentration of adenosine. Error bars indicate standard deviations (n = 3).

The particle spacing change depends on the adenosine concentration because, as aforementioned in Section 3.1, aptamer−adenosine binding induces particle spacing increases. As the concentration of adenosine increases, the amount of aptamer−adenosine binding increases. The increased amount of aptamer−adenosine binding breaks a greater amount of hydrogel DNA crosslinks, generating a larger osmotic pressure that causes the hydrogel to increasingly swell. As the hydrogel swells more, the particle spacing of the embedded 2DPC array increases. This adenosine concentration-dependent response enables the use of these 2DPC hydrogels as adenosine sensors.

Since the particle spacing change depends on the amount of aptamer−adenosine binding, the dissociation constant (K_D) of the adenosine-binding aptamer in our 2DPC hydrogel can be estimated from the particle spacing data shown in Figure 3-6 (see the Supporting Information for detailed calculation). The K_D was estimated to be ∼68 μM, which is slightly larger than the reported K_D for the adenosine-binding aptamer in solution (∼10 μM).[34,39] We hypothesize that this decrease in binding affinity is caused by competitive binding of the aptamer with its complementary DNA and spatial restrictions that result from the aptamer's covalent attachment to the hydrogel network. Our estimated K_D is smaller than that reported for the duplexed adenosine-binding aptamer in solution (∼600 μM),[64] suggesting that the duplexed aptamer's binding affinity for adenosine has been largely preserved despite polymerization into the hydrogel network.

The concentration of adenosine can be determined from the particle spacing change at a short fixed detection time of 30 min. The particle spacing change data at T = 30 min were taken from Figure 3-6 and are replotted in Figure 3-7 as a function of adenosine concentration. Figure 3-7 shows that the particle spacing change was proportional to the logarithm of adenosine

concentration (20 µM to 2 mM adenosine). The linear fit line can be used as a calibration curve for adenosine detection. The LoD was calculated to be 13.9 µM (S/N = 3).

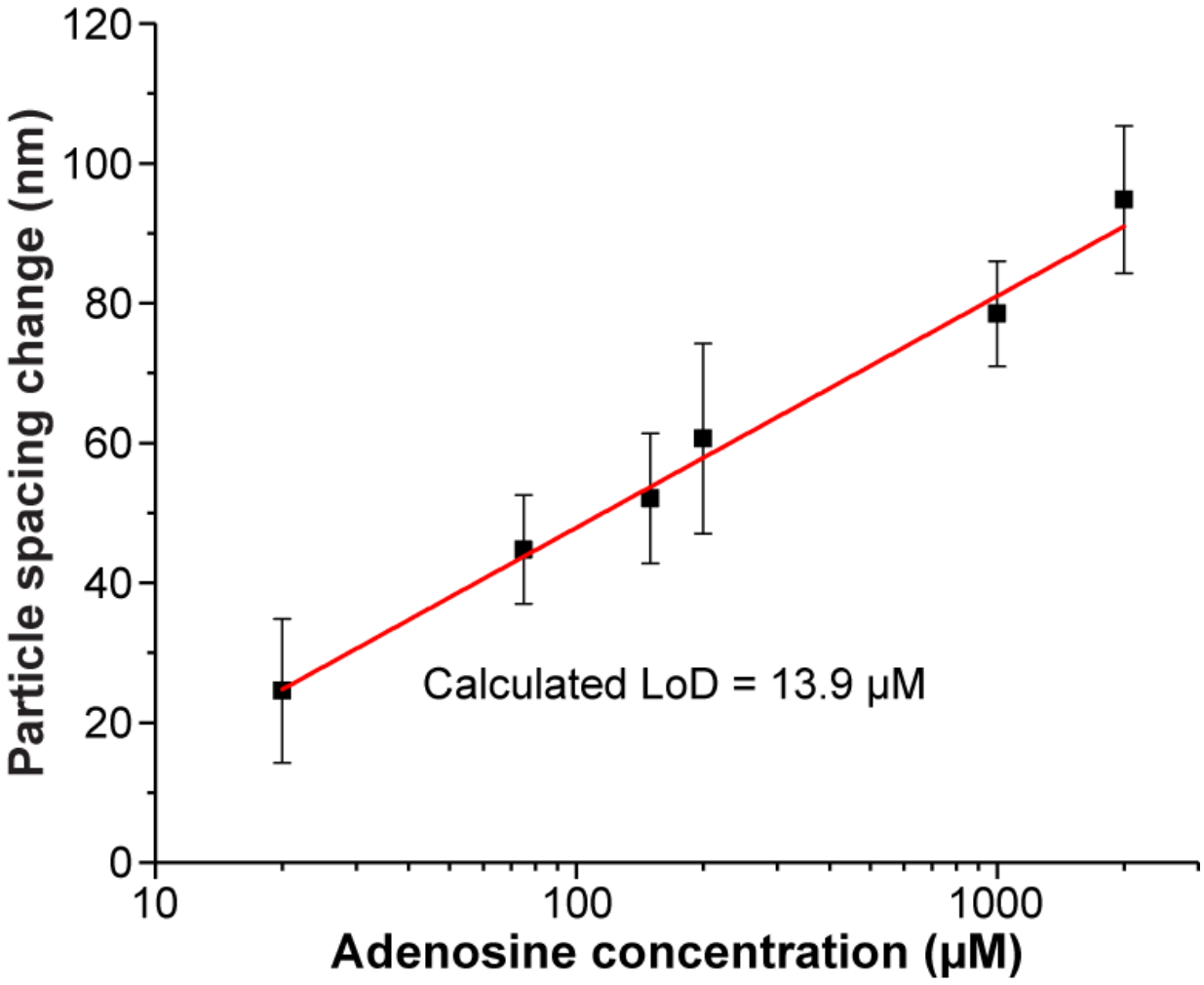

Figure 3-7. Particle spacing changes' dependence on adenosine concentration in buffer solutions (detection time = 30 min). The X-axis is in a logarithmic scale. The red line shows a linear fit (adjusted R-squared = 0.9874). Error bars indicate standard deviations (n = 3).

3.3.4 Selectivity of Adenosine-Sensing 2DPC Hydrogels

Figure 3-8 shows data supporting the selectivity of the adenosine-sensing 2DPC hydrogels. To verify that adenosine actuated the 2DPC hydrogel response, we first measured the 2DPC particle spacing in a blank solution containing no adenosine. Compared to samples containing adenosine, which showed a large increase in particle spacing, samples containing no adenosine showed negligible changes.

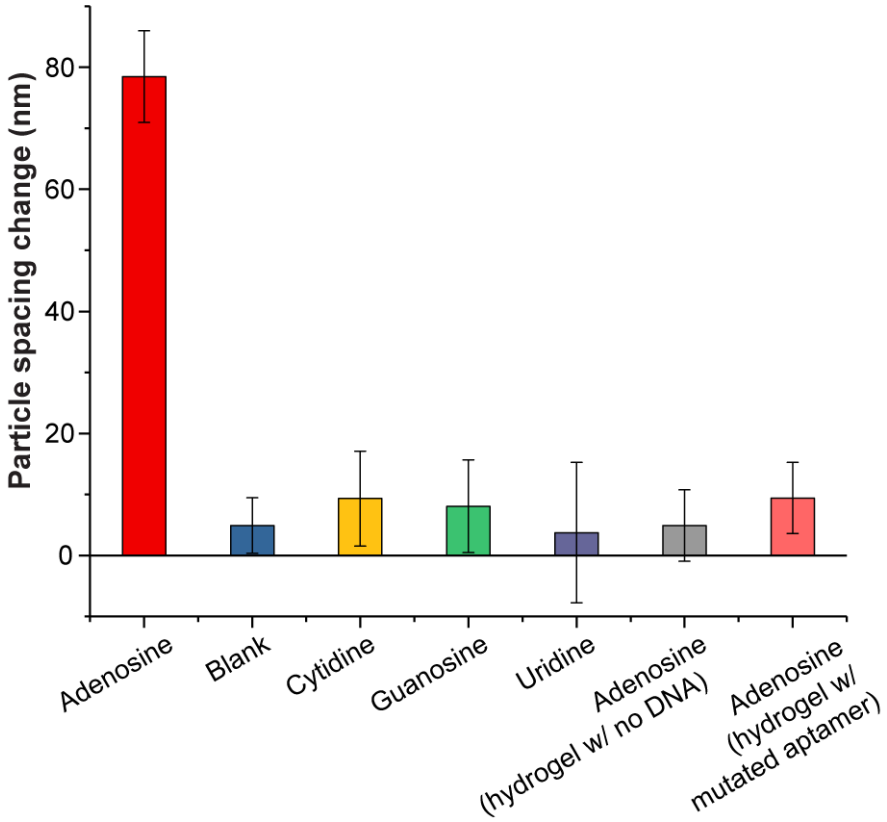

Figure 3-8. Selectivity of adenosine-sensing 2DPC hydrogels. The 2DPC hydrogel particle spacing was measured in a blank sample containing no nucleosides and in samples containing a 1 mM concentration of adenosine, cytidine, guanosine, or uridine. Each 2DPC hydrogel contained the adenosine-binding aptamer, except for a control containing no DNA ("hydrogel w/no DNA") and a control containing a mutated aptamer that did not bind adenosine ("hydrogel w/mutated aptamer"). The particle spacing change of each sample was measured after immersion in each solution for 30 min. Error bars indicate standard deviations (n = 3).

The adenosine aptamer used in our hydrogels has been reported to bind adenine derivatives such as adenosine but not bind other nucleosides.[34] To verify this selectivity for adenosine, we measured the 2DPC particle spacing of samples containing 1 mM solutions of cytidine, guanosine, or uridine, respectively (Figure 3-8). Compared to the large response in 1 mM adenosine, these other nucleosides induced negligible particle spacing changes, similar to that in the blank measurement. This indicates that the 2DPC hydrogel response was actuated by the selective adenosine-binding aptamer.

We further confirmed the selectivity of the adenosine-binding aptamer in actuating sensor response using two different controls (Figure 3-8). The first control hydrogel was fabricated with only acrylamide and MBAAm and without DNA. This sample showed a negligible particle spacing change in 1 mM adenosine solution because it did not have any target recognition groups. The other control hydrogel contained DNA crosslinks (hybridized between DNA strands 2 and 3) and was nearly identical to the adenosine-sensing hydrogels (hybridized between DNA strands 1 and 2). However, in the control, double mutations occurred within the adenosine-binding site of DNA strand 1, which inactivated the mutant strand (DNA strand 3) to adenosine.[64] This control also showed a negligible particle spacing change in adenosine solution, confirming that the active adenosine-binding aptamer was required to actuate adenosine sensing.

3.3.5 Adenosine Sensing in FBS

The response of the DNA-crosslinked 2DPC hydrogels was validated in a complex matrix, FBS. Based on preliminary data, serum proteins were removed to minimize interference. The protein-removed FBS solutions were diluted to 50% with the serum diluting buffer (40 mM Tris, pH 7.5; 19 mM $MgCl_2$; and 450 mM NaCl) to maintain the optimal adenosine-binding conditions.

As with measurements in buffer solutions, 2DPC hydrogel particle spacing changes were monitored after 30 min in serum solutions spiked with adenosine.

Figure 3-9 shows that, as in pure buffer, the particle spacing change was proportional to the logarithm of adenosine concentration (20 μM to 2 mM adenosine). Notably, the adenosine-induced particle spacing changes were slightly less in FBS solutions than in pure buffer. We hypothesize that this decrease in responsivity was caused by interferences in the serum matrix that inhibited the aptamer−adenosine binding. The calculated LoD was 26.7 μM adenosine (S/N = 3). While this LoD is greater than that in pure buffer (LoD = 13.9 μM), it is of the same order of magnitude. This indicates that the hydrogel sensor responsivity has been largely preserved and that our DNA-crosslinked 2DPC hydrogels can be used for adenosine detection in complex matrices.

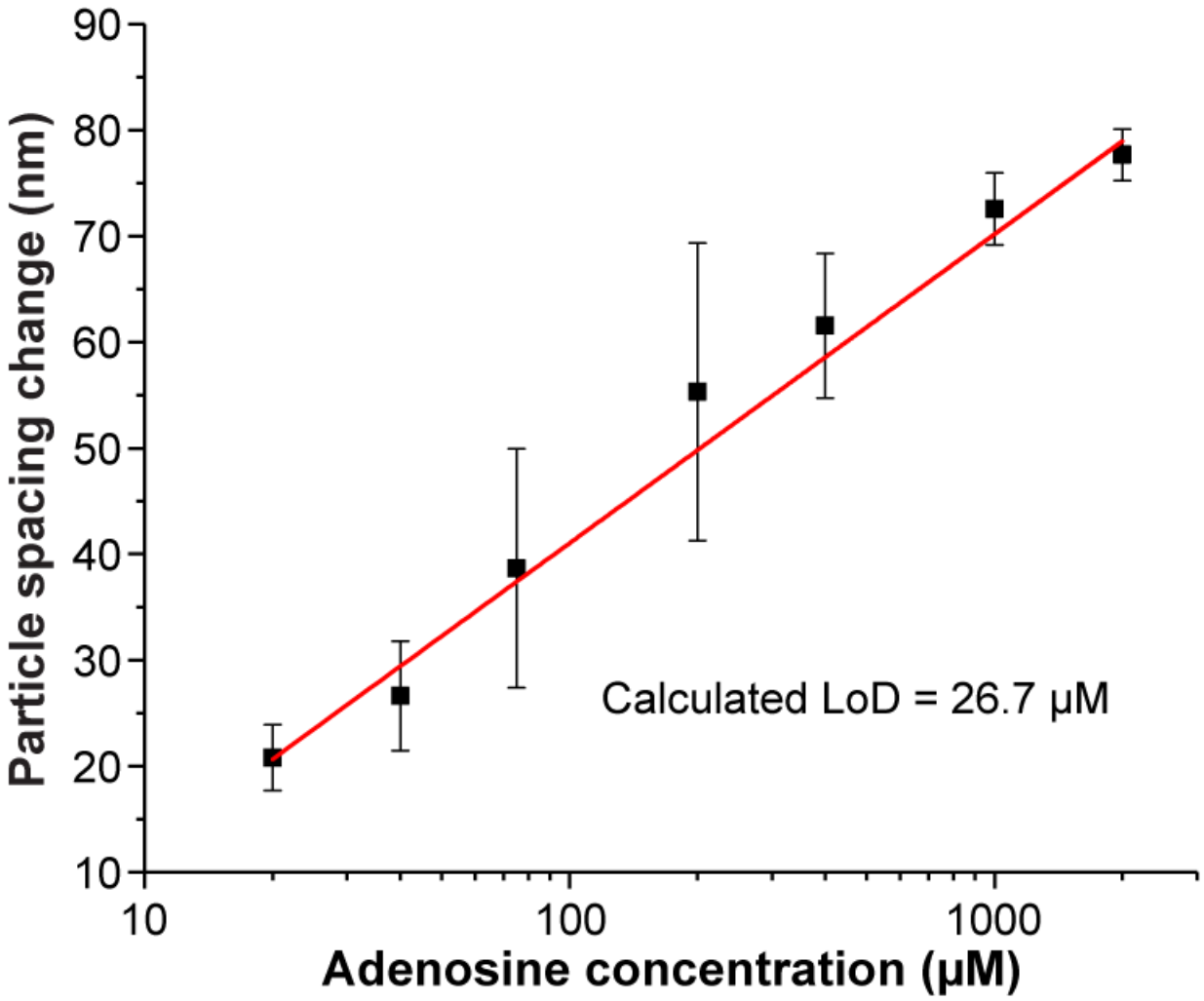

Figure 3-9. Particle spacing changes' dependence on adenosine concentration in 50% protein-removed FBS (detection time = 30 min). The X-axis is in a logarithmic scale. The red line shows a linear fit (adjusted R-squared = 0.9936). Error bars indicate standard deviations (n = 3).

3.4 Conclusions

We report the first fabrication of a DNA-crosslinked 2DPC hydrogel sensor that is actuated by a DNA aptamer. As proof of concept, we created an adenosine sensor using an adenosine-binding aptamer. When adenosine is introduced into the 2DPC hydrogel sensor, aptamer−adenosine binding occurs, breaking preformed DNA crosslinks and actuating the sensor response. As DNA crosslinks break, the hydrogel swells, increasing the particle spacing of the embedded 2DPC array. The linear range was observed to be 20 μM to 2 mM. The calculated LoDs are 13.9 μM in adenosine-binding buffer and 26.7 μM in 50% protein-removed FBS (detection time = 30 min).

The reported sensing motif using DNA-crosslinked 2DPC hydrogels is simple and rapid and requires only a laser pointer. We expect that the sample volume required for testing can be greatly reduced by using smaller hydrogel pieces. Additionally, our group has previously demonstrated the use of 2DPC and three-dimensional PC hydrogels for developing colorimetric sensors that give visual readouts similar to a pH strip.[29] Thus, while requiring additional studies, the aptamer-actuated hydrogels described in this work may have potential clinical applications, especially in resource-limited settings.

In future work, we plan to systematically investigate DNA crosslinks in the system to further understand the sensing mechanism and optimize the sensor performance. It is possible that the length of DNA strands, the number of hybridized base pairs, and the placement of the aptamer sequence within the longer DNA strand will impact sensor response.[64,65] We will test these properties along with the effect of DNA concentration on sensor performance.

While requiring further studies, we hypothesize that this sensing motif is generalizable and that other sensors can be easily fabricated by simply exchanging the aptamer that serves as a

molecular recognition group. High-affinity aptamers for a variety of analytes, ranging from small molecules to whole cells, have been reported. New aptamers can be developed rapidly, enabling the fabrication of sensors for a wide range of targets with ultralow LoDs. We are continuing to investigate the versatility of this novel sensing motif and are working to develop aptamer-actuated 2DPC hydrogel sensors that can detect proteins in solution.

3.4.1 Acknowledgements

The authors acknowledge the University of Pittsburgh for providing instrumentation and financial support.

3.5 References

(1) Mabey, D.; Peeling, R. W.; Ustianowski, A.; Perkins, M. D., Diagnostics for the Developing World. *Nat. Rev. Microbiol.* **2004,** 2, 231-240.

(2) Gubala, V.; Harris, L. F.; Ricco, A. J.; Tan, M. X.; Williams, D. E., Point of Care Diagnostics: Status and Future. *Anal. Chem.* **2012,** 84, 487-515.

(3) Sharma, S.; Zapatero-Rodríguez, J.; Estrela, P.; O'Kennedy, R., Point-of-Care Diagnostics in Low Resource Settings: Present Status and Future Role of Microfluidics. *Biosensors* **2015,** 5, 577-601.

(4) The Diabetes Control and Complications Trial Research Group, The Effect of Intensive Treatment of Diabetes on the Development and Progression of Long-Term Complications in Insulin-Dependent Diabetes Mellitus. *N. Engl. J. Med.* **1993,** 329, 977-986.

(5) Ellington, A. D.; Szostak, J. W., In Vitro Selection of RNA Molecules That Bind Specific Ligands. *Nature* **1990,** 346, 818-822.

(6) Tuerk, C.; Gold, L., Systematic Evolution of Ligands by Exponential Enrichment: RNA Ligands to Bacteriophage T4 DNA Polymerase. *Science* **1990,** 249, 505-510.

(7) Li, J.; Mo, L.; Lu, C.-H.; Fu, T.; Yang, H.-H.; Tan, W., Functional Nucleic Acid-Based Hydrogels for Bioanalytical and Biomedical Applications. *Chem. Soc. Rev.* **2016,** 45, 1410-1431.

(8) Cho, E. J.; Lee, J.-W.; Ellington, A. D., Applications of Aptamers as Sensors. *Annu. Rev. Anal. Chem.* **2009,** 2, 241-264.

(9) Chi, C.-W.; Lao, Y.-H.; Li, Y.-S.; Chen, L.-C., A Quantum Dot-Aptamer Beacon Using a DNA Intercalating Dye as the FRET Reporter: Application to Label-Free Thrombin Detection. *Biosens. Bioelectron.* **2011,** 26, 3346-3352.

(10) Zhu, Y.; Cai, Y.; Xu, L.; Zheng, L.; Wang, L.; Qi, B.; Xu, C., Building An Aptamer/Graphene Oxide FRET Biosensor for One-Step Detection of Bisphenol A. *ACS Appl. Mater. Interfaces* **2015,** 7, 7492-7496.

(11) Li, J.; Zhong, X.; Zhang, H.; Le, X. C.; Zhu, J.-J., Binding-Induced Fluorescence Turn-On Assay Using Aptamer-Functionalized Silver Nanocluster DNA Probes. *Anal. Chem.* **2012,** 84, 5170-5174.

(12) Xu, W.; Lu, Y., Label-Free Fluorescent Aptamer Sensor Based on Regulation of Malachite Green Fluorescence. *Anal. Chem.* **2010,** 82, 574-578.

(13) Subramanian, P.; Lesniewski, A.; Kaminska, I.; Vlandas, A.; Vasilescu, A.; Niedziolka-Jonsson, J.; Pichonat, E.; Happy, H.; Boukherroub, R.; Szunerits, S., Lysozyme Detection on Aptamer Functionalized Graphene-Coated SPR Interfaces. *Biosens. Bioelectron.* **2013,** 50, 239-243.

(14) Zhu, Z.; Feng, M.; Zuo, L.; Zhu, Z.; Wang, F.; Chen, L.; Li, J.; Shan, G.; Luo, S.-Z., An Aptamer Based Surface Plasmon Resonance Biosensor for the Detection of Ochratoxin A in Wine and Peanut Oil. *Biosens. Bioelectron.* **2015,** 65, 320-326.

(15) Kuang, H.; Chen, W.; Xu, D.; Xu, L.; Zhu, Y.; Liu, L.; Chu, H.; Peng, C.; Xu, C.; Zhu, S., Fabricated Aptamer-Based Electrochemical "Signal-Off" Sensor of Ochratoxin A. *Biosens. Bioelectron.* **2010,** 26, 710-716.

(16) Liu, Y.; Tuleouva, N.; Ramanculov, E.; Revzin, A., Aptamer-Based Electrochemical Biosensor for Interferon Gamma Detection. *Anal. Chem.* **2010,** 82, 8131-8136.

(17) Xu, X.; Goponenko, A. V.; Asher, S. A., Polymerized PolyHEMA Photonic Crystals: pH and Ethanol Sensor Materials. *J. Am. Chem. Soc.* **2008,** 130, 3113-3119.

(18) Tian, E.; Ma, Y.; Cui, L.; Wang, J.; Song, Y.; Jiang, L., Color-Oscillating Photonic Crystal Hydrogel. *Macromol. Rapid Commun.* **2009,** 30, 1719-1724.

(19) Ye, B.-F.; Zhao, Y.-J.; Cheng, Y.; Li, T.-T.; Xie, Z.-Y.; Zhao, X.-W.; Gu, Z.-Z., Colorimetric Photonic Hydrogel Aptasensor for the Screening of Heavy Metal Ions. *Nanoscale* **2012,** 4, 5998-6003.

(20) Du, X.; Zhai, J.; Li, X.; Zhang, Y.; Li, N.; Xie, X., Hydrogel-Based Optical Ion Sensors: Principles and Challenges for Point-of-Care Testing and Environmental Monitoring. *ACS Sensors* **2021,** 6, 1990-2001.

(21) Asher, S. A.; Alexeev, V. L.; Goponenko, A. V.; Sharma, A. C.; Lednev, I. K.; Wilcox, C. S.; Finegold, D. N., Photonic Crystal Carbohydrate Sensors: Low Ionic Strength Sugar Sensing. *J. Am. Chem. Soc.* **2003,** 125, 3322-3329.

(22) Sharma, A. C.; Jana, T.; Kesavamoorthy, R.; Shi, L.; Virji, M. A.; Finegold, D. N.; Asher, S. A., A General Photonic Crystal Sensing Motif: Creatinine in Bodily Fluids. *J. Am. Chem. Soc.* **2004,** 126, 2971-2977.

(23) Hu, X.; Li, G.; Li, M.; Huang, J.; Li, Y.; Gao, Y.; Zhang, Y., Ultrasensitive Specific Stimulant Assay Based on Molecularly Imprinted Photonic Hydrogels. *Adv. Funct. Mater.* **2008,** 18, 575-583.

(24) Jang, K.; Horne, W. S.; Asher, S. A., Human Serum Phenylpyruvate Quantification Using Responsive 2D Photonic Crystal Hydrogels via Chemoselective Oxime Ligation: Progress toward Developing Phenylalanine-Sensing Elements. *ACS Appl. Mater. Interfaces* **2020,** 12, 39612-39619.

(25) Rizvi, A. S.; Murtaza, G.; Yan, D.; Irfan, M.; Xue, M.; Meng, Z. H.; Qu, F., Development of Molecularly Imprinted 2D Photonic Crystal Hydrogel Sensor for Detection of L-Kynurenine in Human Serum. *Talanta* **2020,** 208, 120403.

(26) Peng, H.; Wang, S.; Zhang, Z.; Xiong, H.; Li, J.; Chen, L.; Li, Y., Molecularly Imprinted Photonic Hydrogels as Colorimetric Sensors for Rapid and Label-Free Detection of Vanillin. *J. Agric. Food. Chem.* **2012,** 60, 1921-1928.

(27) Cai, Z.; Zhang, J.-T.; Xue, F.; Hong, Z.; Punihaole, D.; Asher, S. A., 2D Photonic Crystal Protein Hydrogel Coulometer for Sensing Serum Albumin Ligand Binding. *Anal. Chem.* **2014,** 86, 4840-4847.

(28) Cai, Z.; Sasmal, A.; Liu, X.; Asher, S. A., Responsive Photonic Crystal Carbohydrate Hydrogel Sensor Materials for Selective and Sensitive Lectin Protein Detection. *ACS Sens.* **2017,** 2, 1474-1481.

(29) Cai, Z.; Smith, N. L.; Zhang, J.-T.; Asher, S. A., Two-Dimensional Photonic Crystal Chemical and Biomolecular Sensors. *Anal. Chem.* **2015,** 87, 5013-5025.

(30) Reese, C. E.; Baltusavich, M. E.; Keim, J. P.; Asher, S. A., Development of an Intelligent Polymerized Crystalline Colloidal Array Colorimetric Reagent. *Anal. Chem.* **2001,** 73, 5038-5042.

(31) Ye, B.; Wang, H.; Ding, H.; Zhao, Y.; Pu, Y.; Gu, Z., Colorimetric Logic Response Based on Aptamer Functionalized Colloidal Crystal Hydrogels. *Nanoscale* **2015,** 7, 7565-7568.

(32) Yang, H.; Liu, H.; Kang, H.; Tan, W., Engineering Target-Responsive Hydrogels Based on Aptamer−Target Interactions. *J. Am. Chem. Soc.* **2008,** 130, 6320-6321.

(33) Zhu, Z.; Wu, C.; Liu, H.; Zou, Y.; Zhang, X.; Kang, H.; Yang, C. J.; Tan, W., An Aptamer Cross-Linked Hydrogel as a Colorimetric Platform for Visual Detection. *Angew. Chem. Int. Ed.* **2010,** 49, 1052-1056.

(34) Huizenga, D. E.; Szostak, J. W., A DNA Aptamer That Binds Adenosine and ATP. *Biochemistry* **1995,** 34, 656-665.

(35) Lin, C. H.; Patei, D. J., Structural Basis of DNA Folding and Recognition in an AMP-DNA Aptamer Complex: Distinct Architectures but Common Recognition Motifs for DNA and RNA Aptamers Complexed to AMP. *Chem. Biol.* **1997,** 4, 817-832.

(36) Liu, J.; Lu, Y., Fast Colorimetric Sensing of Adenosine and Cocaine Based on a General Sensor Design Involving Aptamers and Nanoparticles. *Angew. Chem. Int. Ed.* **2006,** 45, 90-94.

(37) Li, F.; Zhang, J.; Cao, X.; Wang, L.; Li, D.; Song, S.; Ye, B.; Fan, C., Adenosine Detection by Using Gold Nanoparticles and Designed Aptamer Sequences. *Analyst* **2009,** 134, 1355-1360.

(38) Helwa, Y.; Dave, N.; Froidevaux, R.; Samadi, A.; Liu, J., Aptamer-Functionalized Hydrogel Microparticles for Fast Visual Detection of Mercury(II) and Adenosine. *ACS Appl. Mater. Interfaces* **2012,** 4, 2228-2233.

(39) Zhang, Z.; Oni, O.; Liu, J., New Insights into a Classic Aptamer: Binding Sites, Cooperativity and More Sensitive Adenosine Detection. *Nucleic Acids Res.* **2017,** 45, 7593-7601.

(40) Stojanovic, M. N.; de Prada, P.; Landry, D. W., Fluorescent Sensors Based on Aptamer Self-Assembly. *J. Am. Chem. Soc.* **2000,** 122, 11547-11548.

(41) Stojanovic, M. N.; de Prada, P.; Landry, D. W., Aptamer-Based Folding Fluorescent Sensor for Cocaine. *J. Am. Chem. Soc.* **2001,** 123, 4928-4931.

(42) Song, K.-M.; Jeong, E.; Jeon, W.; Jo, H.; Ban, C., A Coordination Polymer Nanobelt (CPNB)-Based Aptasensor for Sulfadimethoxine. *Biosens. Bioelectron.* **2012,** 33, 113-119.

(43) Bock, L. C.; Griffin, L. C.; Latham, J. A.; Vermaas, E. H.; Toole, J. J., Selection of Single-Stranded DNA Molecules That Bind and Inhibit Human Thrombin. *Nature* **1992,** 355, 564-566.

(44) Gopinath, S. C. B.; Sakamaki, Y.; Kawasaki, K.; Kumar, P. K. R., An Efficient RNA Aptamer against Human Influenza B Virus Hemagglutinin. *J. Biochem.* **2006,** *139*, 837-846.

(45) Cho, S.-J.; Woo, H.-M.; Kim, K.-S.; Oh, J.-W.; Jeong, Y.-J., Novel System for Detecting SARS Coronavirus Nucleocapsid Protein Using an ssDNA Aptamer. *J. Biosci. Bioeng.* **2011,** 112, 535-540.

(46) Chen, Z.; Wu, Q.; Chen, J.; Ni, X.; Dai, J., A DNA Aptamer Based Method for Detection of SARS-CoV-2 Nucleocapsid Protein. *Virologica Sinica* **2020,** 35, 351-354.

(47) Dwivedi, H. P.; Smiley, R. D.; Jaykus, L.-A., Selection and Characterization of DNA Aptamers with Binding Selectivity to Campylobacter Jejuni Using Whole-Cell SELEX. *Appl. Microbiol. Biotechnol.* **2010,** 87, 2323-2334.

(48) Rong, Y.; Chen, H.; Zhou, X.-F.; Yin, C.-Q.; Wang, B.-C.; Peng, C.-W.; Liu, S.-P.; Wang, F.-B., Identification of an Aptamer Through Whole Cell-SELEX for Targeting High Metastatic Liver Cancers. *Oncotarget* **2016,** 7, 8282-8294.

(49) Lv, Z.; Liu, J.; Zhou, Y.; Guan, Z.; Yang, S.; Li, C.; Chen, A., Highly Sensitive Fluorescent Detection of Small Molecules, Ions, and Proteins Using a Universal Label-Free Aptasensor. *Chem. Commun.* **2013,** 49, 5465-5467.

(50) Zhang, F.; Cao, L.; Yang, W., Preparation of Monodisperse and Anion-Charged Polystyrene Microspheres Stabilized with Polymerizable Sodium Styrene Sulfonate by Dispersion Polymerization. *Macromol. Chem. Phys.* **2010,** 211, 744-751.

(51) Zhang, J.-T.; Wang, L.; Lamont, D. N.; Velankar, S. S.; Asher, S. A., Fabrication of Large-Area Two-Dimensional Colloidal Crystals. *Angew. Chem. Int. Ed.* **2012,** 51, 6117-6120.

(52) Smith, N.; Coukouma, A.; Dubnik, S.; Asher, S., Debye Ring Diffraction Elucidation of 2D Photonic Crystal Self-Assembly and Ordering at the Air–Water Interface. *Phys. Chem. Chem. Phys.* **2017,** 19, 31813-31822.

(53) Zhang, J.-T.; Chao, X.; Liu, X.; Asher, S. A., Two-Dimensional Array Debye Ring Diffraction Protein Recognition Sensing. *Chem. Commun.* **2013,** 49, 6337-6339.

(54) Prevo, B. G.; Velev, O. D., Controlled, Rapid Deposition of Structured Coatings from Micro- and Nanoparticle Suspensions. *Langmuir* **2004,** 20, 2099-2107.

(55) Rehman, F. N.; Audeh, M.; Abrams, E. S.; Hammond, P. W.; Kenney, M.; Boles, T. C., Immobilization of Acrylamide-Modified Oligonucleotides by Co-Polymerization. *Nucleic Acids Res.* **1999,** 27, 649-655.

(56) Flory, P. J., *Principles of Polymer Chemistry*. Cornell University Press: 1953.

(57) Shibayama, M.; Tanaka, T., Volume Phase Transition and Related Phenomena of Polymer Gels. *Adv. Polym. Sci.* **1993,** 109, 1-62.

(58) Owczarzy, R.; You, Y.; Moreira, B. G.; Manthey, J. A.; Huang, L.; Behlke, M. A.; Walder, J. A., Effects of Sodium Ions on DNA Duplex Oligomers: Improved Predictions of Melting Temperatures. *Biochemistry* **2004,** 43, 3537-3554.

(59) Owczarzy, R.; Moreira, B. G.; You, Y.; Behlke, M. A.; Walder, J. A., Predicting Stability of DNA Duplexes in Solutions Containing Magnesium and Monovalent Cations. *Biochemistry* **2008,** 47, 5336-5353.

(60) Zhao, W.; Chiuman, W.; Lam, J. C. F.; McManus, S. A.; Chen, W.; Cui, Y.; Pelton, R.; Brook, M. A.; Li, Y., DNA Aptamer Folding on Gold Nanoparticles: From Colloid Chemistry to Biosensors. *J. Am. Chem. Soc.* **2008,** 130, 3610-3618.

(61) Xia, T.; Yuan, J.; Fang, X., Conformational Dynamics of an ATP-Binding DNA Aptamer: A Single-Molecule Study. *J. Phys. Chem. B* **2013,** 117, 14994-15003.

(62) Singer, V. L.; Jones, L. J.; Yue, S. T.; Haugland, R. P., Characterization of PicoGreen Reagent and Development of a Fluorescence-Based Solution Assay for Double-Stranded DNA Quantitation. *Anal. Biochem.* **1997,** 249, 228-238.

(63) Dragan, A. I.; Casas-Finet, J. R.; Bishop, E. S.; Strouse, R. J.; Schenerman, M. A.; Geddes, C. D., Characterization of PicoGreen Interaction with dsDNA and the Origin of Its Fluorescence Enhancement upon Binding. *Biophys. J.* **2010,** 99, 3010-3019.

(64) Nutiu, R.; Li, Y., Structure-Switching Signaling Aptamers. *J. Am. Chem. Soc.* **2003,** 125, 4771-4778.

(65) Munzar, J. D.; Ng, A.; Juncker, D., Duplexed Aptamers: History, Design, Theory, and Application to Biosensing. *Chem. Soc. Rev.* **2019,** 48, 1390-1419.

4.0 Aptamer-Functionalized 2D Photonic Crystal Hydrogels for Detection of Adenosine

This chapter was previously published in the journal *Microchimica Acta* as Shen, P.; Jang, K.; Cai, Z.; Zhang, Y.; Asher, S. A., Aptamer-Functionalized 2D Photonic Crystal Hydrogels for Detection of Adenosine. *Microchim. Acta* **2022**, 189, 418, and is reprinted with permission. P.S. and K.J. contributed equally. This manuscript was prepared by P.S. and K.J. with the assistance of Z.C., Y.Z. and S.A.A.

Aptamer-functionalized two-dimensional photonic crystal (2DPC) hydrogels are reported for the detection of adenosine (AD). As a molecular recognition group, an AD-binding aptamer was covalently attached to 2DPC hydrogels. This aptamer selectively and sensitively binds AD, changing the conformation of the aptamer from a long single-stranded structure (AD-free conformation) to a short hairpin loop structure (AD-bound conformation). The AD binding-induced changes of aptamer conformation reduced the volume of the 2DPC hydrogels and decreased the interparticle spacing of the 2DPC embedded in the hydrogel network. The particle spacing changes being dependent on AD concentration were determined by measuring 2DPC light diffraction using a simple laser pointer. The 2DPC hydrogel sensor showed a large particle spacing decrease of ~110 nm in response to 1 mM AD in phosphate-buffered saline (PBS). The linear range of determination of AD was 0.1 nM to 1 mM and the limit of detection was 0.09 nM. The hydrogel sensor response for real samples was then validated in diluted fetal bovine serum (FBS) and human urine. The average % difference in particle spacing changes measured between diluted FBS and pure PBS was only 3.99 %. In diluted human urine, the recoveries for the detection of AD were 95-101% and the relative standard deviations were 4.9-7.8%. The results demonstrate the potential applicability of the hydrogel sensor for real samples. This sensing concept, using the

aptamer-functionalized 2DPC hydrogels, allows for a simple, sensitive, selective, and reversible detection of AD. It may enable sensor development for a wide variety of analytes by simply changing the aptamer recognition group.

4.1 Introduction

Adenosine (AD), a purine nucleoside, plays essential roles in many biochemical processes, such as neuromodulation, neuroprotection, epigenetic control, cellular metabolism, and cell viability.[1–3] Importantly, the physiological concentration of AD can be elevated by many diseases or underlying conditions, including epilepsy,[4] paroxysmal supraventricular tachycardia,[5] and tumors.[6] Therefore, developing simple and reliable AD detection methods has been of great interest to understand specific physiological processes, diagnose and prognose certain diseases or conditions, and adjust treatments accordingly. Many conventional analytical techniques have been used to detect AD, including gas/liquid chromatography-mass spectrometry,[7] high-performance liquid chromatography,[8] and capillary electrophoresis.[9] These methods are sensitive and reliable; however, their clinical or practical applications are limited especially in resource-restricted environments because they require extensive sample preparation, complicated and expensive instruments, and well-trained personnel.

The development of simpler AD-sensing techniques has been explored using AD-binding aptamers. Aptamers, short single-stranded DNA or RNA oligonucleotides, have recently been utilized in the development of various sensors due to their high binding affinities to specific targets, ease of fabrication and modification, and low cost compared to antibodies.[10,11] Importantly, the AD-binding DNA aptamer has been extensively used as a model aptamer for the development of

aptasensors that employ numerous techniques and materials.[12] For example, various AD aptasensors were developed utilizing (1) colorimetric analysis with gold nanoparticles[13] or nanorods,[14] (2) fluorometric measurement with carbon quantum dots,[15] and (3) electrochemical techniques with ZnNi MOF microspheres.[16] Unfortunately, many of the current AD aptasensors can still be expensive and too complex to use.

Recently, stimuli-responsive photonic crystal (PC) hydrogels have been used to fabricate simple chemical and biological sensors for pH,[17] small molecules,[18-21] proteins,[22,23] microorganisms,[24-26] etc. In particular, hydrogel sensors using two-dimensional (2D) PC have attracted wide interest because they are more affordable, easier to fabricate, and require minimal sample preparation and instrumentation, compared to three-dimensional PC hydrogels.[27,28] The PC hydrogels were functionalized with different recognition agents that specifically interacted with their target analytes. The target recognition caused hydrogel volume phase transitions that altered the particle spacing of the PC embedded in each hydrogel.[27,29] The target-specific particle spacing changes then shifted the light diffraction, which was monitored to determine the analyte concentrations. Ye et al. were the first to report the development of three-dimensional PC hydrogels using aptamers as molecular recognition groups.[30,31] They utilized aptamers for the detection of heavy metal ions, Hg^{2+} and Pb^{2+}. Recently, Chen et al. demonstrated the use of 2DPC DNA hydrogels containing double-network structures for the detection of Ag^{+} and cysteine.[32] Jang et al. fabricated DNA strands crosslinked 2DPC hydrogels that responded to AD.[33] The response of the sensor was not reversible and the limit of detection (LoD) was of 26.7 μM, which was too high to be used for determining physiologically relevant AD concentrations in human blood (10 nM to 30 μM).[34]

Here, we report new 2DPC hydrogels that utilize the AD-binding aptamers for the sensitive, selective, and reversible detection of AD in real samples. As molecular recognition groups, the AD aptamers were covalently linked to the 2DPC hydrogels via post-polymerization functionalization reactions. Upon AD binding, the hydrogel volume was reduced because the conformation of the aptamer changed from a long single-stranded structure (AD-free conformation) to a short hairpin loop structure (AD-bound conformation). The reduction in hydrogel volume, which was induced by AD, in turn decreased the particle spacing of the 2DPC embedded in hydrogels. The particle spacing changes that depend on AD concentration were determined by measuring 2DPC light diffraction using a laser pointer without the need of any sophisticated instrumentation. The AD-sensing 2DPC hydrogels were first tested and optimized in phosphate-buffered saline (PBS) solutions. The linear range was observed to be 0.1 nM to 1 mM and the LoD was calculated to be 0.09 nM. It was also demonstrated that the 2DPC hydrogels can determine AD in real complex biological samples containing fetal bovine serum (FBS) and human urine. This shows that the hydrogel sensor could be used clinically for AD detection, especially in resource-constrained environments. In addition, these new aptamer-functionalized 2DPC hydrogels may provide a versatile strategy for developing various aptasensors by simply changing the aptamer recognition groups.

4.2 Experimental

4.2.1 Materials and Characterization

AD and adenosine deaminase (ADA, Type X, ≥130 units/mg) from bovine spleen were purchased from Sigma-Aldrich. Acrylamide (AAm), acrylic acid (AAc), N,N'-methylenebisacrylamide (Bis), 2-hydroxy-4 ′ -(2-hydroxyethoxy)-2-methylpropiophenone (Irgacure 2959), 1-ethyl-3-(3-dimethylaminopropyl) carbodiimide hydrochloride (EDC), thymidine, guanosine, cytidine, and uridine were acquired from Aladdin. N-hydroxysuccinimide (NHS) was purchased from Beijing J&K Scientific. The AD-binding DNA aptamer (5'-NH_2-$(CH_2)_6$-AGA GAA CCT GGG GGA GTA **T**TG CGG AG**G** AAG GT-$(CH2)_6$-NH_2-3') and a mutant DNA (5'-NH_2-$(CH_2)_6$-AGA GAA CCT GGG GGA GTA **A**TG CGG AG**C** AAG GT-$(CH_2)_6$-NH_2-3') were purchased from Sangon Biotech. FBS was purchased from Boehringer-Ingelheim. Human urine from a lung cancer patient was provided by the Yan'an University Affiliated Hospital. The human urine was centrifuged at 3000 g for 10 min and filtered through a nylon filter (0.45 μm). The filtered urine was diluted 15-fold with PBS and stored at -20 ℃ until use.[35] AAc was purified by distillation. All other chemicals were used as received. Monodisperse polystyrene (PS) particles of ~960 nm diameter were synthesized by dispersion polymerization.[36] The nanopure water (18.2 mΩ·cm) obtained from a Duro Pro 12FV water purification system was used for all experiments. PBS solutions (10 mM, pH = 7.4) were used for sample preparations.

The ordering of PS 2DPC was characterized using a scanning electron microscope (SEM) (JSM-7610F, JEOL) at an accelerating voltage of 15 kV after sputter-coating the samples with gold for 50 s at 10 mA (JEC-3000FC, JEOL).

4.2.2 Preparation of AD-Sensing 2DPC Hydrogels

First, 2DPC hydrogels (1 × 1 cm^2 pieces) were fabricated as previously reported.[22,37] The detailed procedures are described in the Electronic Supplementary Material. After the fabrication, the 2DPC hydrogels were functionalized with the AD-binding aptamers. Each 2DPC hydrogel was placed in 1 mL of PBS solution containing 15 mg of EDC and 3 mg of NHS for 1 h.[30,38] The hydrogels were washed with PBS for 6 min (the solution was changed every 2 min). Then, a 20 μL of AD-binding aptamer solution (10, 50, 100, or 150 μM aptamer in PBS) was pipetted onto each piece of the hydrogel. The hydrogels were stored at room temperature for 1 h and then at 4 ℃ overnight. Finally, the resulting aptamer-functionalized 2DPC hydrogels were washed with PBS for 6 h (the solution was changed every 1 h). The hydrogels were stored in PBS solution at room temperature prior to use.

4.2.3 2DPC Particle Spacing Measurement

AD-induced hydrogel volume changes were monitored by measuring the nearest neighbor particle spacing, d of the 2DPC hydrogels (Figure 4-1).[27]

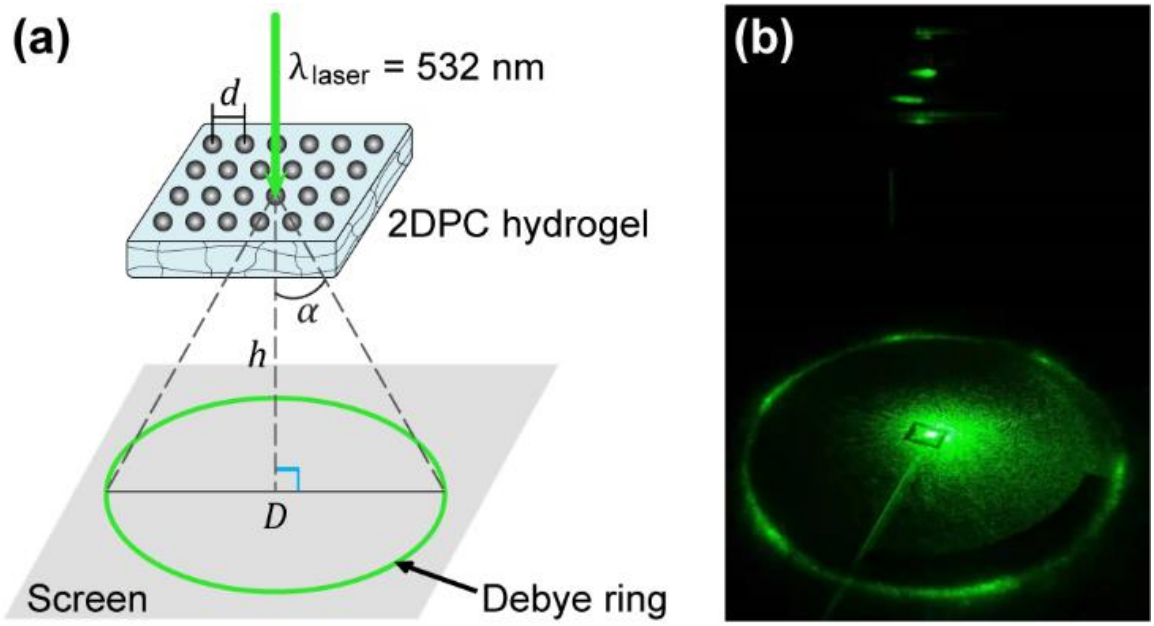

Figure 4-1. (a) Schematic illustration of experimental setup and (b) a photograph of Debye ring. When the 2DPC (hydrogel) is irradiated by a monochromatic light (laser pointer) along the array normal, the diffraction produces a Debye ring on the bottom screen. The 2DPC particle spacing can be calculated by measuring the Debye ring diameter.

According to the Bragg diffraction condition, when the hexagonally ordered 2DPC array is irradiated by light along the array normal, the array diffracts light at an angle α that depends on d and the incident light wavelength λ (eq 4-1).

$$\sin\alpha = 2\lambda/(\sqrt{3}d) \quad (4\text{-}1)$$

If the incident light is monochromatic, the diffraction produces a Debye ring on the screen because the 2DPC consists of numerous small rotationally disordered crystals.[39] Then, d can be calculated by measuring D the Debye ring diameter, and h the distance between the 2DPC array plane and the bottom screen (eq 4-2).[40]

$$d = \frac{4\lambda\sqrt{(D/2)^2 + h^2}}{\sqrt{3}D} \quad (4\text{-}2)$$

In this study, λ and h were fixed at 532 nm and 116 mm, respectively. For each particle spacing determination, 3 pieces of the 2DPC hydrogels were used, and 3 different d values were measured from each hydrogel. From the total 9 measurements, the averaged d and the standard deviation were calculated.

4.2.4 AD-Sensing in PBS

All solutions were freshly prepared in PBS and used immediately. Before taking each 2DPC particle spacing measurement, the hydrogels were washed with PBS solution for 1 h. **(1)** To optimize the hydrogel sensor composition, 2DPC hydrogels fabricated from different candidate polymerizable monomer solutions (listed in Table C-1 in Electronic Supplementary Material) were immersed in 2 mL solutions of 10 mM AD for 1 h. Then, the composition-optimized 2DPC hydrogels were used for subsequent experiments. **(2)** To test the AD-sensing kinetics, pieces of the 2DPC hydrogels were placed in 2 mL solutions of 10 nM, 1 μM, and 1 mM AD, respectively.

The particle spacing was measured at 10-min intervals. **(3)** To further test the particle spacing changes' dependence on AD, pieces of the 2DPC hydrogels were placed in 2 mL solutions containing various concentrations of AD (0.1 nM, 1 nM, 10 nM, 100 nM, 1 μM, 10 μM, 100 μM, 1mM, and 10 mM). After a fixed reaction time of 1 h, each particle spacing was measured. **(4)** To test the detection selectivity, pieces of the 2DPC hydrogels were placed separately in 2 mL solutions of 1 mM thymidine, guanosine, cytidine, or uridine To further test the anti-interference ability, 2DPC hydrogels were also placed in 2 mL solutions containing 1 mM each of AD, thymidine, guanosine, cytidine, and uridine together. After a reaction time of 1 h, each particle spacing was measured. **(5)** To show the reversibility of the AD-sensing, pieces of the 2DPC hydrogels were placed in 2 mL solutions of 100 μM AD for 1 h. Then, the 2DPC hydrogels were placed in 2 mL of ADA solutions (1.67 units/mL of ADA in PBS) for 4 h. The ADA-treated hydrogels were washed with PBS solution for 6 h (the solution was changed every 1 h). The same 2DPC hydrogels were further reacted with AD and ADA alternately over multiple cycles.

4.2.5 AD-Sensing in FBS and Human Urine

The response of the AD-sensing 2DPC hydrogels was validated in FBS and human urine. The FBS was diluted tenfold with PBS solution. The frozen human urine was thawed at room temperature and then further diluted to 450-fold with PBS solution.[35] Pieces of the 2DPC hydrogels were placed in 2 mL solutions of diluted FBS or human urine containing different concentrations of AD for 40 min. Then, the particle spacing change was monitored.

4.3 Results and Discussion

4.3.1 Preparation and Characterizations of AD-Sensing 2DPC Hydrogels

Scheme 4-1 summarizes the reactions used to prepare AD-sensing 2DPC hydrogels. As described above, 2DPC hydrogels were first prepared by co-polymerizing AAm, Bis (crosslinker), and AAc, and thus contained carboxyl groups. The carboxyl groups in the hydrogel were then activated by the reaction with EDC and NHS. Lastly, amide bonds were formed between the activated carboxyl groups in the hydrogels and the terminal amino groups in the aptamers. The resulting aptamer-functionalized 2DPC hydrogels were used for AD-sensing.

Scheme 4-1. Reactions used to prepare aptamer functionalized AD-sensing hydrogels

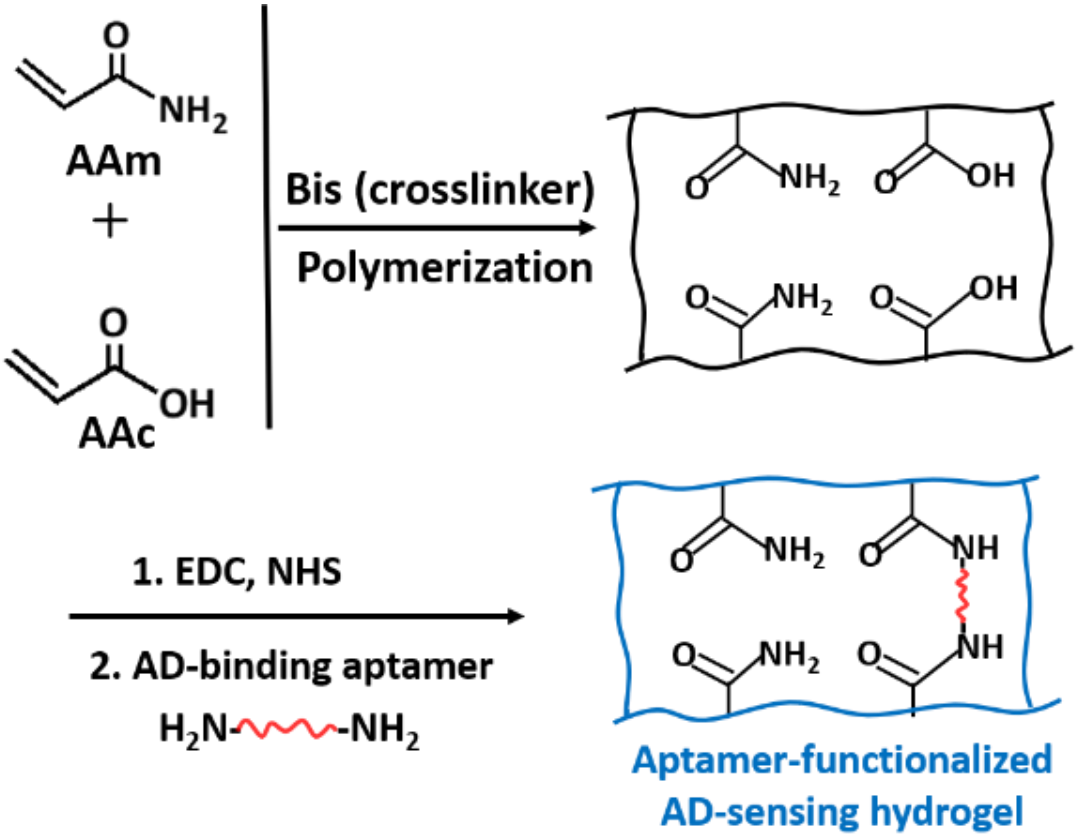

To confirm the aptamer attachment to the hydrogels, Fourier transform infrared (FTIR) spectra were measured. For FTIR characterization, the hydrogels without 2DPC were prepared and thoroughly washed with nanopure water to avoid any unwanted interference. Figure C-2 (Electronic Supporting Material) shows the FTIR spectra of hydrogels before and after the aptamer functionalization reaction. The appearance of a new absorption peak at 1232 cm^{-1}, which derives from the P = O vibration of the DNA phosphate backbone,[41] clearly demonstrates that the aptamer was covalently attached to the hydrogel polymer network.

We used SEM to show the hexagonal ordering of 2DPC array. Figure 4-2a shows the hcp structure of the 2DPC array prepared on a glass slide. The 2DPC array was embedded within the crosslinked 2DPC hydrogel network. Figure 4-2b shows that the hcp structure was maintained. After the 2DPC hydrogel was washed and equilibrated in PBS, the hydrogel swelled homogeneously. As a result, the 2DPC became non-close-packed by increasing the spacing between particles (Figure 4-2c). When illuminated by a white flashlight, the 2DPC array and 2DPC hydrogels diffracted the light at different angles depending on the wavelength, producing vivid iridescent colors (Figure 4-2 insets).

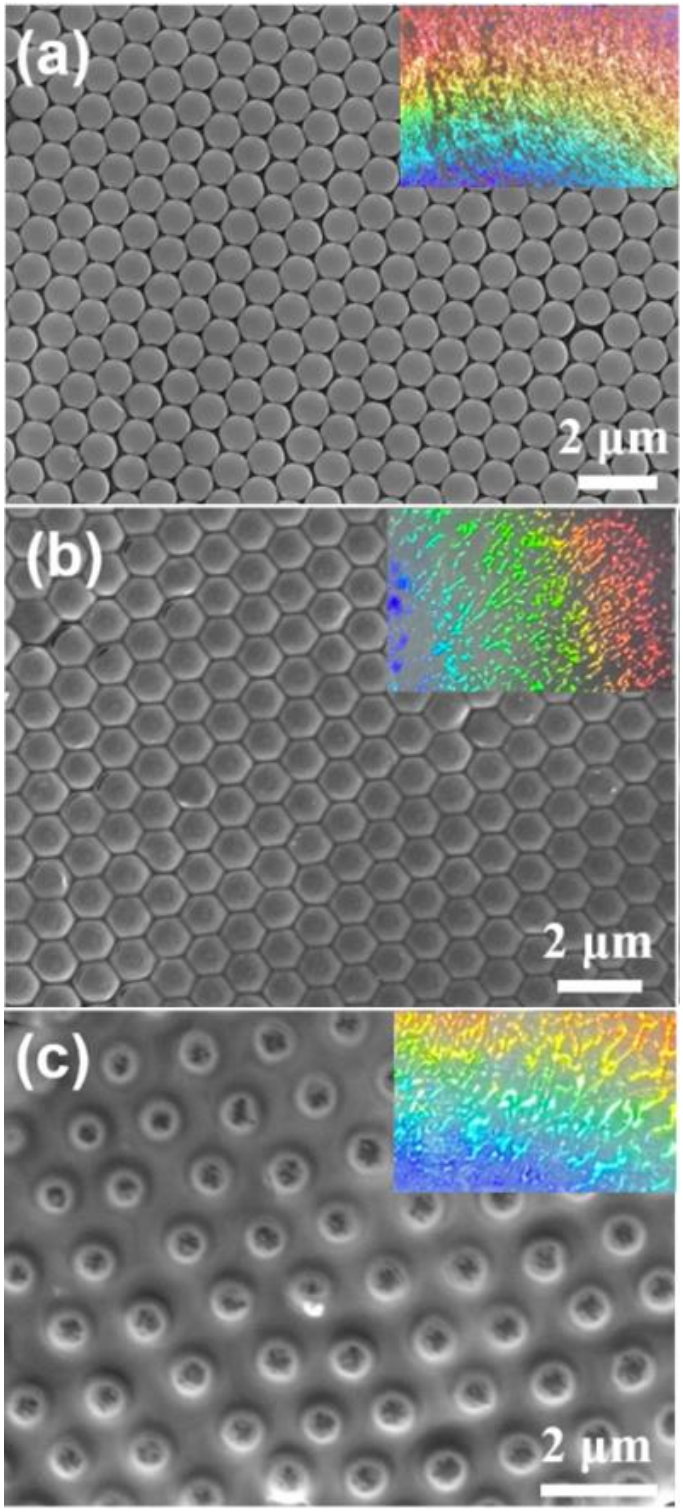

Figure 4-2. SEM images of (a) the hcp 2DPC on a glass slide, (b) the hcp 2DPC embedded in non-swollen hydrogel, and (c) the non-close-packed 2DPC embedded in swollen hydrogel. Insets: photographs of the corresponding samples showing iridescent colors when they are illuminated by a white flashlight.

4.3.2 Reversible AD-Sensing Mechanism Using Aptamer-Functionalized 2DPC Hydrogels

Figure 4-3 shows a schematic diagram of the AD-sensing mechanism that uses the aptamer-functionalized 2DPC hydrogels. When AD is introduced, the AD aptamer specifically binds AD and undergoes a conformational change from a long single-stranded structure (AD-free conformation) to a short hairpin loop structure (AD-bound conformation). Because AD aptamer strands are covalently attached to the hydrogel polymer network, the AD binding-induced aptamer conformation changes reduce the volume of the hydrogel. These changes also decrease the interparticle spacing of the 2DPC embedded in the hydrogel network. The particle spacing changes that are dependent on the AD concentration are monitored by measuring 2DPC light diffraction.

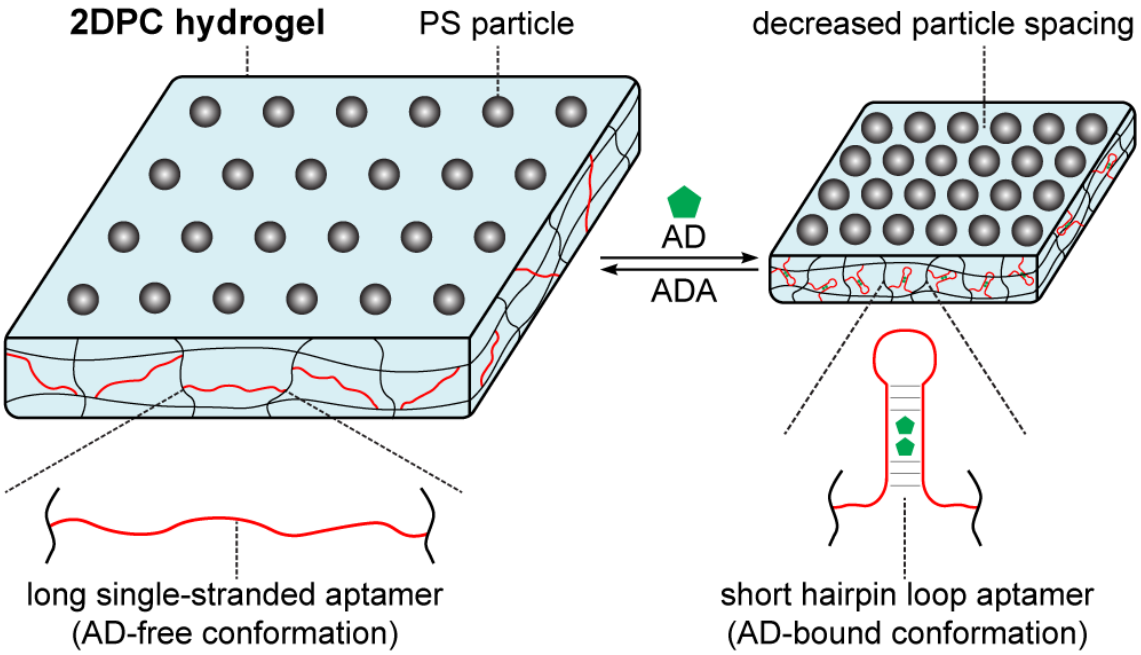

Figure 4-3. Reversible AD-sensing mechanism using aptamer functionalized 2DPC hydrogels. Upon binding AD, the AD aptamer undergoes a conformational change, which decreases the interparticle spacing of the 2DPC embedded in the hydrogel network. The AD-bound 2DPC hydrogels can be recycled by removing the bound AD with the enzyme ADA.

The 2DPC hydrogels can be reused by removing the bound AD with the enzyme ADA. When ADA is added to the system, the enzyme converts the bound AD to inosine.[42] The ADA enzymatic product, inosine, is no longer the target of the AD-binding aptamer. Thus, it can be removed from the 2DPC hydrogels by a subsequent PBS wash. Without the AD-binding, the conformation of the AD aptamer reverts to the long single-stranded structure (AD-free conformation). As a result, the AD-free 2DPC hydrogels swell back to the original state and can then be reused to detect AD.

4.3.3 AD-sensing in PBS

We optimized the 2DPC hydrogel sensor composition by testing various 2DPC hydrogels, prepared with different concentrations of AAc (C_{AAc}), Bis (C_{Bis}), and AD-binding aptamer ($C_{Aptamer}$), against the same concentration of AD. Figure C-3 shows the particle spacing changes of various 2DPC hydrogels in response to 10 mM AD in PBS for 1 h. As described, the AD-sensing 2DPC hydrogels showed particle spacing decreases upon AD binding. Importantly, a hydrogel with larger particle spacing decreases for the same concentration of AD indicates that the corresponding hydrogel is more sensitive to AD. Thus, the experimentally determined optimal C_{AAc}, C_{Bis}, and $C_{Aptamer}$ (3 wt%, 0.4 wt%, and 100 μM, respectively) were used for subsequent experiments (see the Electronic Supplementary Material for more detailed discussion).

Control experiments confirmed that the particle spacing changes of the 2DPC hydrogels were specifically induced by the aptamer-AD binding (Figure 4-4). First, 2DPC hydrogels were fabricated with the optimized amounts of monomers, but no aptamer was attached to the hydrogels. Without any aptamers attached, this control hydrogel showed a negligible particle spacing change of 2.8 ± 1.8 nm in response to 10 mM AD in PBS for 1 h. However, when the AD-binding aptamers

were attached, the 2DPC hydrogels showed a significant particle spacing change, -110.2 ± 2.3 nm, in response to the same concentration of AD. As an additional control, the aptamer-functionalized 2DPC hydrogels were immersed in a blank PBS solution for 1 h. After the immersion without AD, a negligible particle spacing change of -4.3 ± 2.7 nm was observed. Lastly, another control sample was prepared by attaching a mutant DNA to 2DPC hydrogels. The sequence of the mutant DNA was almost identical to that of the AD-binding aptamer; however, the inclusion of a double mutation in the AD-binding site caused the loss of the AD-binding ability.[43] In response to 10 mM AD, this control sample prepared with the mutant DNA showed a nearly negligible particle spacing change, -9.25 ± 2.6 nm. Therefore, these control experiments collectively confirmed that the aptamer-AD binding indeed induced the significant particle spacing changes.

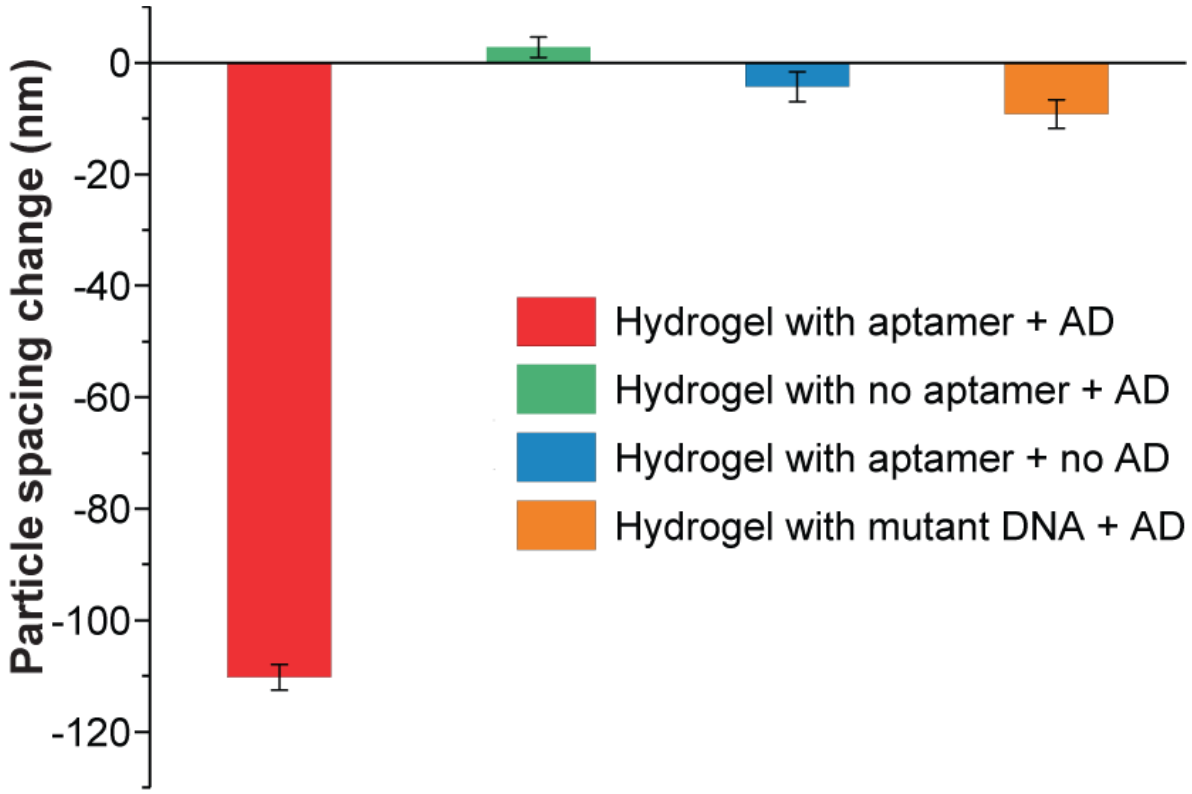

Figure 4-4. Particle spacing changes of different 2DPC hydrogels upon exposure to PBS solutions with and without AD. The mutant DNA does not bind AD. Error bars represent the mean ± standard deviation (*n* = *3*).

The composition-optimized 2DPC hydrogels were used to investigate the AD-induced particle spacing changes in PBS solutions. First, pieces of the 2DPC hydrogels were placed in 2 mL solutions of 10 nM, 1 μM, and 1 mM AD, respectively. To test the AD-sensing kinetics, the particle spacing was measured at 10-min intervals. Figure 4-5a shows that significant particle spacing changes were observed during the first 20 min regardless of AD concentration (C_{AD}). The initial particle spacing changes were presumably driven by the diffusion of AD into the hydrogel network. As the aptamer-AD binding reaction gradually reached equilibrium after 20 min, the particle spacing changes began to level off. Notably, larger particle spacing changes were observed with higher C_{AD}. This is because the higher the C_{AD}, the more AD molecules were bound to the aptamer, resulting in a greater hydrogel volume shrinkage.

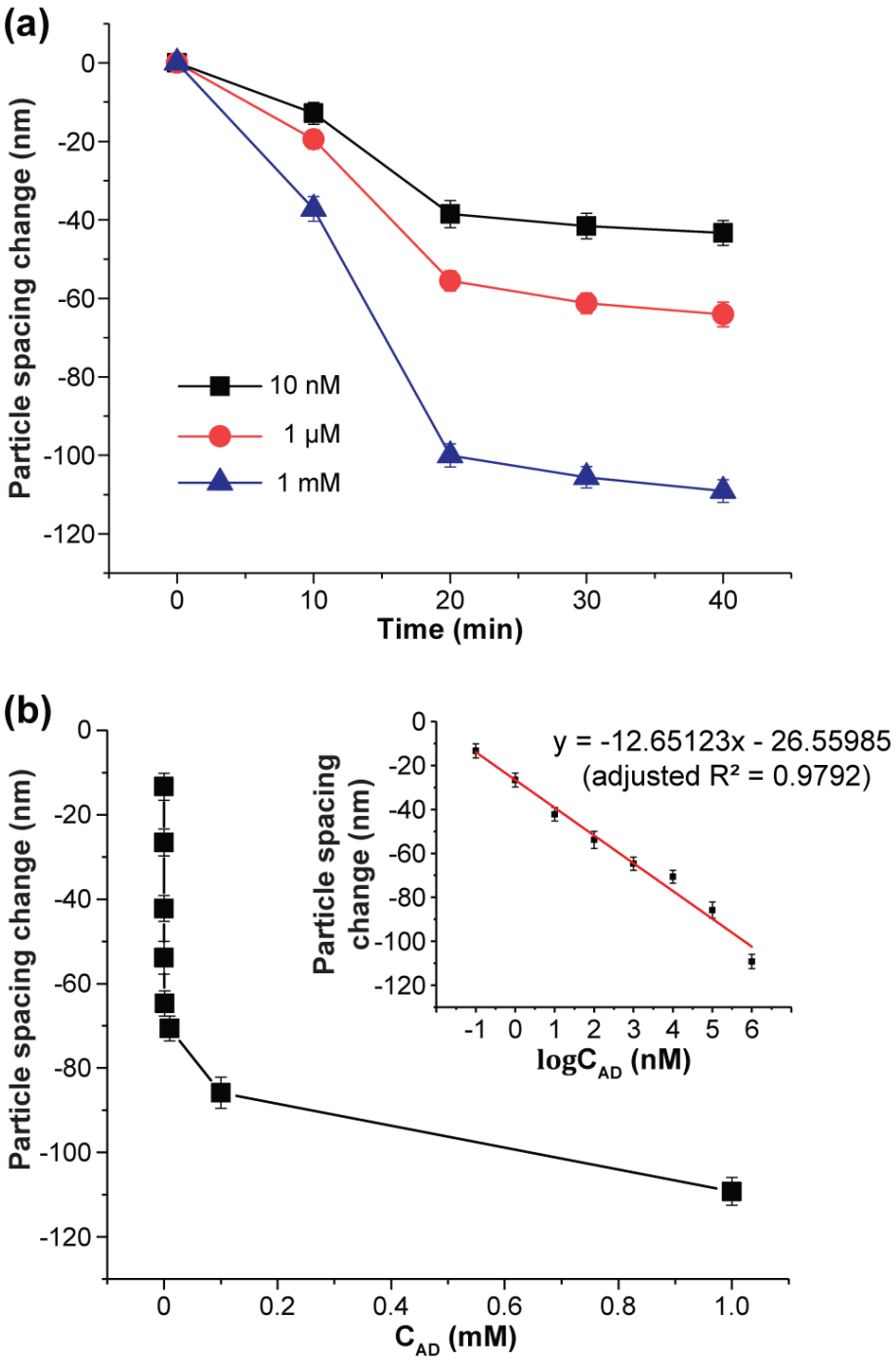

Figure 4-5. (a) Monitoring of the 2DPC particle spacing change in response to different concentrations of AD. (b) Particle spacing changes' dependence on C_{AD}. The C_{AD} were varied from 0.1 nM to 1 mM. After a fixed AD reaction time of 1 h, each particle spacing change was measured. The inset shows the particle spacing change vs. logC_{AD}. The red line shows a linear fit. Error bars represent the mean ± standard deviation (n = 3).

To further examine the particle spacing changes' dependence on C_{AD}, pieces of the 2DPC hydrogels were placed in solutions containing various C_{AD}. After a fixed reaction time of 1 h, each particle spacing change was measured. Figure 4-5b shows that the magnitude of the particle spacing change increased over the C_{AD} range from 0.1 nM to 1 mM. In addition, the magnitude of the particle spacing change showed a linear correlation with the logarithm of C_{AD} (Figure 4-5b inset). Again, as the C_{AD} increased, the more AD molecules were bound to the aptamer, resulting in greater particle spacing changes. Further increase in C_{AD} did not lead to a significantly larger particle spacing change, probably because the aptamer-AD binding reaction was saturated when the C_{AD} exceeded 1 mM. The LoD was calculated to be 0.09 nM AD (S/N = 3).

Compared with other AD aptasensors listed in Table C-2 (Electronic Supplementary Material), our 2DPC hydrogels have the advantages of both high sensitivity and wide detection range. Most importantly, the particle spacing changes that depend on AD concentration were measured using a simple laser pointer without the need of any sophisticated instrumentation, which is ideal for resource-limited settings. Furthermore, this new sensing strategy may be generalizable by simply changing the aptamer recognition groups for the development of other chemical and biological sensors.

We examined the selectivity of the 2DPC hydrogel sensor by placing pieces of hydrogels into four other chemically related nucleosides individually (1 mM of thymidine, guanosine, cytidine, and uridine). After a fixed reaction time of 1 h, the particle spacing change was measured. Figure 4-6a clearly shows that only AD induced a significant particle spacing change of -110.2 ± 3.3 nm. On the other hand, thymidine, guanosine, cytidine, and uridine all showed negligible or very small particle spacing changes, as the blank PBS solution did. This is because the AD aptamer specifically bound AD, not other nucleosides. Only when the specific binding occurred, significant

particle spacing changes were observed. The very small particle spacing changes by the other nucleosides were probably due to the very minor non-specific interactions between the AD aptamer and these nucleosides. The 2DPC hydrogels were also tested with a mixture containing all nucleosides (1 mM each of AD, thymidine, guanosine, cytidine, and uridine together). After the same reaction time of 1 h, a particle spacing change of -109.6 ± 3.1 nm was observed, which is very similar to that in 1 mM AD, -110.2 ± 3.3 nm. The results demonstrate that the AD detection does not significantly change even in the presence of other chemically relevant species, proving the excellent anti-interference ability of our aptamer-functionalized 2DPC hydrogels.

Figure 4-6b demonstrates that the AD-induced particle spacing changes are reversible, as described in the AD-sensing mechanism section. The initial particle spacing of fresh 2DPC hydrogels was measured at 1452.5 ± 3.6 nm. The particle spacing decreased to 1368.1 ± 2.8 nm after the reaction with 100 μM AD. Then, the same AD-reacted 2DPC hydrogels were placed in 2 mL of ADA solutions (1.67 units/mL of ADA in PBS). After 4 h of ADA treatment and 6 h of subsequent PBS wash, the particle spacing of the 2DPC hydrogels increased to 1446.8 ± 4.5 nm, similar to the initial state. The same 2DPC hydrogels were further reacted with AD and ADA alternately over multiple cycles, showing consistent particle spacing changes after each reaction. The results clearly indicate that the AD-induced particle spacing changes are reversible and the 2DPC hydrogels are reusable after the ADA enzymatic treatment.

Lastly, we tested the sensor stability using 2DPC hydrogels stored in PBS solutions at 4 ℃ for 1 to 2 months. The aged hydrogels were reacted with AD and then showed particle spacing

changes very similar to those of freshly prepared 2DPC hydrogels. This demonstrates that the AD-sensing 2DPC hydrogels are stable for a long time.

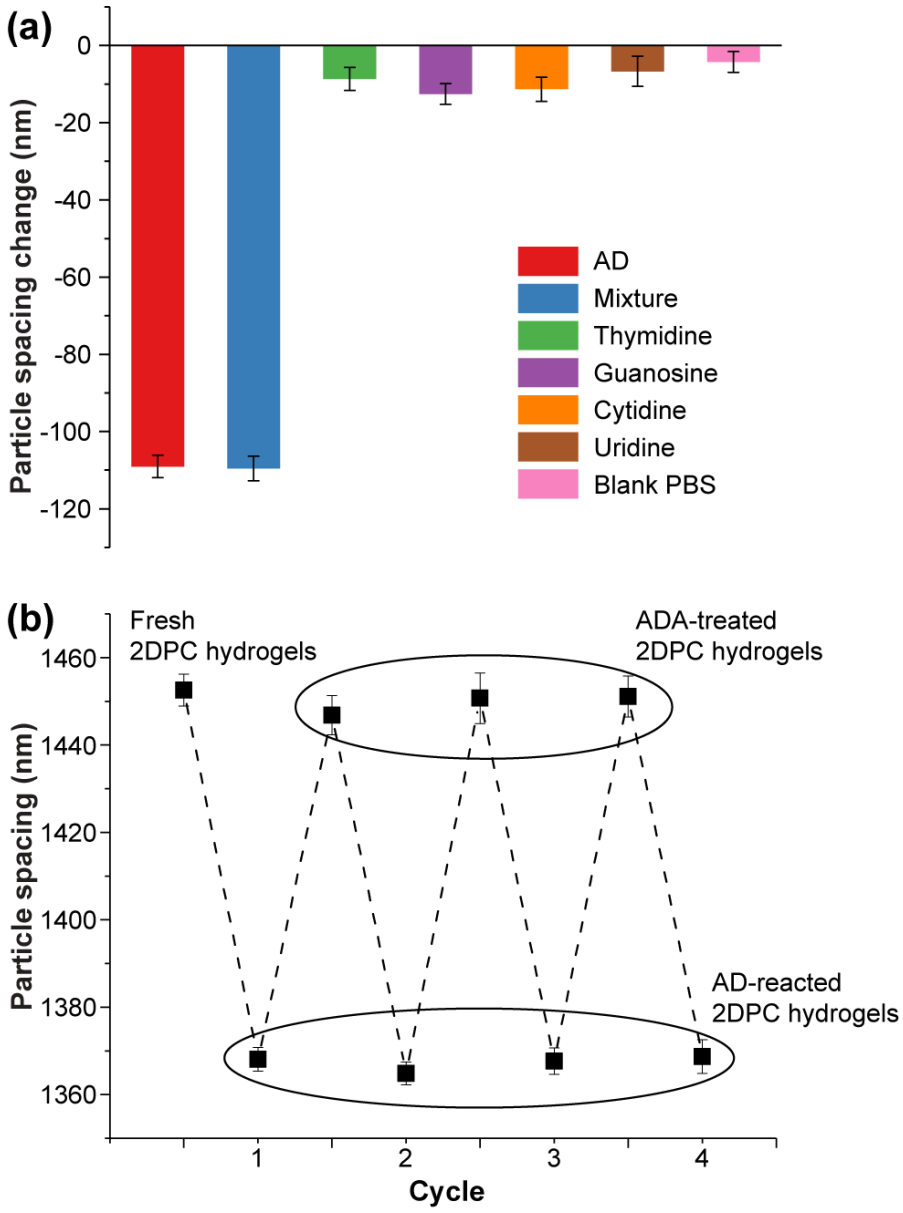

Figure 4-6. (a) Selectivity and anti-interference ability of the AD-sensing 2DPC hydrogels. 2DPC hydrogels were reacted with other chemically relevant nucleosides individually (thymidine, guanosine, cytidine, and uridine). The mixture contained AD, thymidine, guanosine, cytidine, and uridine together. After a reaction time of 1 h, each particle spacing change was monitored. (b) Reversible detection of AD. Fresh 2DPC hydrogels were alternately reacted with AD (100 μM) and ADA (1.67 units/mL). After each reaction, the particle spacing was monitored. Error bars represent the mean ± standard deviation (n = 3).

4.3.4 AD-Sensing in FBS and Human Urine

The response of the AD-sensing 2DPC hydrogels was validated in more complex biological environments. In order to minimize unexpected interference, the real samples were diluted in PBS solutions and the AD concentrations were determined. The circulating concentrations of AD are in the range from 10 nM to 30 μM, although there are differences in the reported concentrations.[34] Based on this range, we chose the spiked concentrations of AD (1 nM, 10 nM, 100 nM, 1 μM, and 10 μM) in tenfold diluted FBS. Considering the dilution factor, we detected AD concentrations in FBS from 10 nM to 100 μM, which includes the reported range. First, the baseline concentration of AD in the unspiked FBS was observed to be below the LoD (0.09 nM AD) of our method. Then, pieces of the 2DPC hydrogels were placed in 2 mL of tenfold diluted FBS solutions containing different concentrations of AD. Figure 4-7 shows the particle spacing changes measured in diluted FBS. As a comparison, the particle spacing change curve measured in pure PBS was plotted together (data taken from Figure 4-5b). As in the PBS solution, larger particle spacing changes were observed with higher C_{AD}. The average % difference in particle spacing changes measured between diluted FBS and pure PBS was only 3.99% (see the Electronic Supplementary Material for detailed calculation). This indicates that the AD concentration in unknown serum samples can be determined using the linear correlation acquired in PBS.

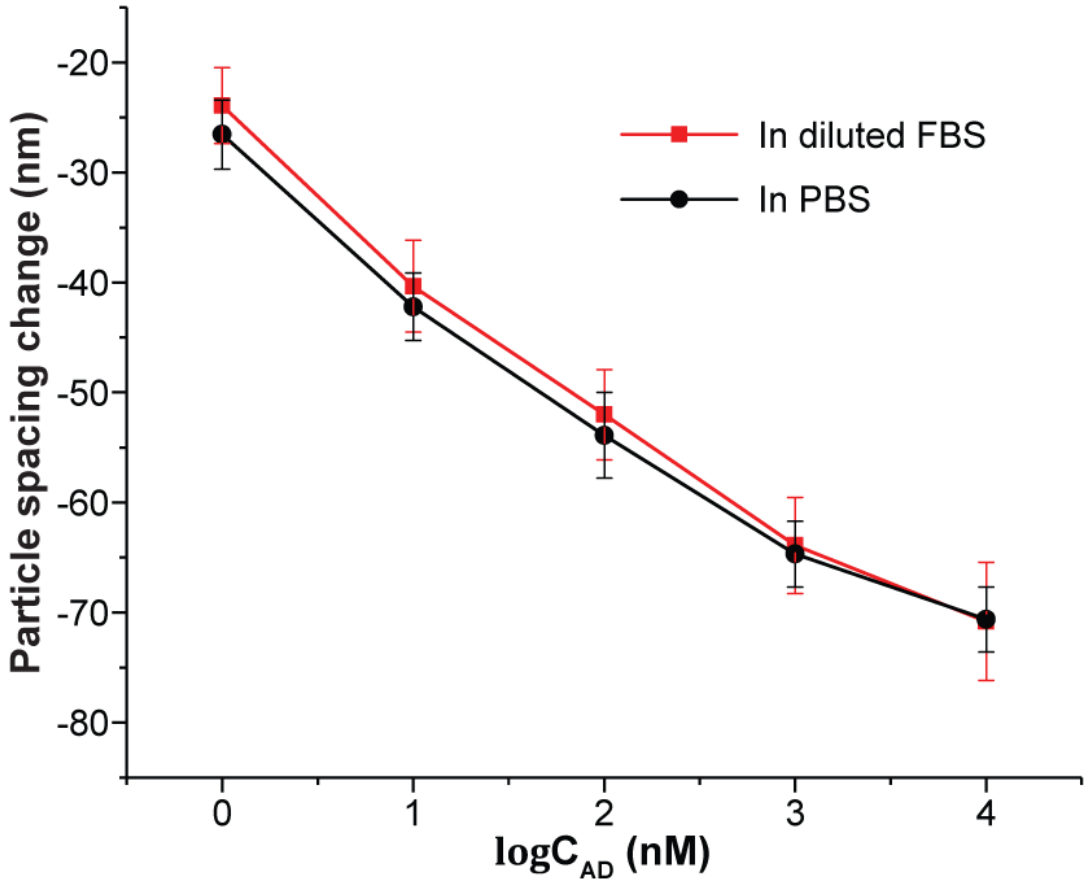

Figure 4-7. Particle spacing changes' dependence on C_{AD}, measured in tenfold diluted FBS. The *X*-axis has a logarithmic scale. Error bars represent the mean ± standard deviation (*n* = 3).

Next, the 2DPC hydrogel sensor response was tested in human urine. Urinary AD concentrations in healthy human are typically in the μM range. It is reported that the concentration of urinary AD can be elevated by many diseases or underlying conditions. For example, the urinary AD concentration can be tenfold or much higher in cancer patients[49]. Thus, we chose the spiked concentrations of AD (90, 490, and 990 nM) in 450-fold diluted human urine. First, the baseline AD concentration in the diluted urine was determined at 10 nM using the particle spacing measurements and the calibration curve in Figure 4-5b inset. Then, the urine samples were spiked with known concentrations of AD (90, 490, and 990 nM AD, respectively). Likewise, the C_{AD} in the spiked urine samples were determined using the particle spacing measurements and the same calibration curve. The % recoveries for the detection of AD were 95-101% and the relative standard deviations (RSD) were 4.9-7.8%, showing adequate accuracy and precision (Table 4-1). Considering the dilution factor and the baseline AD concentration in the unspiked sample, we detected AD concentrations in human urine from 4.5 to 450 μM, which are relevant to the both normal and abnormal physiological levels. Combining the results above, it was demonstrated that the reported 2DPC hydrogels can be used to detect AD in more complex matrices.

Table 4-1. Determination of AD in diluted human urine (*n* = 3)

Added (nM)	Found (nM)	Recovery (%)	RSD (%) (*n* = 3)
0	10	-	0.94
90	101	101	7.8
490	476	95.2	4.9
990	971	97.1	5.8

4.4 Conclusions

We developed aptamer-functionalized 2DPC hydrogels for the selective, sensitive, and reversible detection of AD. The hydrogel sensor utilized the AD-binding aptamer as a recognition group, which induced particle spacing changes upon AD binding. The AD-induced particle spacing changes were monitored by simple 2DPC light diffraction measurements. The AD-sensing methodology was first tested in PBS and showed a calculated LoD of 0.09 nM. The hydrogel sensor response for real samples was then validated in diluted FBS and human urine. This new 2DPC hydrogel aptasensor for AD was fabricated from inexpensive materials. It provides a simple readout with minimal sample preparation or instrumentation. Although further work is needed, these 2DPC hydrogels may have important clinical applications, especially in resource-limited settings. More importantly, this new sensing strategy may be generalizable by simply changing the aptamer recognition groups for the development of other chemical and biological sensors.

4.4.1 Acknowledgements

The authors gratefully acknowledge the National Natural Science Foundation of China (grant no. 21663032 to Y. Z.), the Open Sharing Platform for Scientific and Technological Resources of Shaanxi Province (grant no. 2021PT-004 to Y. Z.), the China Scholarship Council (grant no. 201701000001 to Y. Z.), the National Natural Science Foundation of China (grant no. 22076008 to Z. C.), and the Defense Threat Reduction Agency (grant no. HDTRA1-15-1-0038 to S. A.) for financial support.

4.5 References

(1) Winn, H. R.; Rubio, G. R.; Berne, R. M., The Role of Adenosine in the Regulation of Cerebral Blood Flow. *J. Cereb. Blood Flow Metab.* **1981**, 1, 239-244.

(2) Ross, A. E.; Venton, B. J., Nafion–CNT Coated Carbon-Fiber Microelectrodes for Enhanced Detection of Adenosine. *Analyst* **2012**, 137, 3045-3051.

(3) Cunha, R. A., How Does Adenosine Control Neuronal Dysfunction and Neurodegeneration? *J. Neurochem.* **2016**, 139, 1019-1055.

(4) Masino, S. A.; Kawamura Jr., M.; Ruskin, D. N., Adenosine Receptors and Epilepsy: Current Evidence and Future Potential. *Int. Rev. Neurobiol.* **2014**, 119, 233-255.

(5) DiMarco, J. P.; Sellers, T. D.; Lerman, B. B.; Greenberg, M. L.; Berne, R. M.; Belardinelli, L., Diagnostic and Therapeutic Use of Adenosine in Patients with Supraventricular Tachyarrhythmias. *J. Am. Coll. Cardiol.* **1985**, 6, 417-425.

(6) Bahreyni, A.; Samani, S. S.; Ghorbani, E.; Rahmani, F.; khayami, R.; Toroghian, Y.; Behnam-Rassouli, R.; Khazaei, M.; Ryzhikov, M.; Parizadeh, M. R.; Hasanzadeh, M.; Avan, A.; Hassanian, S. M., Adenosine: An Endogenous Mediator in the Pathogenesis of Gynecological Cancer. *J. Cell. Physiol.* **2018**, 233, 2715-2722.

(7) Huang, L.-F.; Guo, F.-Q.; Liang, Y.-Z.; Li, B.-Y.; Cheng, B.-M., Simple and Rapid Determination of Adenosine in Human Synovial Fluid with High Performance Liquid Chromatography–Mass Spectrometry. *J. Pharm. Biomed. Anal.* **2004**, 36, 877-882.

(8) Jeon, J.-S.; Kim, H.-T.; Kim, M.-G.; Oh, M.-S.; Hong, S.-R.; Yoon, M.-H.; Cho, S.-M.; Shin, H.-C.; Shim, J.-H.; Ramadan, A.; Abd El-Aty, A. M., Simultaneous Determination of Water-Soluble Whitening Ingredients and Adenosine in Different Cosmetic Formulations by High-Performance Liquid Chromatography Coupled with Photodiode Array Detection. *Int. J. Cosmet. Sci.* **2016**, 38, 286-293.

(9) Fang, H.; Pajski, M. L.; Ross, A. E.; Venton, B. J., Quantitation of Dopamine, Serotonin and Adenosine Content in a Tissue Punch From a Brain Slice Using Capillary Electrophoresis with Fast-Scan Cyclic Voltammetry Detection. *Anal. Methods* **2013**, 5, 2704-2711.

(10) Liu, J.; Cao, Z.; Lu, Y., Functional Nucleic Acid Sensors. *Chem. Rev.* **2009**, 109, 1948-1998.

(11) Xiong, X.; Wu, C.; Zhou, C.; Zhu, G.; Chen, Z.; Tan, W., Responsive DNA-Based Hydrogels and Their Applications. *Macromol. Rapid Commun.* **2013**, 34, 1271-1283.

(12) Li, Y.; Liu, J., Aptamer-Based Strategies for Recognizing Adenine, Adenosine, ATP and Related Compounds. *Analyst* **2020**, 145, 6753-6768.

(13) Ma, L.; Ma, L.; Su, M.; Wang, Z., Exonuclease III Assisted Aptasensor for Adenosine Detection with Gold Nanoparticle Probes. *Anal. Methods* **2014**, 6, 4366-4372.

(14) Zhang, X.; Kong, C.; Liu, Q.; Zuo, X.; Li, K.; Chen, Z., Colorimetric Adenosine Assay Based on the Self-Assembly of Aptamer-Functionalized Gold Nanorods. *Microchim. Acta* **2019**, 186, 587.

(15) Yousefi, S.; Saraji, M., Developing a Fluorometric Aptasensor Based on Carbon Quantum Dots and Silver Nanoparticles for the Detection of Adenosine. *Microchem. J.* **2019**, 148, 169-176.

(16) Tian, K.; Ma, Y.; Liu, Y.; Wang, M.; Guo, C.; He, L.; Song, Y.; Zhang, Z.; Du, M., Hierarchically Structured Hollow Bimetallic ZnNi MOF Microspheres as a Sensing Platform for Adenosine Detection. *Sens. Actuators B Chem.* **2020**, 303, 127199.

(17) Shin, J.; Braun, P. V.; Lee, W., Fast Response Photonic Crystal pH Sensor Based on Templated Photo-Polymerized Hydrogel Inverse Opal. *Sens. Actuators B Chem.* **2010**, 150, 183-190.

(18) Sharma, A. C.; Jana, T.; Kesavamoorthy, R.; Shi, L.; Virji, M. A.; Finegold, D. N.; Asher, S. A., A General Photonic Crystal Sensing Motif: Creatinine in Bodily Fluids. *J. Am. Chem. Soc.* **2004**, 126, 2971-2977.

(19) Zhang, C.; Cano, G. G.; Braun, P. V., Linear and Fast Hydrogel Glucose Sensor Materials Enabled by Volume Resetting Agents. *Adv. Mater.* **2014**, 26, 5678-5683.

(20) Jang, K.; Horne, W. S.; Asher, S. A., Human Serum Phenylpyruvate Quantification Using Responsive 2D Photonic Crystal Hydrogels via Chemoselective Oxime Ligation: Progress toward Developing Phenylalanine-Sensing Elements. *ACS Appl. Mater. Interfaces* **2020**, 12, 39612-39619.

(21) Chen, Q.; Wei, Z.; Wang, S.; Zhou, J.; Wu, Z., A Self-Healing Smart Photonic Crystal Hydrogel Sensor for Glucose and Related Saccharides. *Microchimica Acta* **2021**, 188, 210.

(22) Zhang, J.-T.; Cai, Z.; Kwak, D. H.; Liu, X.; Asher, S. A., Two-Dimensional Photonic Crystal Sensors for Visual Detection of Lectin Concanavalin A. *Anal. Chem.* **2014**, 86, 9036-9041.

(23) Cai, Z.; Sasmal, A.; Liu, X.; Asher, S. A., Responsive Photonic Crystal Carbohydrate Hydrogel Sensor Materials for Selective and Sensitive Lectin Protein Detection. *ACS Sens.* **2017**, 2, 1474-1481.

(24) Cai, Z.; Kwak, D. H.; Punihaole, D.; Hong, Z.; Velankar, S. S.; Liu, X.; Asher, S. A., A Photonic Crystal Protein Hydrogel Sensor for Candida Albicans. *Angew. Chem. Int. Ed.* **2015**, 54, 13036-13040.

(25) Murtaza, G.; Rizvi, A. S.; Irfan, M.; Yan, D.; Khan, R. U.; Rafique, B.; Xue, M.; Meng, Z. H.; Qu, F., Glycated Albumin Based Photonic Crystal Sensors for Detection of

Lipopolysaccharides and Discrimination of Gram-Negative Bacteria. *Anal. Chim. Acta* **2020**, 1117, 1-8.

(26) Murtaza, G.; Rizvi, A. S.; Xue, M.; Qiu, L.; Meng, Z., Consensus Receptor-Binding Domain-Targeted Aptamer Selection and Designing of a Photonic Crystal-Decorated Aptasensor for SARS-CoV-2. *Anal. Chem.* **2022**, 94, 7391-7399.

(27) Cai, Z.; Smith, N. L.; Zhang, J.-T.; Asher, S. A., Two-Dimensional Photonic Crystal Chemical and Biomolecular Sensors. *Anal. Chem.* **2015**, 87, 5013-5025.

(28) Shen, P.; Zhang, Y.; Cai, Z.; Liu, R.; Xu, X.; Li, R.; Wang, J.-J.; Yang, D. a., Three-Dimensional/Two-Dimensional Photonic Crystal Hydrogels for Biosensing. *J. Mater. Chem. C* **2021**, 9, 5840-5857.

(29) Holtz, J. H.; Holtz, J. S. W.; Munro, C. H.; Asher, S. A., Intelligent Polymerized Crystalline Colloidal Arrays: Novel Chemical Sensor Materials. *Anal. Chem.* **1998**, 70, 780-791.

(30) Ye, B.-F.; Zhao, Y.-J.; Cheng, Y.; Li, T.-T.; Xie, Z.-Y.; Zhao, X.-W.; Gu, Z.-Z., Colorimetric Photonic Hydrogel Aptasensor for the Screening of Heavy Metal Ions. *Nanoscale* **2012**, 4, 5998-6003.

(31) Ye, B.; Wang, H.; Ding, H.; Zhao, Y.; Pu, Y.; Gu, Z., Colorimetric Logic Response Based on Aptamer Functionalized Colloidal Crystal Hydrogels. *Nanoscale* **2015**, 7, 7565-7568.

(32) Chen, Q.; Wang, S.; Huang, T.; Xiao, F.; Wu, Z.; Yu, R., Construction and Research of Multiple Stimuli-Responsive 2D Photonic Crystal DNA Hydrogel Sensing Platform with Double-Network Structure and Signal Self-Expression. *Anal. Chem.* **2022**, 94, 5530-5537.

(33) Jang, K.; Westbay, J. H.; Asher, S. A., DNA-Crosslinked 2D Photonic Crystal Hydrogels for Detection of Adenosine Actuated by an Adenosine-Binding Aptamer. *ACS Sensors* **2022**, 7, 1648-1656.

(34) Löfgren, L.; Pehrsson, S.; Hägglund, G.; Tjellström, H.; Nylander, S., Accurate Measurement of Endogenous Adenosine in Human Blood. *PloS one* **2018**, 13, e0205707-e0205707.

(35) Yousefi, S.; Saraji, M., Optical Aptasensor Based on Silver Nanoparticles for the Colorimetric Detection of Adenosine. *Spectrochim. Acta A* **2019**, 213, 1-5.

(36) Zhang, F.; Cao, L.; Yang, W., Preparation of Monodisperse and Anion-Charged Polystyrene Microspheres Stabilized with Polymerizable Sodium Styrene Sulfonate by Dispersion Polymerization. *Macromol. Chem. Phys.* **2010**, 211, 744-751.

(37) Zhang, J.-T.; Wang, L.; Lamont, D. N.; Velankar, S. S.; Asher, S. A., Fabrication of Large-Area Two-Dimensional Colloidal Crystals. *Angew. Chem. Int. Ed.* **2012**, 51, 6117-6120.

(38) Li, G.; Xiao, F.; Liao, S.; Chen, Q.; Zhou, J.; Wu, Z.; Yu, R., Label-Free 2D Colloidal Photonic Crystal Hydrogel Biosensor for Urea and Urease Inhibitor. *Sens. Actuators B Chem.* **2018**, 277, 591-597.

(39) Prevo, B. G.; Velev, O. D., Controlled, Rapid Deposition of Structured Coatings from Micro- and Nanoparticle Suspensions. *Langmuir* **2004**, 20, 2099-2107.

(40) Cai, Z.; Zhang, J.-T.; Xue, F.; Hong, Z.; Punihaole, D.; Asher, S. A., 2D Photonic Crystal Protein Hydrogel Coulometer for Sensing Serum Albumin Ligand Binding. *Anal. Chem.* **2014**, 86, 4840-4847.

(41) Thomas, L. C.; Chittenden, R. A., Characteristic Infrared Absorption Frequencies of Organophosphorus Compounds — I. The Phosphoryl (P=O) Group. *Spectrochim. Acta* **1964**, 20, 467-487.

(42) Zhang, K.; Wang, K.; Xie, M.; Zhu, X.; Xu, L.; Yang, R.; Huang, B.; Zhu, X., DNA-Templated Silver Nanoclusters Based Label-Free Fluorescent Molecular Beacon for the Detection of Adenosine Deaminase. *Biosens. Bioelectron.* **2014**, 52, 124-128.

(43) Nutiu, R.; Li, Y., Structure-Switching Signaling Aptamers. *J. Am. Chem. Soc.* **2003**, 125, 4771-4778.

(44) Sun, J.; Jiang, W.; Zhu, J.; Li, W.; Wang, L., Label-Free Fluorescence Dual-Amplified Detection of Adenosine Based on Exonuclease III-Assisted DNA Cycling and Hybridization Chain Reaction. *Biosens. Bioelectron.* **2015**, 70, 15-20.

5.0 Summary and Future Work

5.1 Summary

This dissertation demonstrates the development of novel 2DPC hydrogel sensors for biomolecular detection. Chapter 1 introduced background theory on the stimuli-responsive hydrogels and 2DPC, which constitute 2DPC hydrogel sensors.

Chapter 2 showed the development of PhPY-sensing 2DPC hydrogels. The hydrogels are functionalized with oxyamine recognition groups that chemoselectively link PhPY to the hydrogel via oxime ligation. The covalent attachment of hydrophilic PhPY causes the hydrogel volume to increase, which in turn increases the particle spacing of the embedded 2DPC array in proportion to the PhPY concentration.

Chapter 3 demonstrated the use of new 2DPC hydrogel sensing motif that utilizes duplexed DNA crosslinks. One strand of the duplexed DNA contains an adenosine-binding aptamer sequence. Upon the introduction of adenosine, the aptamer segment binds adenosine with high affinity, resulting in the breakage of the preformed DNA crosslinks. This change decreases the hydrogel elasticity, which homogeneously increases the 2DPC particle spacing in proportion to the adenosine concentration.

Chapter 4 showed another type of 2DPC hydrogel sensing motif utilizing DNA aptamer recognition groups. Unlike the DNA aptamers in Chapter 3, both ends of the DNA aptamers are covalently attached to the hydrogel network. Upon binding adenosine, the DNA aptamer changes its conformation from a long single-stranded structure to a short hairpin loop structure. The adenosine-binding induced aptamer conformational changes reduce the hydrogel volume, resulting

in decreased particle spacing of the embedded 2DPC array in proportion to the analyte concentration.

5.2 Future Work

5.2.1 Development of L-Phe- and L-Lactate-Sensing Elements Utilizing Enzymes and the Oxyamine-Functionalized 2DPC Hydrogels

In Chapter 2, we fabricated the 2DPC hydrogels capable of chemoselectively detecting PhPY in human serum. Our hypothesis is that the oxyamine-functionalized 2DPC hydrogels could be applied to develop L-Phe-sensing elements with the enzyme L-phenylalanine dehydrogenase (L-PheDH), which converts L-Phe to PhPY (Figure 5-1a).[1,2] The concentrations of enzymatically produced PhPY are proportional to the L-Phe concentrations. Thus, the oxyamine-functionalized hydrogels will be tested to detect enzymatically produced PhPY in order to determine the concentration of L-Phe. The L-Phe-sensing hydrogels will be further utilized to develop point-of-care L-Phe sensors for PKU patients.

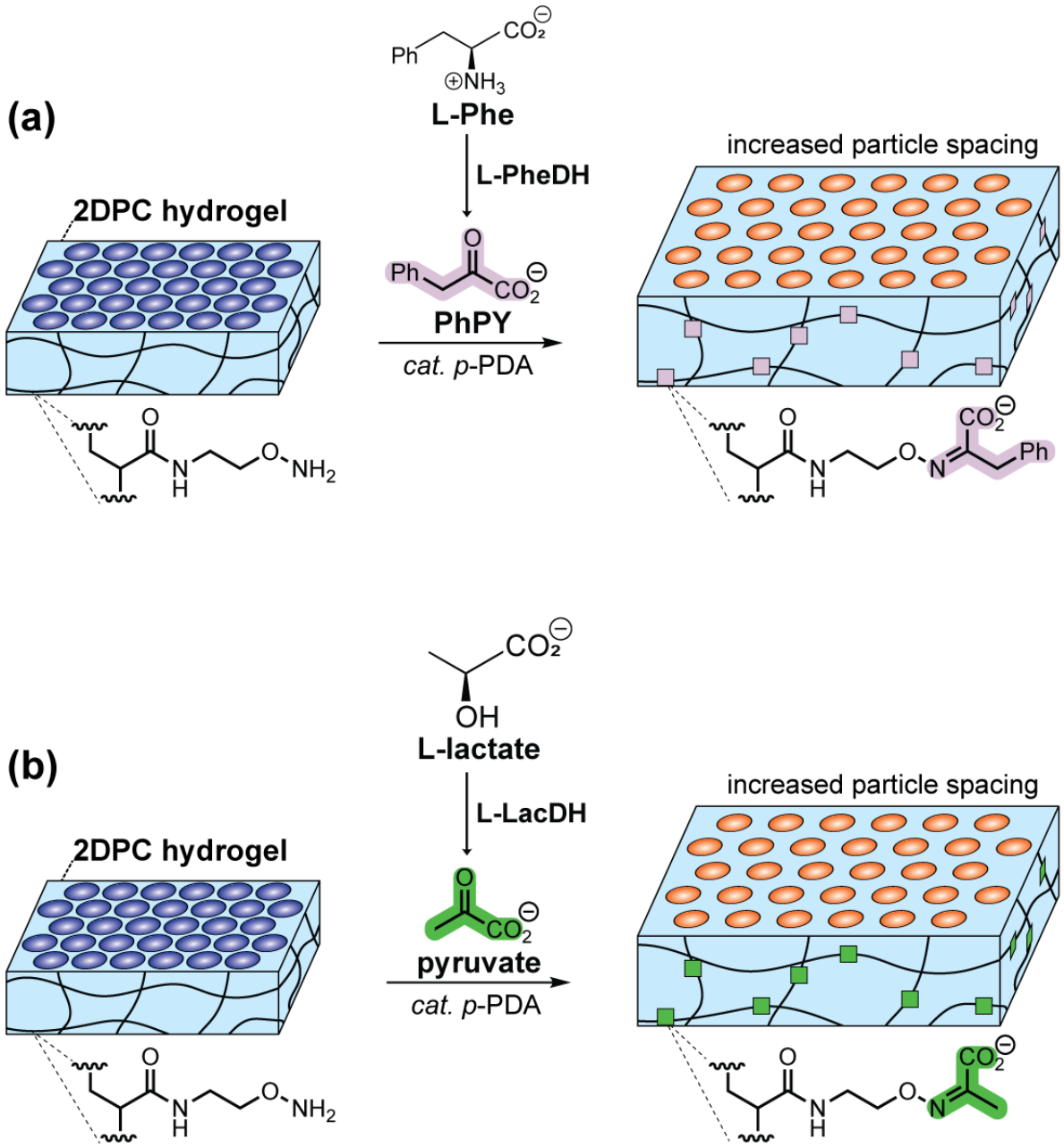

Figure 5-1. Proposed mechanisms for (a) L-Phe and (b) L-lactate detection.

We also hypothesize that an L-lactate sensor could be developed by utilizing the oxyamine-functionalized 2DPC hydrogels with the enzyme L-lactate dehydrogenase (L-LacDH). L-lactate is one of the biomarkers used to evaluate the development of sepsis.[3,4] L-LacDH converts L-lactate to pyruvate (Figure 5-1b),[5,6] which has a carbonyl functional group that can be linked to the

oxyamines in the hydrogels via oxime ligation. The concentrations of enzymatically produced pyruvate are proportional to the L-lactate concentrations. Thus, our oxyamine-functionalized 2DPC hydrogels will be tested to quantify enzymatically produced pyruvate in order to determine the concentration of L-lactate.

5.2.2 Future Work in the Aptamer-Functionalized 2DPC Hydrogel Materials

The sensor performance using the aptamer-functionalized 2DPC hydrogels reported in Chapters 3 and 4 can be further optimized and characterized. First, the detection sensitivity can be improved by testing hydrogels prepared with various pre-gel solutions containing different concentrations of monomers and DNA strands. In particular, in the DNA-crosslinked hydrogel fabrication, (1) the length of each DNA strand, (2) the number of bases that form the DNA-crosslinks, and (3) the placement of the aptamer sequence in the longer DNA strand can be systematically altered. The results will advance the understanding of the properties of DNA crosslinks that can be used to further optimize the hydrogel sensor responsivity.

Furthermore, thrombin-sensing 2DPC hydrogels can be developed by changing the aptamer recognition group, demonstrating that the aptamer-functionalized sensing motifs are generalizable to develop protein sensors. We propose four different mechanisms for the thrombin detection using two different thrombin-binding aptamers (TBAs). One TBA is a 15-mer and the other TBA is a 29-mer, targeting different exosites of thrombin.[7-9] Here, the first three mechanisms are shown using the 15-mer 2TBA; however, the same mechanisms can also be tested with the 29-mer TBA.

Figure 5-2 shows the mechanism utilizing the sensing-motif that we reported in Chapter 3. The only change is that the thrombin-binding aptamer (TBA), not the adenosine-binding aptamer,

is now incorporated into the hydrogel network. When thrombin is introduced to the hydrogels, the TBA sequence in the longer DNA strand competitively binds thrombin, breaking the DNA-crosslinks. As a result, this will increase the 2DPC particle spacing in proportion to the thrombin concentration.

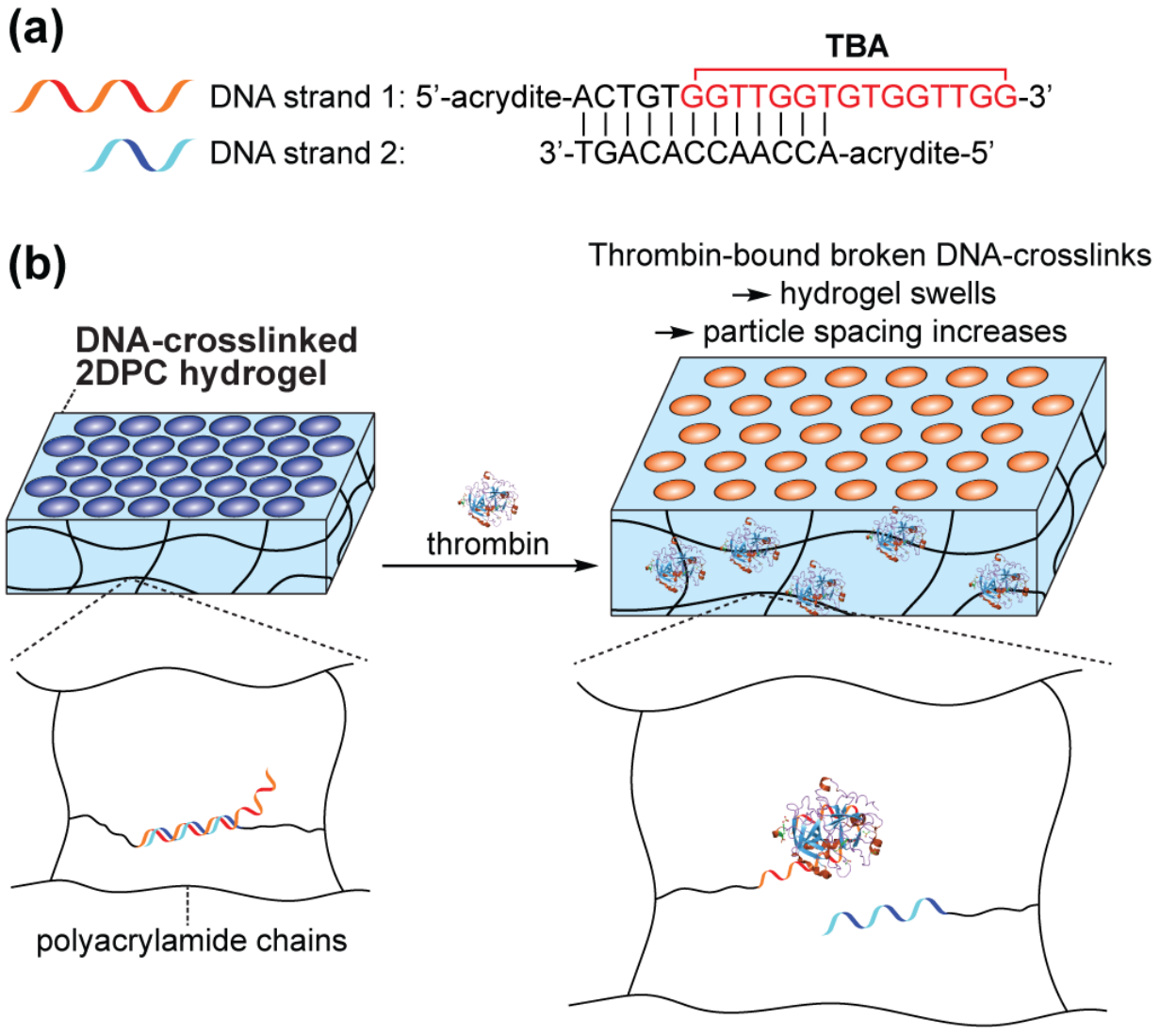

Figure 5-2. Proposed thrombin detection mechanism 1.

Figure 5-3 shows the second mechanism for the thrombin detection using only the DNA strand containing TBA. As thrombin is a large and charged molecule, it is possible that the TBA-thrombin binding induces a large change in the free energy of mixing and the ionic free energy of the hydrogels. As a result, the 2DPC particle spacing will change in proportion to the thrombin concentration.

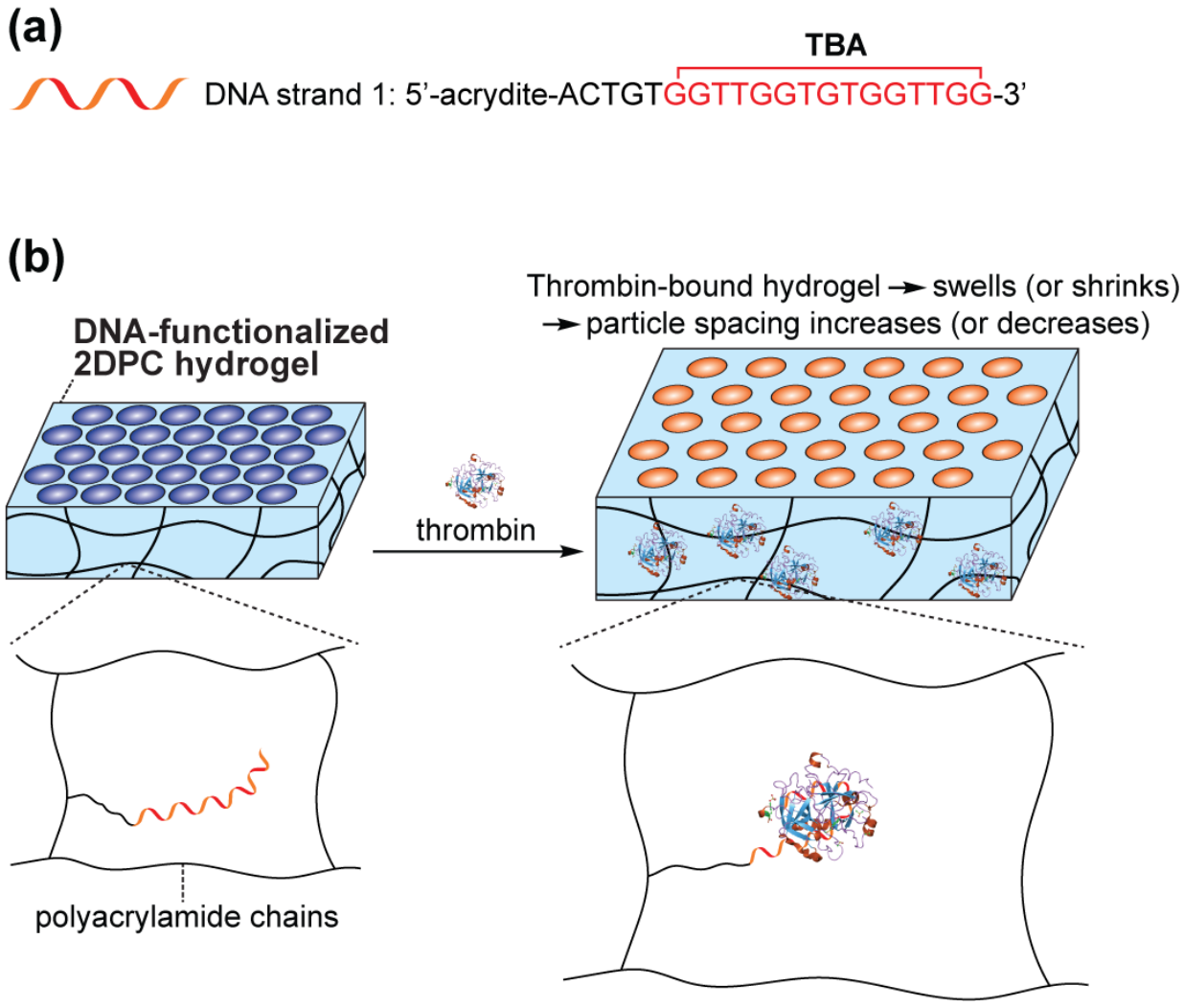

Figure 5-3. Proposed thrombin detection mechanism 2.

The third thrombin detection mechanism uses the sensing motif developed in Chapter 4 in conjunction with the TBA (Figure 5-4). Upon binding thrombin, the TBA will change its conformation to a shorter hairpin loop structure, which reduces the 2DPC particle spacing and reports the thrombin concentration.

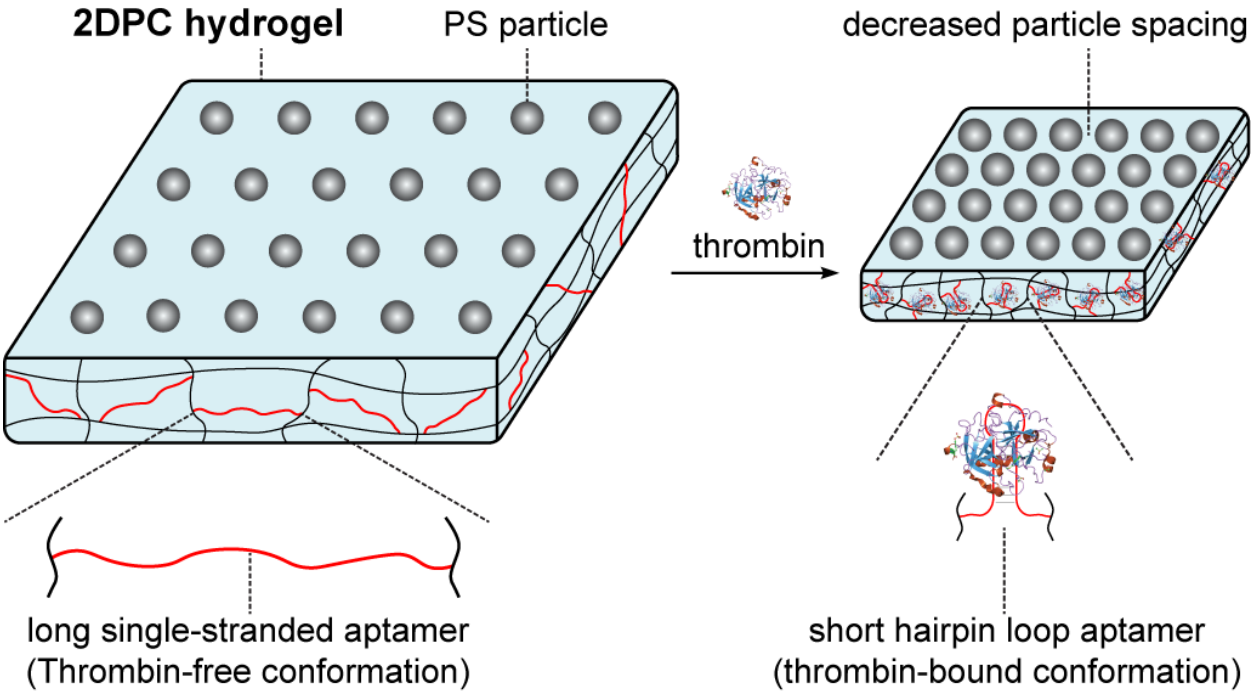

Figure 5-4. Proposed thrombin detection mechanism 3.

Figure 5-5 shows the last thrombin detection mechanism using the 2DPC hydrogels functionalized with two different TBAs. When thrombin is introduced to the hydrogels, the 15-mer and the 29-mer TBAs bind different exosites within the same thrombin, forming an additional crosslink. Therefore, the elastic restoring force of the hydrogel network will increase in proportion to the amount of thrombin, reducing the 2DPC particle spacing.

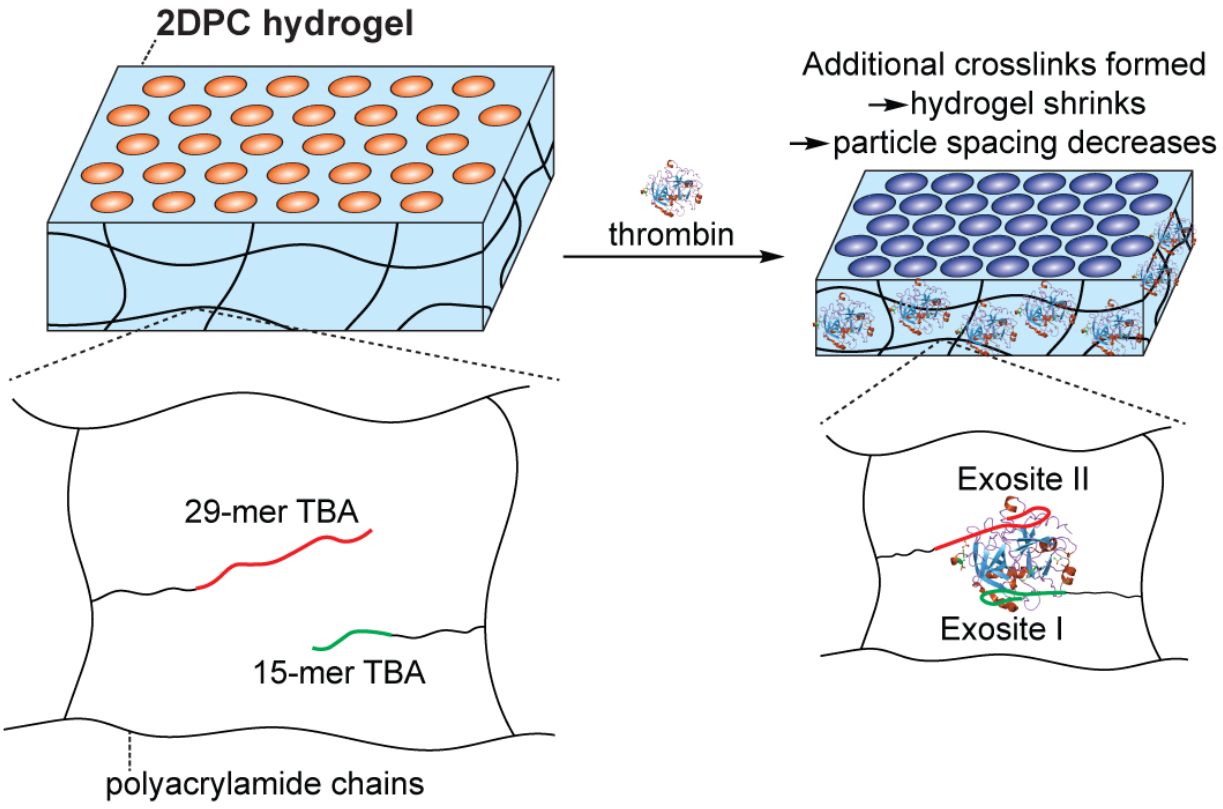

Figure 5-5. Proposed thrombin detection mechanism 4.

In the future, the aptamer-functionalized 2DPC hydrogel sensing motifs can be further utilized to develop sensors for other small molecules, proteins, microorganisms, and viruses by altering the aptamer recognition groups.

5.3 References

(1) Asano, Y.; Nakazawa, A.; Endo, K., Novel Phenylalanine Dehydrogenases from *Sporosarcina Ureae* and *Bacillus Sphaericus*. Purification and Characterization. *J. Biol. Chem.* **1987**, 262, 10346-10354.

(2) Brunhuber, N. M.; Thoden, J. B.; Blanchard, J. S.; Vanhooke, J. L., *Rhodococcus* L-Phenylalanine Dehydrogenase: Kinetics, Mechanism, and Structural Basis for Catalytic Specifity. *Biochemistry* **2000**, 39, 9174-9187.

(3) Rattu, G.; Khansili, N.; Maurya, V. K.; Krishna, P. M., Lactate Detection Sensors for Food, Clinical and Biological Applications: A Review. *Environ. Chem. Lett.* **2021,** 19, 1135-1152.

(4) Rathee, K.; Dhull, V.; Dhull, R.; Singh, S., Biosensors Based on Electrochemical Lactate Detection: A Comprehensive Review. *Biochem. Biophys. Rep.* **2016,** 5, 35-54.

(5) Javed, M. H.; Azimuddin, S. M. I.; Hussain, A. N.; Ahmed, A.; Ishaq, M., Purification and Characterization of Lactate Dehydrogenase from *Varanus* Liver. *Exp. Mol. Med.* **1997,** 29, 25-30.

(6) Vanderlinde, R., Measurement of Total Lactate Dehydrogenase Activity. *Ann. Clin. Lab. Sci.* **1985,** 15, 13-31.

(7) Bock, L. C.; Griffin, L. C.; Latham, J. A.; Vermaas, E. H.; Toole, J. J., Selection of Single-Stranded DNA Molecules That Bind and Inhibit Human Thrombin. *Nature* **1992**, 355, 564-566.

(8) Tasset, D. M.; Kubik, M. F.; Steiner, W., Oligonucleotide Inhibitors of Human Thrombin That Bind Distinct Epitopes. *J. Mol. Biol.* **1997**, 272, 688-698.

(9) Musumeci, D.; Montesarchio, D., Polyvalent Nucleic Acid Aptamers and Modulation of Their Activity: A Focus on the Thrombin Binding Aptamer. *Pharmacol. Ther.* **2012**, 136, 202-215.

Appendix A Supporting Information for Chapter 2

Appendix A.1 High-Resolution Mass Spectrometry (HRMS) Spectra of Synthesized Compounds

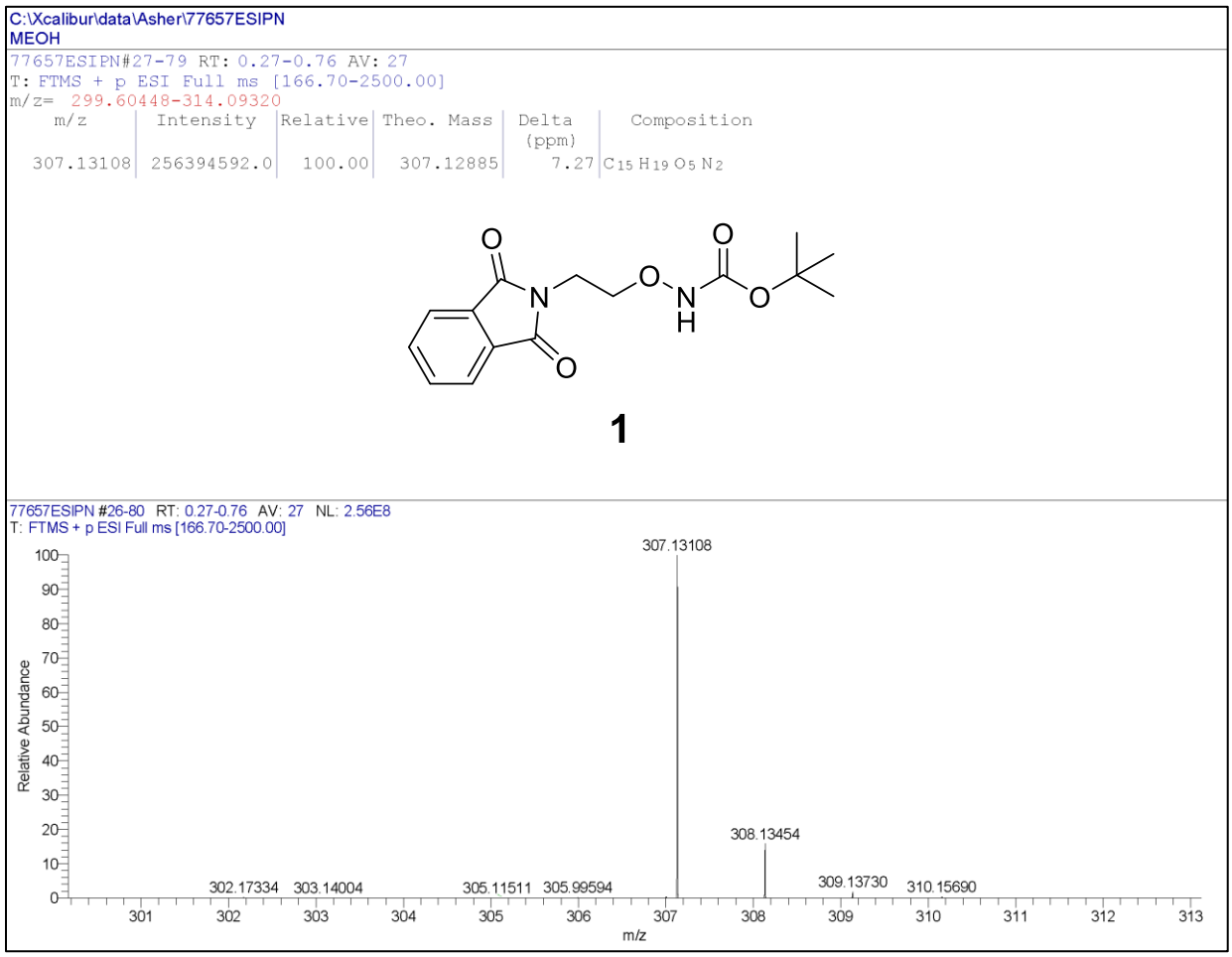

Appendix Figure A-1. HRMS spectrum of compound 1.

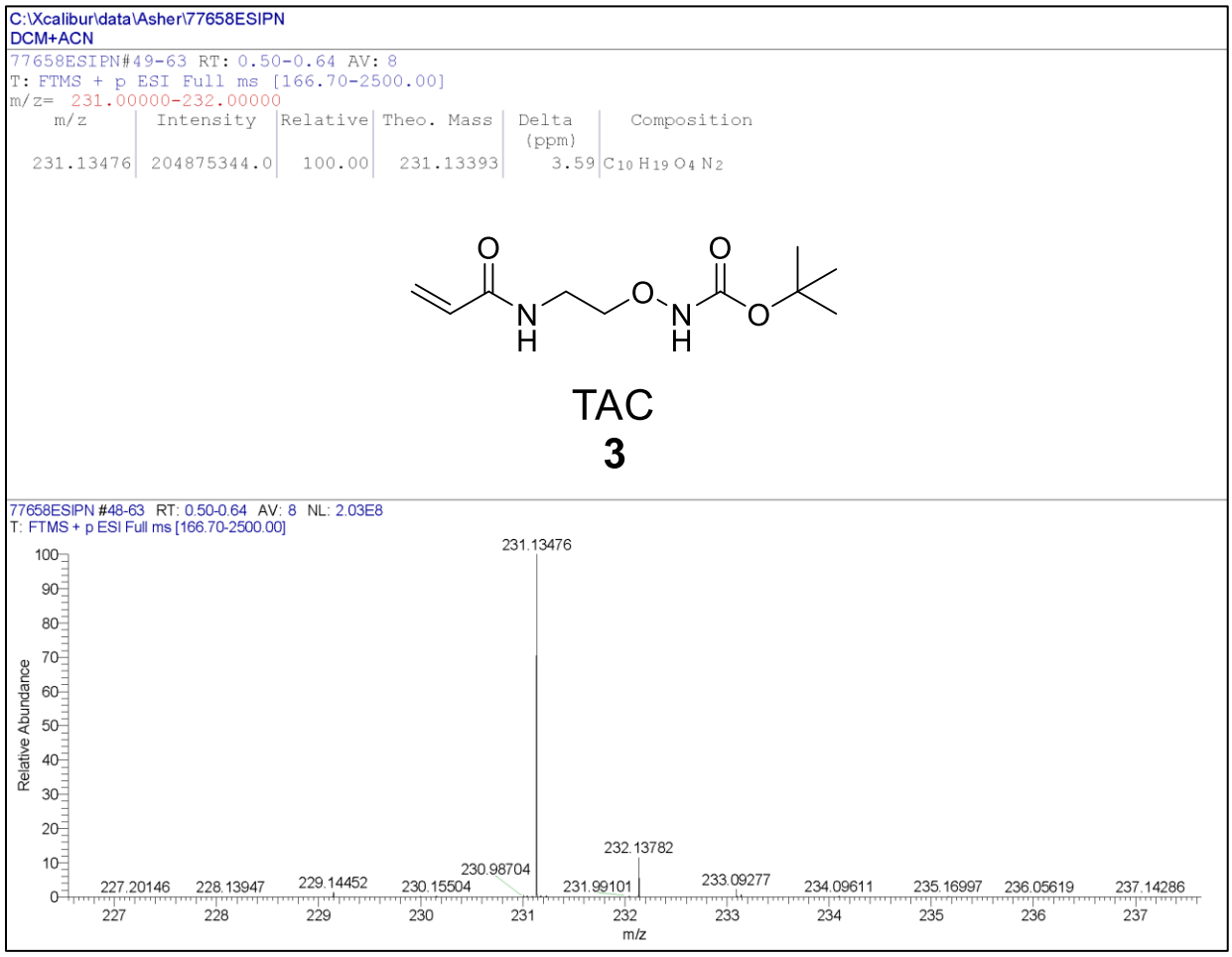

Appendix Figure A-2. HRMS spectrum of compound 3.

Appendix A.2 ^{1}H and ^{13}C NMR Spectra of Synthesized Compounds

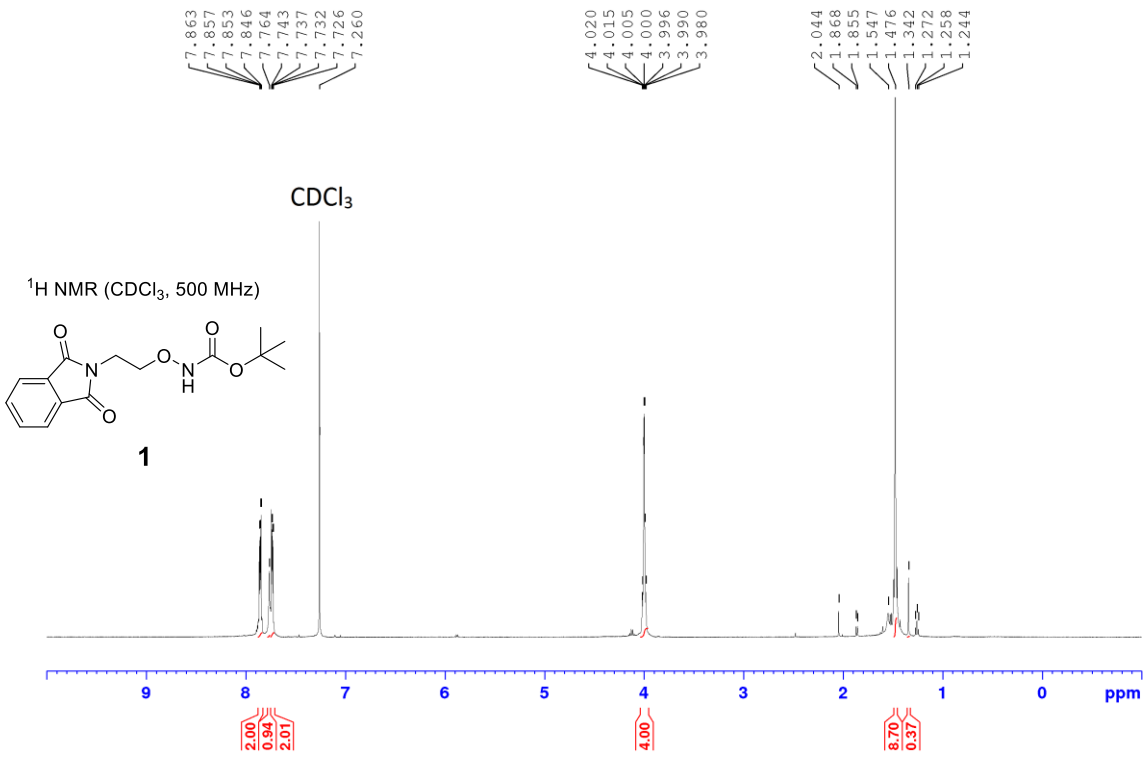

Appendix Figure A-3. ^{1}H NMR spectrum of compound 1.

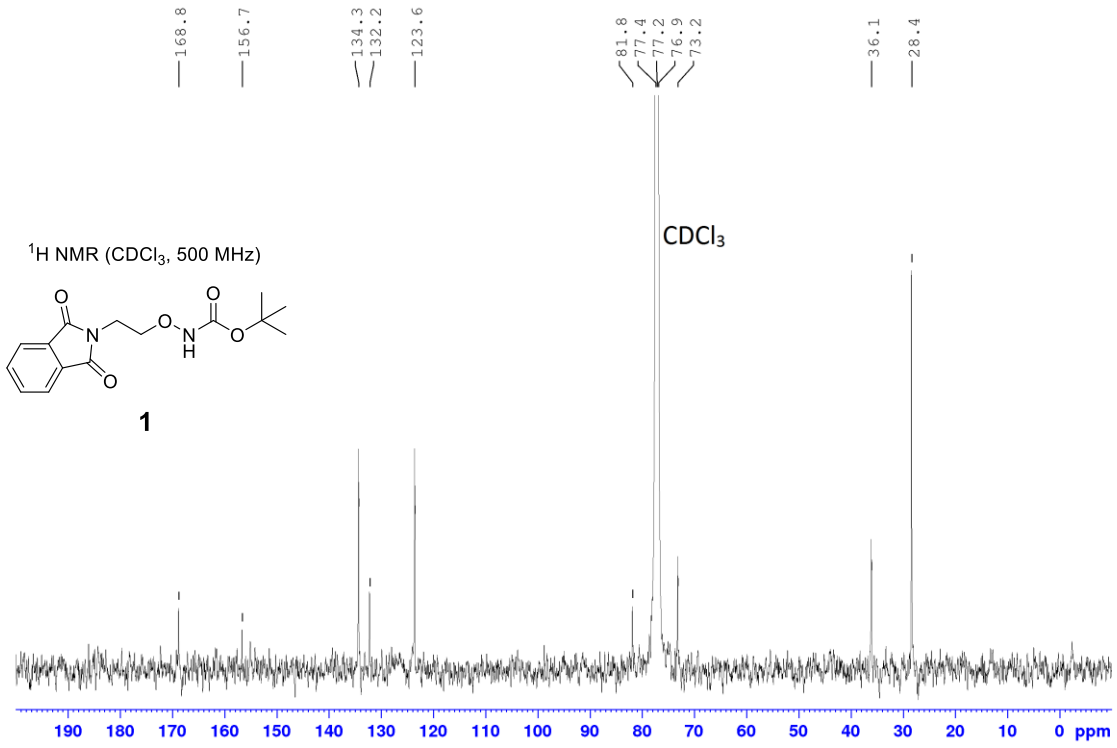

Appendix Figure A-4. ^{13}C NMR spectrum of compound 1.

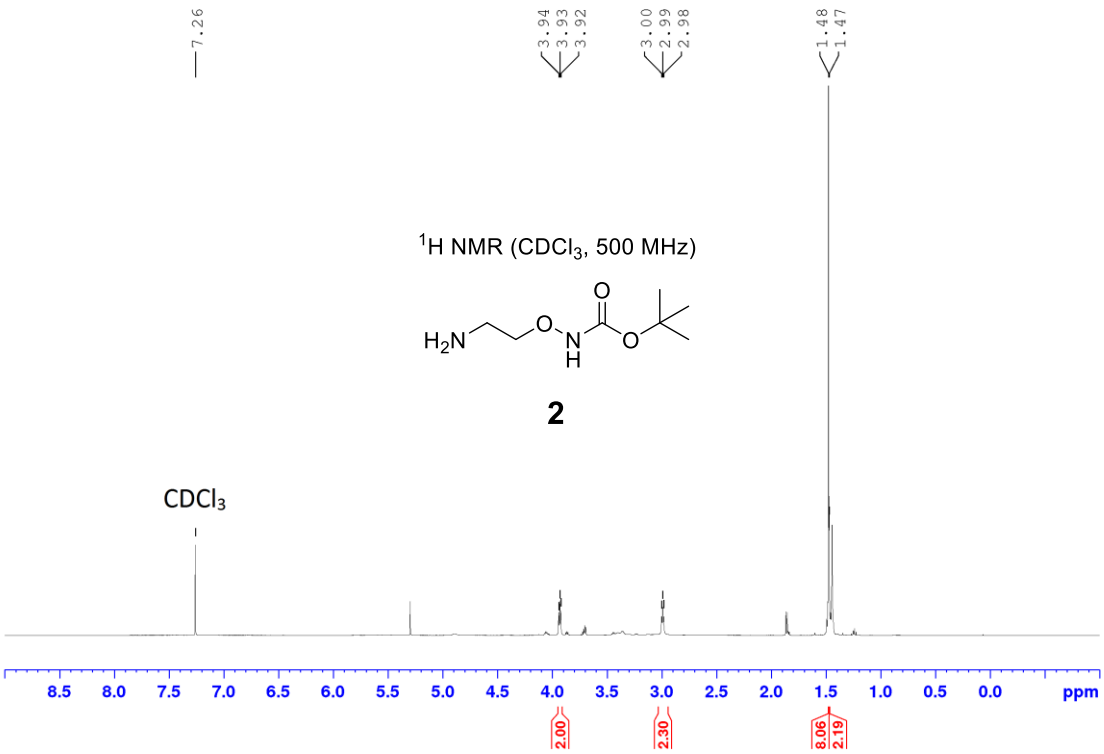

Appendix Figure A-5. ^{1}H NMR spectrum of compound 2.

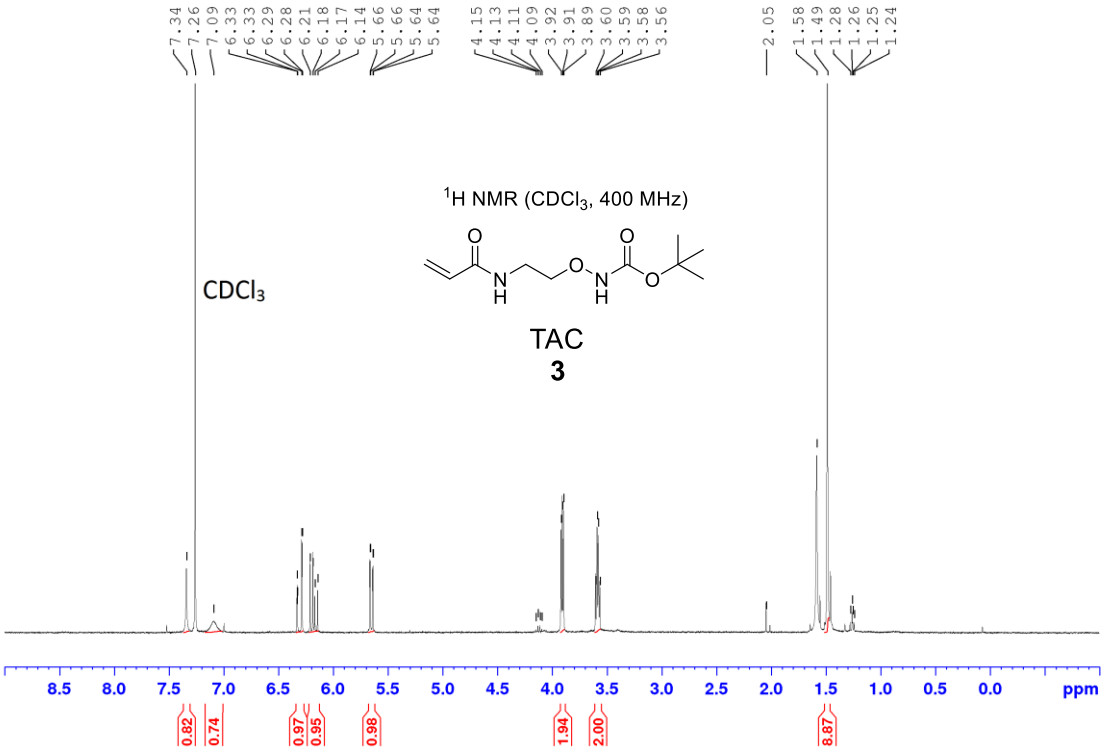

Appendix Figure A-6. ^{1}H NMR spectrum of compound 3.

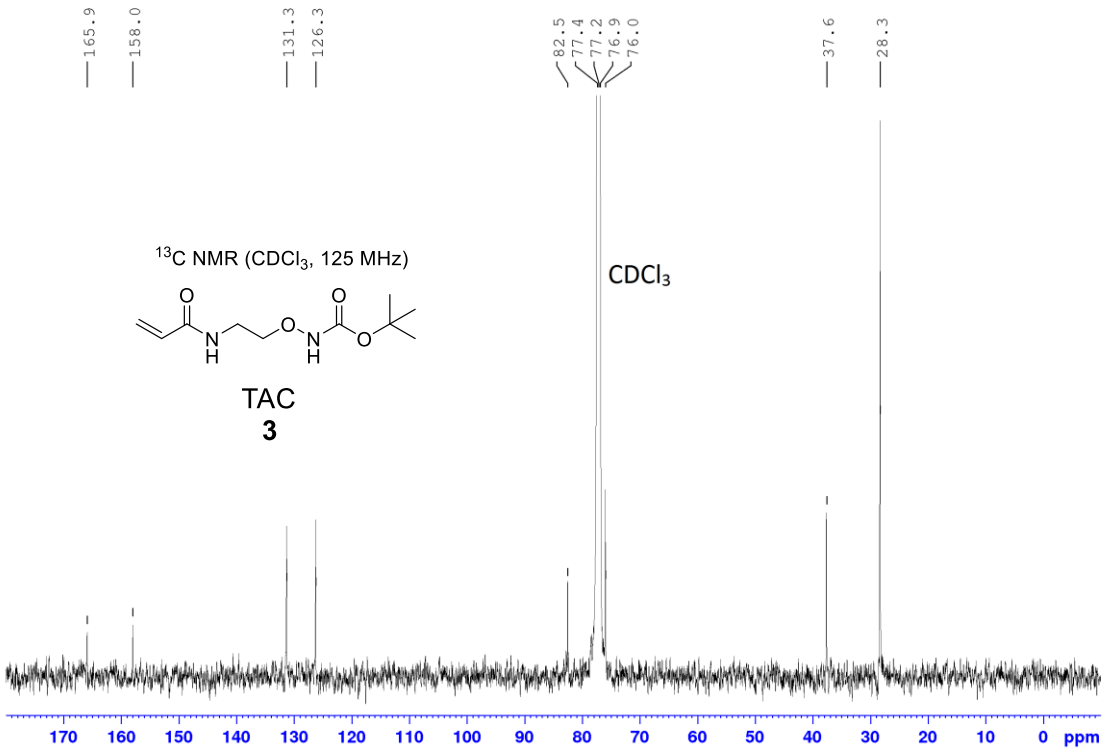

Appendix Figure A-7. ^{13}C NMR spectrum of compound 3.

Appendix B Supporting Information for Chapter 3

Appendix B.1 Calculating Dissociation Constant of the Adenosine-Binding Aptamer

The fraction of bound aptamer, f_{bound}, is defined as:

$$f_{bound} = \frac{[aptamer \cdot adenosine]}{[free\ aptamer] + [aptamer \cdot adenosine]}$$

Where $[aptamer \cdot adenosine]$ is the concentration of adenosine-bound aptamer and $[free\ aptamer]$ is the concentration of aptamer that has not bound adenosine. Dividing the numerator and denominator by $[aptamer \cdot adenosine]$ gives:

$$f_{bound} = \frac{1}{\frac{[free\ aptamer]}{[aptamer \cdot adenosine]} + 1}$$

The dissociation constant, K_D, of the adenosine-binding aptamer is:

$$K_D = \frac{[free\ aptamer][free\ adenosine]}{[aptamer \cdot adenosine]}$$

Where $[free\ adenosine]$ is the concentration of adenosine that the aptamer has not bound. Thus, f_{bound} can be written as:

$$f_{bound} = \frac{1}{\frac{K_D}{[free\ adenosine]} + 1}$$

Multiplying the numerator and denominator by $[free\ adenosine]$ gives:

$$f_{bound} = \frac{[free\ adenosine]}{K_D + [free\ adenosine]}$$

If $K_D = [free\ adenosine]$, then $f_{bound} = \frac{1}{2}$. Assuming the particle spacing change is proportional to f_{bound}, and the concentration of adenosine added is equal to $[free\ adenosine]$,

K_D can be estimated as the concentration of adenosine when the particle spacing change is at half-maximum.

Using measured particle spacing changes at t = 60 min, we constructed a calibration curve relating log([adenosine]) to particle spacing change and generated a linear fit using the software OriginLab (Figure B-1). We observed a maximum particle spacing change of 97.746 nm at an adenosine concentration of 2000 μM. The half-maximum particle spacing was thus 48.873 nm. The linear fit was then used to calculate an adenosine concentration of 74.36 μM, which was taken as the estimated K_D of the adenosine-binding aptamer.

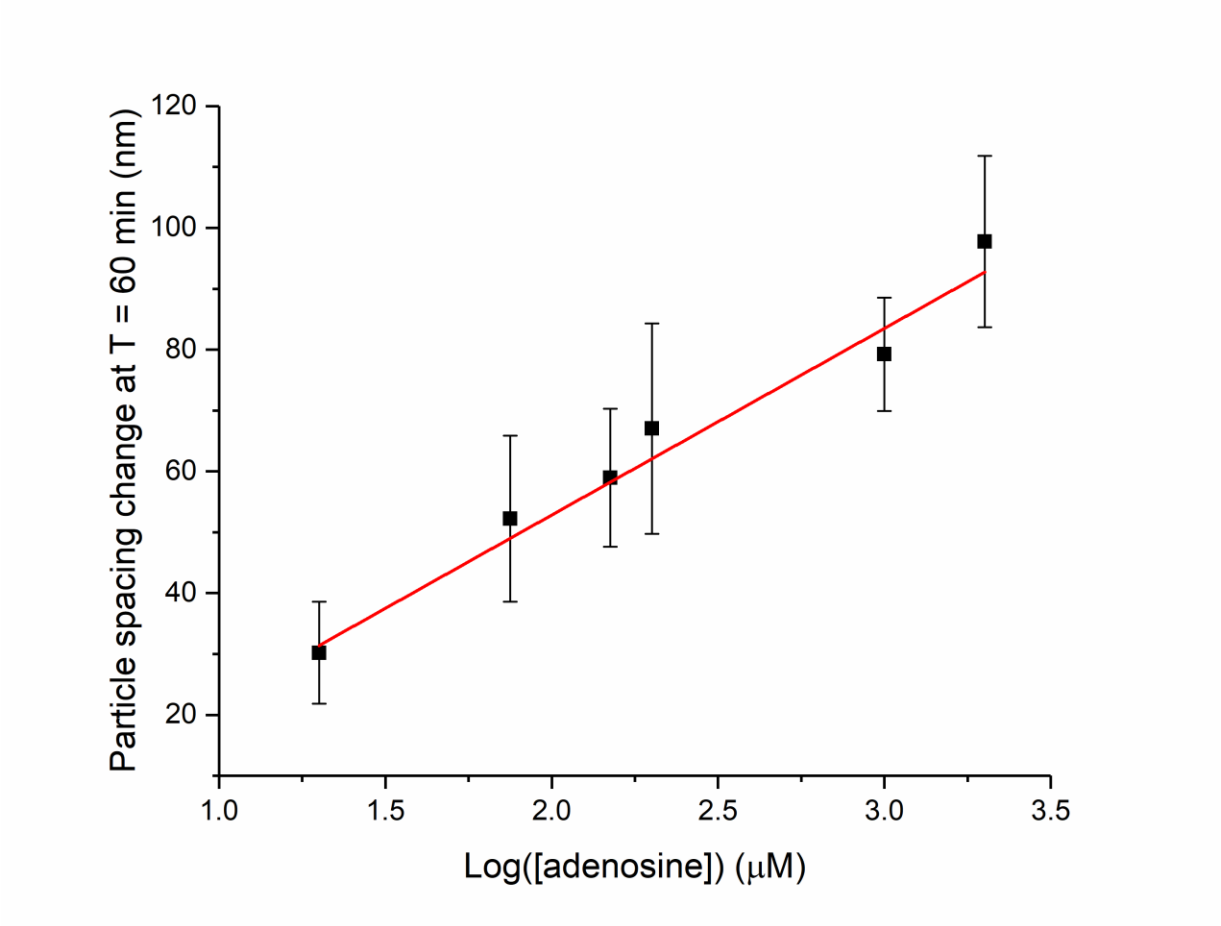

Appendix Figure B-1. Log ([adenosine]) vs. particle spacing change. A weighted-least square method in OriginLab was used to generate a linear fit of $y = 30.65366x - 8.49099$ (adjusted R-Squared = 0.9746).

Appendix B.2 Optimizing Acrylamide (AAm) Monomer and MBAAm Crosslinker Concentrations in 2DPC Hydrogel Fabrication

To find the optimal 2DPC hydrogel fabrication conditions for this proof-of-concept study, we systematically varied the concentrations of AAm monomer and MBAAm crosslinker. 2DPC hydrogels are expected to be more sensitive to adenosine if a lower amount of crosslinker is used, as the sensor response is induced by altering the crosslinking density of the hydrogel. However, hydrogels cannot embed a 2DPC array into the network if they do not have sufficient mechanical robustness. It is important that the 2DPC array fully embeds into the hydrogel because it affects the quality of light diffraction that is used to monitor particle spacing changes in 2DPC hydrogels. Thus, the main goal was to minimize the amount of MBAAm, while ensuring appropriate mechanical robustness of the 2DPC hydrogels. After fabricating 2DPC hydrogels with different recipes, we visually evaluated how much of the 2DPC array was successfully embedded into the hydrogel. A recipe was deemed successful if over 90% of the 2DPC array was embedded in the corresponding hydrogel.

As summarized in Table B-1 below, 2DPC hydrogels with 25% (w/v) AAm and 0.02% (w/v) MBAAm successfully embedded a 2DPC array with the lowest amount of MBAAm crosslinker. Thus, this composition was adopted to fabricate DNA-crosslinked 2DPC hydrogels. We will continue to investigate hydrogel formulations in future studies by systematically altering DNA concentration in addition to AAm and MBAAm.

Appendix Table B-1. Concentrations of AAm and MBAAm used in preparation of 2DPC hydrogels

AAm concentration (%, w/v)	MBAAm concentration (%, w/v)	Was >90% of 2DPC array embedded in the 2DPC hydrogel?
20	0.03	✓
20	0.02	×
25	0.03	✓
25	0.02	✓
25	0.01	×

*For this test, no DNA was added.

Appendix C Supporting Information for Chapter 4

Appendix C.1 Fabrication of two-dimensional photonic crystal (2DPC) hydrogels

First, the polystyrene (PS) 2DPC array was prepared on a water surface by using the needle-tip-flow method (Figure C-1a).[1] The suspension of PS particles (~20 wt% in water) was mixed with 1-propanol at a volume ratio of 3:1. The mixture was vortexed for 2 min and injected onto a water surface. With a steady injection flow, the negatively-charged PS particles spread outward and self-assembled into a hexagonal-close-packed (hcp) 2DPC array (Figure C-1b). The 2DPC array on water was then transferred onto a glass slide (2.4 × 7.6 cm^2) and air-dried (Figure C-1c). 120 μL of each candidate polymerizable monomer solution (Table C-1) was dripped on a 2DPC array (Figure C-1d) and a coverslip was placed on top of the sample (Figure C-1e). Then, the free radical polymerization reaction was allowed to proceed at room temperature for 30 min by irradiating the sample with 365 nm UV light. This embedded the 2DPC into the crosslinked hydrogel network (2DPC hydrogel) (Figure C-1f).

The 2DPC hydrogel was peeled from the glass substrates and thoroughly washed with nanopure water to remove unreacted monomers for at least 6 h (the water was changed every 2 h). Subsequently, the 2DPC hydrogels were washed with phosphate-buffered saline (PBS) solution for 6 h (the solution was changed every 2 h). The hydrogels were then left in fresh PBS solution for 24 h. The equilibrated 2DPC hydrogels were cut into 1 × 1 cm^2 pieces.

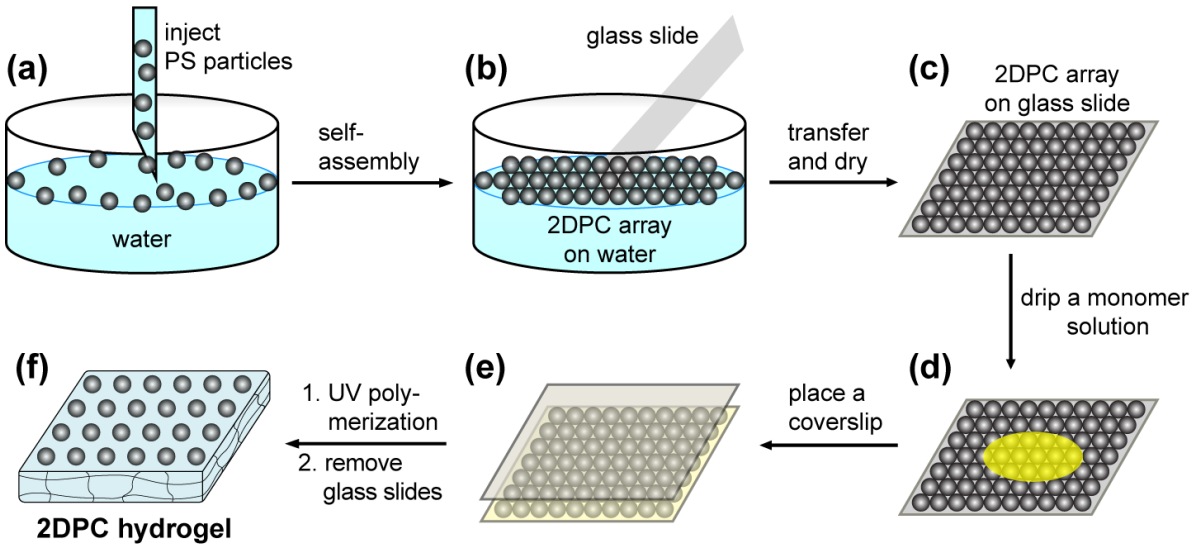

Appendix Figure C-1. Schematic illustration of 2DPC hydrogel fabrication.

Appendix Table C-1. Compositions of polymerizable monomer solutions used to prepare various 2DPC hydrogels

Sample #	AAm* (g)	AAc* (g)	Bis* (g)	H_2O (g)	Total** (g)
1	0.8	0.1	0.050	9.050	10
2	0.8	0.2	0.050	8.950	10
3	0.8	0.3	0.050	8.850	10
4	0.8	0.4	0.050	8.750	10
5	0.8	0.3	0.045	8.855	10
6	0.8	0.3	0.040	8.860	10
7	0.8	0.3	0.035	8.865	10
8	0.8	0.3	0.030	8.870	10

*AAm, AAc, and Bis are the abbreviations of acrylamide, acrylic acid, and N,N'-methylenebisacrylamide, respectively. **20 µL of 33% (w/v) Irgacure 2959 in DMSO was added to each 1 g of polymerizable monomer solution.

Appendix C.2 Fourier transform infrared (FTIR) characterization

For FTIR characterization, the hydrogels without 2DPC were prepared and thoroughly washed with nanopure water to avoid any unwanted interference. Then, the hydrogels were completely dried and ground with dry KBr. The resulting powder was then pressed to form a pellet. The FTIR spectra were acquired using the Themo Scientific Nicolet iS5 FTIR Spectrometer at room temperature.

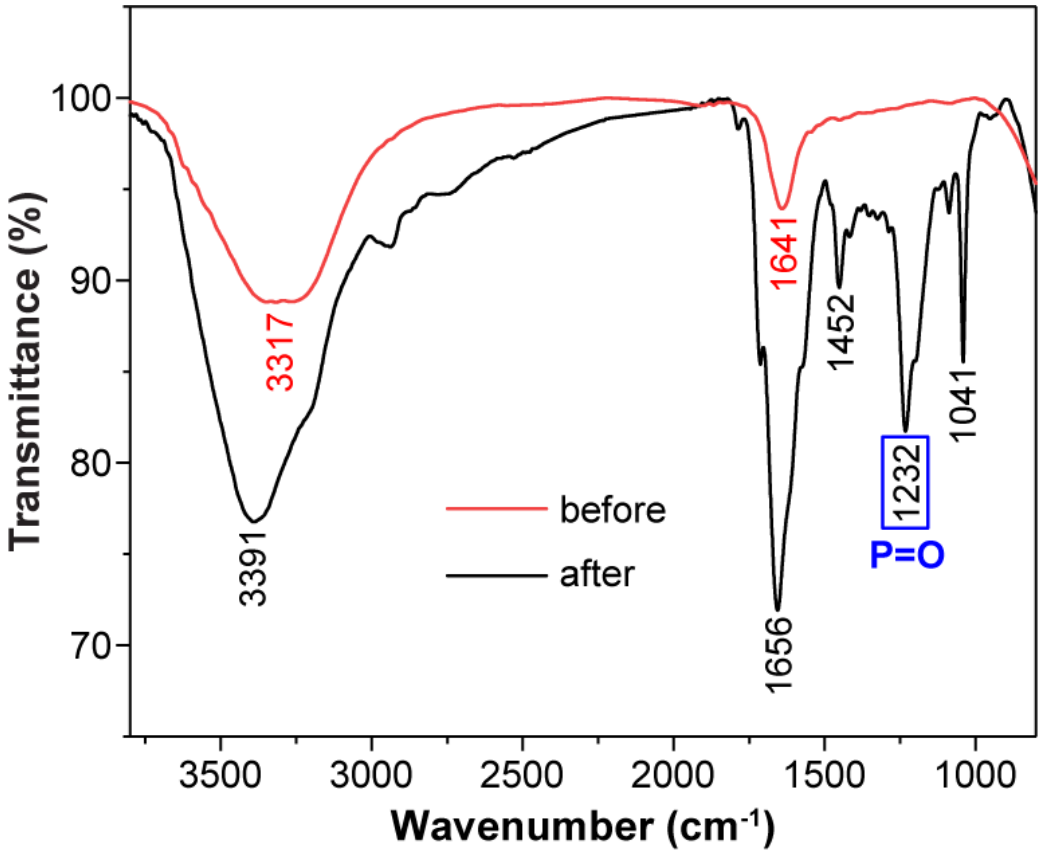

Appendix Figure C-2. FTIR spectra of hydrogels before and after the aptamer functionalization reaction. The appearance of a new absorption peak at 1232 cm^{-1}, which derives from the P=O vibration of the DNA phosphate backbone,[2] demonstrates that the aptamer was covalently attached to the hydrogel polymer network.

Appendix C.3 Optimization of hydrogel sensor composition

First, to optimize the concentration of AAc (C_{AAc}) for adenosine (AD)-sensing, 2DPC hydrogels were fabricated with different C_{AAc}, while the concentrations of AAm (C_{AAm}), Bis (C_{Bis}), and AD-binding aptamer ($C_{Aptamer}$) were fixed at 8 wt%, 0.5 wt%, and 100 μM, respectively (samples 1 to 4 in Table C-1). All 2DPC hydrogels showed particle spacing decreases in response to 10 mM AD in PBS for 1 h (Figure C-3a). Most importantly, a hydrogel with larger particle spacing decreases for the same concentration of AD indicates that the corresponding hydrogel is more sensitive to AD. Thus, for the next optimization experiments, the 2DPC hydrogels were prepared using 3 wt% AAc, which showed the largest particle spacing decrease, -90.9 ± 3.8 nm.

Next, various C_{Bis} were used to prepare the 2DPC hydrogels. While changing the C_{Bis}, we kept the C_{AAc} and $C_{Aptamer}$ at 3 wt% and 100 μM, respectively (samples 3 and 5 to 8 in Table C-1). Figure C-3b shows the particle spacing changes of these hydrogels in response to 10 mM AD in PBS for 1 h. Again, the particle spacings of all samples decreased upon sensing AD, indicating that the target recognition induced the hydrogel volume decrease. The largest particle spacing change, -111.5 ± 3.2 nm, was observed from the 2DPC hydrogel fabricated with 0.4 wt% Bis. This C_{Bis} was then used to prepare further samples for additional experiments.

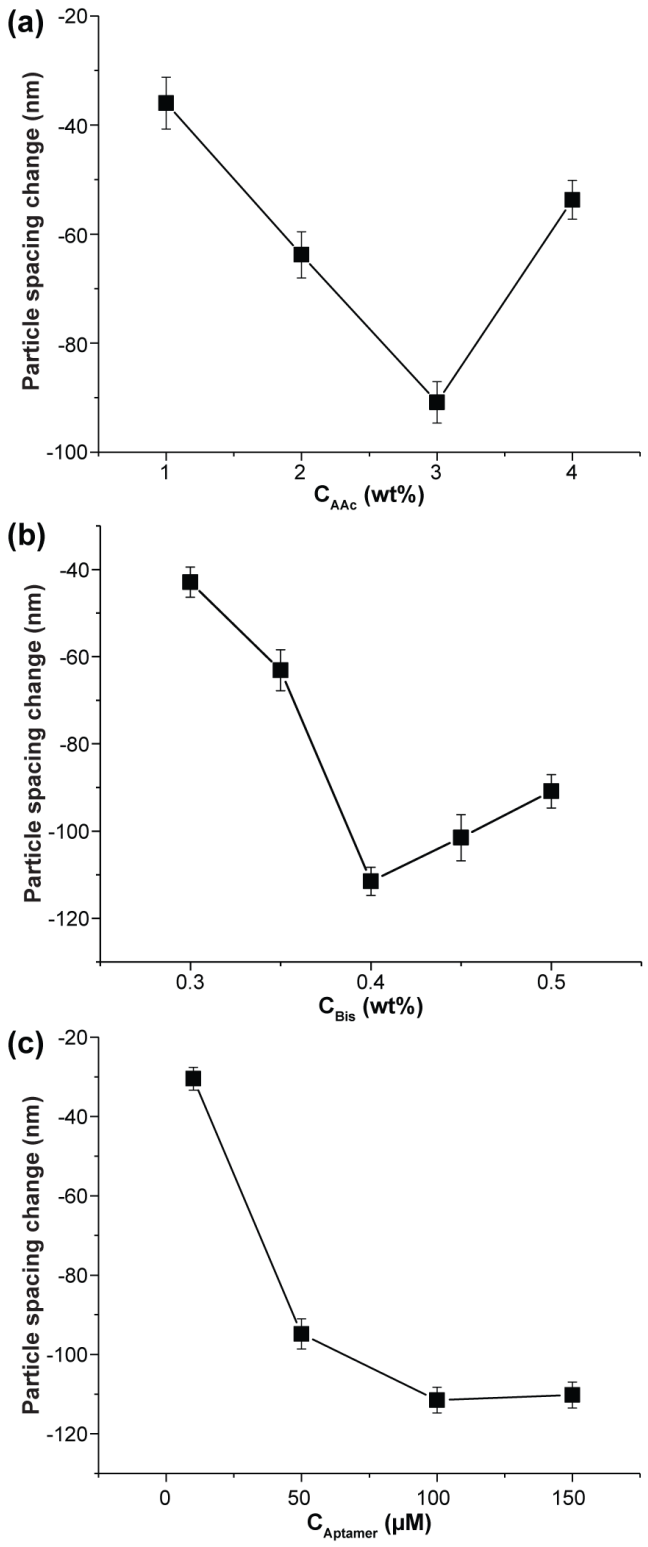

Appendix Figure C-3. Particle spacing changes of various 2DPC hydrogels in response to 10 mM AD in PBS for 1 h. The 2DPC hydrogels were prepared with different (a) C_{AAc}, (b) C_{Bis}, and (c) $C_{Aptamer}$.

Lastly, various $C_{Aptamer}$ (10, 50, 100, and 150 μM) were tested for the aptamer attachment reaction to further optimize the hydrogel sensor responsivity. (The C_{AAc} and C_{Bis} were fixed at 3 wt% and 0.4 wt%, respectively.) Figure C-3c shows the particle spacing changes of these hydrogels in response to 10 mM AD in PBS for 1 h. The magnitude of the particle spacing change increased from -30.5 ± 2.9 nm to -110.5 ± 3.2 nm, as the $C_{Aptamer}$ increased from 10 to 100 μM. This is because the higher the $C_{Aptamer}$, the greater the number of aptamers were linked to the hydrogel, making the hydrogel more sensitive to AD. Further increases in the $C_{Aptamer}$ to 150 μM showed a negligible further decrease on the particle spacing. We hypothesize that this is because the covalent linkage formation reaction between the aptamer and the hydrogel carboxyl group reached saturation when the $C_{Aptamer}$ exceeded 100 μM. Thus, these experimentally determined optimal C_{AAc}, C_{Bis}, and $C_{Aptamer}$ (3 wt%, 0.4 wt%, and 100 μM, respectively) were used for subsequent experiments.

Appendix C.4 An overview on recently reported aptamer-based AD sensors

Appendix Table C-2. Comparison of the performance of our 2DPC hydrogels with other aptasensors for AD detection

Detection method	Materials	Linear range	LoD	Ref.
Debye ring measurement	2DPC hydrogels	0.1 nM – 1 mM	0.09 nM	This work
Debye ring measurement	DNA-crosslinked hydrogels	20 μM – 2 mM	26.7 μM	3
Electrochemistry	ZnNi MOF microspheres	100 fM – 1 nM	76 fM	4
Electrochemistry	Reduced graphene oxide and gold nanoclusters	0.1 nM – 1 mM	0.1 nM	5
UV–Vis absorption	Creatinine-Ag+/AuNPs	1.0 – 5.0 μM	45 nM	6
Chemiluminescence	DNA hydrogel with Au@HKUST-1 encapsulation	0.4 – 150 pM	0.104 pM	7
Chemiluminescence	DNA cross-linked hydrogel-capped magnetic mesoporous silica nanoparticles	0.1 nM – 1 μM	0.14 nM	8
Fluorometry	Carbon dots	10 – 500 nM	4.2 nM	9
Fluorometry	T7 exonuclease	5 μM – 0.7 mM	0.98 μM	10
Fluorometry	Carbon quantum dots and silver nanoparticles	50 – 200 nM	13 nM	11
Fluorometry	Gold film	-	42 μM	12
Fluorometry	Polymerase/nicking template	0.5 – 20 μM	84 nM	13
Fluorometry	CdTe quantum dots	0.333 – 167 nM	0.217 nM	14
Colorimetry	Silver nanoparticles	60 – 280 nM	21 nM	15
Colorimetry	Gold nanorods	10 pM – 5 nM	3.3 pM	16
Colorimetry	Gold nanoparticles	10 nM – 1 mM	5.6 nM	17
Colorimetry	Gold nanoparticles	0.1 – 100 μM	18 nM	18
Surface plasmon resonance	Gold nanoparticles	0.5 – 50 pM	0.21 pM	19
Surface plasmon resonance	Streptavidin-coated Au-NPs	0.005 – 0.5 pM, 1 – 20 pM	4 fM	20

Appendix C.5 Calculating the average % difference in particle spacing changes measured between diluted FBS and pure PBS

Figure 4-7 shows the AD-induced particle spacing changes measured in diluted FBS and pure PBS. The % difference in particle spacing changes measured between diluted FBS and pure PBS at each AD concentration (1 nM, 10 nM, 100 nM, 1 µM, and 10 µM) was calculated using the equation below.

% difference $= \frac{|\boldsymbol{a}-\boldsymbol{b}|}{|(\boldsymbol{a}+\boldsymbol{b})/\mathbf{2}|} \times 100$ (%), where $\boldsymbol{a}$ is the particle spacing change in diluted FBS and $\boldsymbol{b}$ is the particle spacing change in pure PBS. The calculated % differences were 10.4, 4.51, 3.53, 1.23, and 0.256%. From the five % differences, the average % difference was calculated to be 3.99%.

Appendix C.6 Calculating the % recoveries for the detection of AD in human urine

The % recoveries were calculated using the equation below, where C_{Found} is the concentration of AD found in the spiked sample, $C_{Baseline}$ is the baseline concentration of AD in the unspiked sample, and C_{Added} is the known concentration of AD added to the sample.

Recovery % = $(C_{Found} - C_{Baseline})/C_{Added}*100$

Appendix C.7 References

(1) Zhang, J.-T.; Wang, L.; Lamont, D. N.; Velankar, S. S.; Asher, S. A., Fabrication of Large-Area Two-Dimensional Colloidal Crystals. *Angew. Chem. Int. Ed.* **2012,** 51, 6117-6120.

(2) Thomas, L. C.; Chittenden, R. A., Characteristic Infrared Absorption Frequencies of Organophosphorus Compounds — I. The Phosphoryl (P=O) Group. *Spectrochim. Acta* **1964**, 20, 467-487.

(3) Jang, K.; Westbay, J. H.; Asher, S. A., DNA-Crosslinked 2D Photonic Crystal Hydrogels for Detection of Adenosine Actuated by an Adenosine-Binding Aptamer. *ACS Sensors* **2022,** 7, 1648-1656.

(4) Tian, K.; Ma, Y.; Liu, Y.; Wang, M.; Guo, C.; He, L.; Song, Y.; Zhang, Z.; Du, M., Hierarchically Structured Hollow Bimetallic ZnNi MOF Microspheres as a Sensing Platform for Adenosine Detection. *Sens. Actuators B Chem.* **2020**, 303, 127199.

(5) Zhang, D.; Ma, J.; Meng, X.; Xu, Z.; Zhang, J.; Fang, Y.; Guo, Y., Electrochemical Aptamer-Based Microsensor for Real-Time Monitoring of Adenosine in vivo. *Anal. Chim. Acta* **2019**, 1076, 55-63.

(6) Du, J.; Ge, H.; Long, S.; Sun, W.; Fan, J.; Peng, X., Gold Nanoparticle-Based Plasmonic Probe for Selective Recognition of Adenosine. *Sens. Actuators B Chem.* **2019**, 296, 126591.

(7) Lin, Y.; Wang, X.; Sun, Y.; Dai, Y.; Sun, W.; Zhu, X.; Liu, H.; Han, R.; Gao, D.; Luo, C., A Chemiluminescent Biosensor for Ultrasensitive Detection of Adenosine Based on Target-Responsive DNA Hydrogel with Au@HKUST-1 Encapsulation. *Sens. Actuators B Chem.* **2019**, 289, 56-64.

(8) Hou, Y.; Han, R.; Sun, Y.; Luo, C.; Wang, X., Chemiluminescence Sensing of Adenosine Using DNA Cross-Linked Hydrogel-Capped Magnetic Mesoporous Silica Nanoparticles. *Anal. Chim. Acta* **2022**, 1195, 339386.

(9) Shen, X.; Xu, L.; Zhu, W.; Li, B.; Hong, J.; Zhou, X., A Turn-on Fluorescence Aptasensor Based on Carbon Dots for Sensitive Detection of Adenosine. *New J. Chem.* **2017**, 41, 9230-9235.

(10) Wang, G.; Wang, L.; Li, X.; Xu, X.; Jiang, W., T7 Exonuclease-Assisted and Target-Triggered Cascade Dual Recycling Signal Amplification Strategy for the Sensitive and Specific Detection of Adenosine. *Talanta* **2019**, 197, 234-238.

(11) Yousefi, S.; Saraji, M., Developing a Fluorometric Aptasensor Based on Carbon Quantum Dots and Silver Nanoparticles for the Detection of Adenosine. *Microchem. J.* **2019**, 148, 169-176.

(12) Sergelen, K.; Liedberg, B.; Knoll, W.; Dostalek, J., A Surface Plasmon Field-Enhanced Fluorescence Reversible Split Aptamer Biosensor. *Analyst* **2017**, 142, 2995-3001.

(13) Xu, X.; Wei, H.; Jiang, W., A Target Triggered Proximity Combination-Based Fluorescence Sensing Strategy for Adenosine Detection. *Analyst* **2017**, 142, 2247-2252.

(14) Song, Y.; Tang, T.; Wang, X.; Xu, G.; Wei, F.; Wu, Y.; Song, Q.; Ma, Y.; Ma, Y.; Cen, Y.; Hu, Q., Highly Selective and Sensitive Detection of Adenosine Utilizing Signal Amplification Based on Silver Ions-Assisted Cation Exchange Reaction with CdTe Quantum Dots. *Sens. Actuators B Chem.* **2017**, 247, 305-311.

(15) Yousefi, S.; Saraji, M., Optical Aptasensor Based on Silver Nanoparticles for the Colorimetric Detection of Adenosine. *Spectrochim. Acta A* **2019**, 213, 1-5.

(16) Zhang, X.; Kong, C.; Liu, Q.; Zuo, X.; Li, K.; Chen, Z., Colorimetric Adenosine Assay Based on the Self-Assembly of Aptamer-Functionalized Gold Nanorods. *Microchim. Acta* **2019**, 186, 587.

(17) Ma, L.; Ma, L.; Su, M.; Wang, Z., Exonuclease III Assisted Aptasensor for Adenosine Detection with Gold Nanoparticle Probes. *Anal. Methods* **2014**, 6, 4366-4372.

(18) Zhu, R.; Song, J.; Zhou, Y.; Lei, P.; Li, Z.; Li, H.-W.; Shuang, S.; Dong, C., Dual Sensing Reporter System of Assembled Gold Nanoparticles toward the Sequential Colorimetric Detection of Adenosine and Cr(III). *Talanta* **2019**, *204*, 294-303.

(19) Yao, G.-H.; Liang, R.-P.; Huang, C.-F.; Zhang, L.; Qiu, J.-D., Enzyme-Free Surface Plasmon Resonance Aptasensor for Amplified Detection of Adenosine via Target-Triggering Strand Displacement Cycle and Au Nanoparticles. *Anal. Chim. Acta* **2015**, 871, 28-34.

(20) Yao, G.-H.; Liang, R.-P.; Yu, X.-D.; Huang, C.-F.; Zhang, L.; Qiu, J.-D., Target-Triggering Multiple-Cycle Amplification Strategy for Ultrasensitive Detection of Adenosine Based on Surface Plasma Resonance Techniques. *Anal. Chem.* **2015**, 87, 929-936.